Available online at www.keaipublishing.com/en/journals/journal-of-magnesium-and-alloys/

ScienceDirect

Journal of Magnesium and Alloys 13 (2025) 3524–3563

www.elsevier.com/locate/jma

Review

Magnesium alloys with rare-earth elements: Research trends applications, and future prospect ☆

Zhiqi Zhu [a,#], Irfan Ayoub [b,#], Jie He [c,#], Jingran Yang [a], HanDong Zhang [d], Zhiqin Zhu [e,*], Qi Hao [f], Ziming Cai [g], Oluwafunmilola Ola [h], Santosh K. Tiwari [i,**]

[a] School of Materials Science and Engineering, Central South University, Changsha 410083, China
[b] Department of Metallurgical Engineering and Materials Science, Indian Institute of Technology Bombay, Mumbai, 400076, India
[c] Powder Metallurgy Research Institute, Central South University, Changsha 410083, China
[d] Light Alloy Research Institute, Central South University, Changsha 410083, China
[e] Department of Hepatology, Southern Medical University Hospital of Integrated Traditional Chinese and Western Medicine, Southern Medical University, Changsha 410083, China
[f] School of Resource and Safety Engineering, Central South University, Changsha 410083, China
[g] School of Electronic Information Engineering, Beijing Jiaotong University, Changsha 410083, China
[h] Advanced Materials Research Group, Faculty of Engineering, The University of Nottingham, Nottingham NG7 2RD, UK
[i] Centre For New Materials & Surface Engineering, Dept of Chemistry, NMAM Institute of Technology, Nitte University, Karnataka 547110, India

Received 22 January 2025; received in revised form 4 July 2025; accepted 21 July 2025
Available online 26 August 2025

Abstract

Magnesium alloys have emerged as promising light weight materials due to their low density, high specific strength, excellent machinability, and superior damping capacity, making them ideal for aerospace, automotive, and electronics applications. However, broader use of magnesium alloys is limited by poor thermo-mechanical performance, corrosion susceptibility, and low formability at room temperature. The addition of rare-earth elements such as gadolinium, yttrium, and neodymium has meaningfully improved these limitations, enhancing the overall performance of magnesium alloys. This review highlights recent advancements in rare-earth magnesium alloys, focusing on their improved thermo-mechanical properties, microstructural evolution, crystallization behavior, and texture development. Herein, strengthening mechanisms associated with rare-earth additions are discussed in detail. Furthermore, the article explores growing relevance of these alloys in advanced applications, including biomedical implants, IoT devices, aerospace structures, defense systems, and general engineering. With their enhanced mechanical and functional properties, rare-earth magnesium alloys represent a new generation of high-performance, functional materials poised to drive innovation across multiple technology sectors.

Keywords: Rare-earth magnesium alloys; Deformation mechanisms; Microstructure; Mechanical properties; Thermal properties; Crystallization processes; Applications.

1. Introduction

Amid resource depletion and environmental concerns, optimizing efficiency is crucial. Rising global warming and crude oil prices drive industries to seek innovative solutions for sustainable and efficient resource utilization in today's evolving technological landscape. This demand has sparked a renewed emphasis on the design, development, and implementation of lightweight materials [1]. Composite materials are currently regarded as the most promising choice for density-optimized

☆ Peer review under the responsibility of Chongqing University

* Corresponding author at: Department of Hepatology, Southern Medical University Hospital of Integrated Traditional Chinese and Western Medicine, Southern Medical University, Changsha 410083, China.
** Corresponding author at: Centre For New Materials & Surface Engineering, Dept of Chemistry, NMAM Institute of Technology, Nitte University, Karnataka 547110, India.
E-mail addresses: 233101034@csu.edu.cn (Z. Zhu), ismgraphene@gmail.com (S.K. Tiwari).
# Contributed equally and regarded as co-first authors.

https://doi.org/10.1016/j.jma.2025.07.012

material applications. When utilized in the design of various structural components, these materials can demonstrate pertinent efficiency and contribute to reductions in fuel consumption by lowering the overall weight of vehicles in the automation and aeronautics sectors. Research indicates that a weight reduction of 10 % in passenger vehicles can result in achieving fuel savings of 20-30 %, without any modifications to the existing design [2]. In this regard, lightweighting has become a core focus of different design manufacturing industries.

To achieve the desired objectives, the primary consideration is the selection of materials and their suitability for specific applications. Among the various materials available, Magnesium (Mg) and its alloys are recognized as some of the lightest options, offering a wide range of applications [3]. Currently, these materials are increasingly replacing commonly used steel and aluminum (Al), establishing a noteworthy role in many engineering fields [4,5]. But, the low corrosion resistance of Mg in various environments puts a limit to its potential applications [6]. Notably, galvanic corrosion is a critical concern, to a great extent when Mg is used alongside materials such as stainless steel and other alloys [4,5]. The reduced corrosion rate of pure Mg can be attributed to the presence of alpha-Mg microstructures, which develop due to trace amounts of impurities such as nickel (Ni), copper (Cu), cobalt (Co), and iron (Fe) [6]. These impurities often exceed acceptable tolerance levels, further affecting the material's performance. But, the excellent benefits of Mg and its alloys have caught the attention of researchers from every domain. Therewithal being effectively used in automation and aeronautics, owing to their biocompatible nature with better mechanical and physical properties they are being intensely scrutinized for the bioimplants [3–6]. The magnesium alloys (MAs) exhibit a greater resistance to hydrogen porosity, resulting in a castability that is 50 % higher than that of copper (Cu) and Al alloys [7]. Furthermore, the properties attained by Mg and its alloys also favors its use for electromagnetic shielding [8,9]. Owing to its adaptability feature it can be easily produced via rolling. Due to high damping ability, it can absorb energy of any substance, thus being effectively used for load-bearing purposes [8]. With its ease of machinability, it is being effectively used for designing complex structures with great dimensional precision [10]. High precision being an important aspect in the biomedical field further increases its applicability in the domain [11,12]. In Contrast to polymers, it possesses high thermal conductivity with cent percent recyclability. The heat dissipation ability of Mg is 100 times more than that of plastic [13].

Despite being rich in properties, the use of Mg and its alloys is limited by several drawbacks, with the most important being their high degradation rate [14]. The addition of various alloying elements can improve the properties of materials; however, selecting the appropriate alloying element is crucial, as it may enhance one property whereas adversely affecting another. Typically, the choice of alloying element is based on the intended application. For instance, Mg, due to its pyrophoric nature, oxidizes quickly when exposed to air [15]. Due to release of hydrogen gas on interacting with the air it is highly prone to corrosion as well [16]. Resolving the issues with due care of enhancing the properties, researches have observed that using rare-earth (RE) elements as alloying elements has provided the better results in every aspect. The unique electronic structure of RE metals, with high electron density and substantial localized characteristics in the 4f electron shell, endows them with high reactivity and responsiveness in the alloy system. There is substantial practical use of RE elements in alloy design and development due to the fact that they tend to increase the mechanical qualities, corrosion resistance, magnetic properties, etc. [17–23].

To provide an all-inclusive understanding of the effects and enhancements of various characteristics of MAs resulting from the incorporation of RE elements, there is currently no consolidated source in the existing literature. This review article aims to present a clear overview of Mg, its alloys, and the influence of RE ions. It will explore the role of RE elements in MAs and how their integration enhances the properties of these materials. A detailed examination of how these elements contribute to the strength of MAs will be conducted, including an analysis of the mechanisms of deformation such as lattice distortion, slip dislocation, and twinning deformation. Besides, the review will address the impact of lattice mismatch on the mechanical properties of RE-incorporated MAs and how RE elements affect twinning behavior, subsequently influencing the ductility and toughness of the alloys. An emphasis will be laid to discuss the unique magnetic properties of these elements and their interactions with microstructural components, including dislocations, grain boundaries, and phase interfaces within the alloys. Finally, the article will outline the applications of these alloys in various sectors, such as automotive, defense, aerospace, electronics, communication, and the medical field.

2. Historical prospect and importance of magnesium and its alloys

Magnesium, the lightest structural metal with a density of 1.74 g/cm^3, has long captured attention in materials science for its unique combination of low weight, high specific strength, and electromagnetic shielding capabilities. The historical trajectory of Mg and its alloys reflects a continual interplay between scientific advancement, technological demand, and strategic importances, highlighting both the challenges and immense potential of this element in engineering applications [24]. Elemental Mg was first isolated by Sir Humphry Davy in 1808 through the electrolysis of a magnesia–mercuric oxide mixture. However, significant industrial production began only in the late 19th and early 20th centuries [25]. The carbothermic and electrolytic extraction processes most notably the development of electrolytic Mg production by IG Farben in Germany enabled large-scale applications [26]. The early 20th century witnessed the rise of magnesium's strategic relevance, mainly during World Wars I and II, when it was widely employed in aircraft components, incendiaries, and structural applications owing to its

low density and availability [27]. During these wartime periods, foundational MAs such as Mg-Al-Zn (AZ) and Mg-Mn systems were developed. Although these alloys offered favorable casting behavior and adequate strength-to-weight ratios, they were hindered by poor corrosion resistance and limited high-temperature performance. Nevertheless, their use in aerospace underscored magnesium's importance in weight-sensitive applications, marking the beginning of sustained interest in improving its mechanical and chemical behavior [28]. Post-war industrial and scientific efforts shifted toward developing wrought MAs, particularly those incorporating zirconium (Zr) and RE elements. The discovery that RE element, such as yttrium (Y), neodymium (Nd), and gadolinium (Gd) could enhance high-temperature strength and creep resistance, thereby significantly broadened the functional domain of MAs. Alloys like WE43, containing Y and Nd, became critical in aerospace and defense sectors [29]. These RE-containing alloys form thermally stable intermetallic phases (e.g., $Mg_{12}RE$, Mg_3RE) that improve their microstructural stability under elevated temperatures, a breakthrough in extending magnesium's use beyond ambient conditions.

The importance of MAs lies primarily in their exceptional specific strength, which makes them indispensable in industries where weight reduction translates directly into improved energy efficiency, that is key aim of this review and will be discussed in details [24]. In the automotive sector, substituting steel and Al with Mg components reduces fuel consumption and CO_2 emissions. For aerospace, the weight savings are even more critical, affecting payload capacity, fuel economy, and performance. These systemic benefits illustrate magnesium's integral role in achieving lightweight, high-performance design in transportation and structural engineering. The 1980s and 1990s saw renewed interest in Mg driven by global energy concerns, automotive efficiency standards, and a rising demand for environmentally conscious materials. Novel alloy systems such as AE42 (Mg-Al-RE) and AS21 (Mg-Al-Si) emerged, offering enhanced creep resistance and improved casting capabilities [30]. Concurrently, advancements in solidification processing; such as thixomolding, squeeze casting, and rapid solidification, allowed better microstructural control and defect minimization, thereby expanding magnesium's design window. But, inherent limitations in magnesium's hexagonal close-packed crystal structure, mainly its limited number of easy slip systems at room temperature constrained its ductility and formability [31]. The addition of RE elements emerged again as a key strategy. RE atoms alter texture development during thermomechanical processing, reduce basal texture intensity, and promote activation of non-basal slip systems. These effects not only enhance ductility but also allow for more uniform plastic deformation [32]. Advanced characterization techniques, including EBSD and in-situ neutron diffraction, have elucidated these mechanisms, confirming the role of REs in improving the overall deformation response.

In recent decades, magnesium's potential in biomedical, electronics, and energy applications has become increasingly evident. Its biodegradability and biocompatibility make Mg alloys attractive candidates for orthopedic implants and bioresorbable vascular stents [33]. Alloy systems like Mg-Zn-Ca and Mg-Sr are being tailored for such uses, with research focused on optimizing corrosion rates and mechanical retention during healing. The environmental importance of Mg is increasingly recognized in the context of sustainability. Compared to heavier structural metals like steel and copper, Mg offers advantage of lower life-cycle emissions when used effectively. Furthermore, it is highly recyclable, and ongoing efforts are focused on developing green extraction technologies, including molten salt electrolysis powered by renewable energy sources [34,35]. Given that over 85 % of global Mg production currently relies on the Pidgeon process an energy-intensive method advancing cleaner production routes remains a key objective [36]. Despite its promising attributes, several challenges persist, including limited ductility, high reactivity, and cost constraints especially for RE-containing alloys. However, the ongoing integration of computational materials science, additive manufacturing, and advanced thermomechanical treatments is accelerating the discovery and deployment of next-generation magnesium alloys.

3. Rare-earth magnesium alloys (REMAs)

3.1. Importance of studying REMAs

The alloying process has meaningfully improved the characteristics of Mg and its alloys; however, REMAs have demonstrated superior performance in various applications due to their enhanced properties [37]. The incorporation of RE elements has shown significant results in texture weakening and in enhancing the deformation capabilities of MAs [38,39]. Their incorporation results in the development of new eutectic phases which in turn enhance the strength of these alloys [40]. Therefore, it is necessary to understand the role of RE interaction with the alloy's microstructure. These elements also tend to enhance the ductility as well as formability of the Mg and its alloys [41]. To comprehend the interaction mechanism, it is essential to understand the deformation mechanism of RE magnets through both theoretical analysis and practical foundations for the selected designs and optimization of MAs. In recent developments, various MAs have been enhanced with RE elements to improve their mechanical properties. Table 1 illustrates the REMAs developed domestically and internationally along with their mechanical properties [23,42–49].

As outlined in Table 1, the alloys are characterized by their unique compositions and have been tested under T6 conditions, which typically involve solution treatment followed by artificial aging to optimize their strength and ductility [50]. The alloys ranges from AZ91, which primarily consists Mg, Al, and Zn, to more complex alloys like VQ182, which includes higher concentrations of Gd and Ag. Some alloys have noticeably showed improvements in their mechanical characteristics due to the inclusion of RE elements, including Y, Nd, and Gd. With ultimate tensile-strength values ranging from 108 MPa for MEZ (Mg-2.5RE-0.5Zn) to 414 MPa for VQ182

(Mg-18.2Gd-1.9Ag-0.3Zr), these alloys have a wide range of industrial uses. This large variation shows how the alloying components affect the tensile-strength (TS) of MAs. Elevated TS values are characteristic of alloys like VQ182 and VW102, which include weighty amounts of Gd and other RE elements. Similar to TS, the yield strength (YS) also varies significantly among the alloys, from 76 MPa for MEZ to 293 MPa for VQ182. The correlation between the YS and the composition of RE elements is evident, indicating that these elements play an important role in increasing the YS of MAs. Alloys like VW114 and VWZ1142 exhibit high TS and YS, showcasing the beneficial effects of combining Gd, Y, and Zn. The presence of these elements, primarily in T6 heat treatment conditions, contributes to the formation of stable phases that resist deformation, thereby enhancing the mechanical properties. When comparing alloys like AZ91 to advanced compositions like VQ182, the substantial impact of RE additions on mechanical properties is clearly evident. This improvement is vital for applications requiring structural integrity under high stress and temperature. Fig. 1 shows a histogram of elongation percentages, with VZ61 alloy exhibiting the highest elongation, indicating superior ductility among the alloys.

From the above discussion, it is clear that the mechanical characteristics of REMAs, especially their TS and YS, have been greatly enhanced due to incorporation of RE elements. The variations in alloy composition highlight the tailored approach in enhancing material properties for specific industrial applications. The data provided in Table 1 serve as a valuable reference for selecting suitable REMAs for engineering applications requiring weight-reducing materials with high strength. Moreover, due to the increasing demands of engineering applications, REMAs are continuously advancing to meet the demands, forming a virtuous cycle of mutual reinforcement.

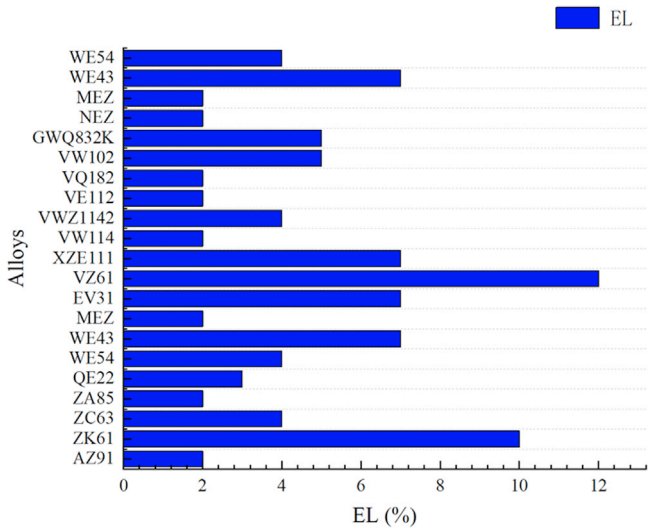

Fig. 1. Elongation strength of REMAs that have been developed across the globe.

3.2. Origin and development

Among the families of MAs, Mg-Mn, Mg-Al, Mg-Zn, Mg-RE, Mg-Th, Mg-Ag, and Mg-Li are the most common, with further variations depending on their principal elements. But,

Table 1
REMAs developed their scientific name, composition and properties.

Alloys	Alloy composition	Test condition	UTS/ MPa	Mechanical property YS/MPa
AZ91	Mg-8.7Al-0.7Zn-0.1Mn	T6	200	120
ZK61	Mg-6Zn-0.7Zr	T6	310	195
ZC63	Mg-6Zn-2.7Cu-0.3Mn	T6	210	125
ZA85	Mg-7.7Zn-4.9Al-0.3Mn	T6	195	138
QE22	Mg-2.5Ag-2.1Di-0.7Zr	T6	260	195
WE54	Mg-5.2Y-3RE-0.7Zr	T6	280	205
WE43	Mg-4Y-3.4RE-0.7Zr	T6	250	180
MEZ	Mg-2.5RE-0.5Zn	T6	108	76
EV31	Mg-3Nd-2Gd-0.6Zn-0.5Zr	T6	292	178
/	Mg-2.6Nd-1.5Gd-0.5Zn-0.5Zr	T6	295	165
VZ61	Mg-6Gd-1Zn-0.6Zr	T6	220	127
XZE111	Mg-1Ca-1Zn-Nd-0.6Zr	T6	227	153
VW114	Mg-11.3Gd-3.8Y-0.7Zr	T6	330	300
VWZ1142	Mg-11.1Gd-4.1Y-1.7Zn-0.5Zr	T6	361	231
VE112	Mg-11Gd-2Nd-0.5Zr	T6	350	230
/	Mg-4.5Gd-2.6Nd-0.5Zn-0.5Zr	T6	325	205
VQ182	Mg-18.2Gd-1.9Ag-0.3Zr	T6	414	293
VW102	Mg-10Gd-2Y-0.5Zr	T6	362	239
GWQ832K	Mg-7.77Gd-2.73Y-2.04Ag-0.37Zr	T6	402	268
NEZ	Mg-3Nd-0.5Zn	T6	165	114
MEZ	Mg-2.5RE-0.5Zn	T6	108	108
/	Mg-8Gd-2.5Nd-0.5Zr	T6	251	228
/	Mg-6Gd-2.5Y-1Nd-0.5Zr	T6	289	241
WE43	Mg-4Y-3.4RE-0.7Zr	T6	345	196
WE54	Mg-5.2Y-3RE-0.7Zr	T6	280	205

because of the lower melting points and greater atomic diffusion capabilities, the strengthening phases of MAs such as $Mg_{17}Al_{12}$, Mg-Zn, and β-phase are highly susceptible to softening and over-aging at high temperature (HT) [52]. Although at HT alloys grain boundary rotation is not affected so much but performance suffers because of grain boundary sliding. The radioactive properties of thorium (Th) restrict the use of Mg-Th series alloys, even though it is the ideal element for enhancing the HT performance of MAs. The extensive usage of Mg-Ag series alloys is further restricted by silver being a valuable metal. Although the impact of Mn on MAs heat resistance is not as strong as that of RE elements, it is nevertheless noticeable. Furthermore, the Mg-Mn alloy series face several challenging issues such as casting problem, solidification shrinkage, and hot cracking. For these reasons, creating heat-resistant MAs that function very well at HTs requires only Mg-RE series alloys [53]. The main function of RE elements in this alloy series is to improve creep resistance and casting characteristics at HTs. Nonetheless, due to the high separation costs of individual RE elements, early research and development of MAs were focused on their mixtures. The light RE elements that make up these mixed REs was La, Ce, Pr, and Nd. The primary categories were La-Ce, and Nd-Pr, mixed RE compositions. Among the first RE elements introduced to Mg-RE series alloys were La, Ce, Pr, and Nd. Haughton and Prytherch found in 1940 that Mg-Ce alloys have a higher tensile strength (TS) when heated to HT. Afterward, in 1949, Leontis' research showed that adding La, Ce, Mishmetal (RE mixture rich in Ce), and Nd greatly tends to improve the HT performance of MAs [54]. By 1951, Leontis had delved deeper insights into the study of Mg-RE deformation (extrusion) alloys. He discovered that these alloys exhibit improved mechanical properties when La, Ce, non-Ce mixed REs, and Nd were added.

Moreover, it has been observed that heat treatment further tends to increase the strength of these alloys. Research on microstructure was first restricted to the study of metallographic structures, whereas these early studies were mostly concentrated on improving mechanical qualities. Findings from this study provided a solid theoretical and practical groundwork for future commercial alloy development and evaluations for the role of RE elements in MAs. With advancements in RE separation technology, by the mid-1960s, it was possible to produce RE metals with 99 % purity, and by the end of the 20th century, purities of up to 99.99 % were achievable. This facilitated the study of phase diagrams between Mg and individual RE elements. Therefore, the phase diagram research of Mg with individual REs that began in the early 20th century achieved considerable results by the late 1980s and early 1990s [55,56]. It has been found that, the Mg-rich regions in most Mg-RE (except in case of Sc) binary phase diagrams exhibited simple eutectic reactions, yielding the high solubility of these elements in Mg and compound phases that coexist with the Mg-based solid solutions, as is clearly depicted pictorially in Fig. 2 [57] and Table 2 [37].

From the Table 2, it is evident that the solubility of the elements in the La series in Mg matrix generally, increases

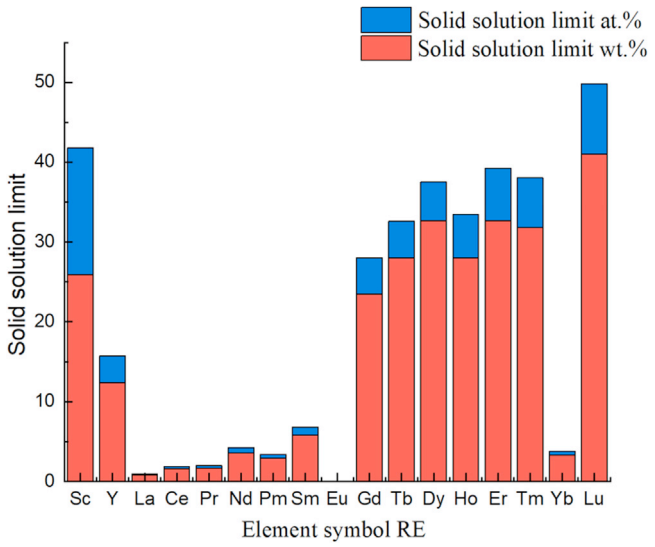

Fig. 2. Maximum solubility and binary compounds of RE metals in Mg matrix. Reproduced with permission from Elsevier [57].

with the increase in their atomic number. But, the solubility of the radioactive element Pm is yet to be determined, whereas the solubility of Eu (with a half-filled 4f electron shell) and Yb shows an abnormal decrease. The solubilities of Sc and Y in Mg-matrix are also relatively high. The strengthening property of the alloys increase due to incorporation of RE elements from La to Dy (with Y falling between Sm and Gd), reaching the highest strength in Mg-Gd, Mg-Tb, and Mg-Dy alloys, whereas the strength of Mg-Ho, Mg-Er, and Mg-Tm alloys slightly decreases [58]. At typical aging temperatures roughly about 12 wt.% of Ho, Er, and Tm is quite soluble in Mg. Even though, they do not attain enough aging strengthening. Considering the phenomenon that increasing the content of RE elements leads to a rise in alloy density and cost, current research and development efforts are primarily focused on binary and multicomponent REMAs containing La-Dy (excluding Pm and Eu) as well as Sc and Y, in order to obtain sufficient aging strengthening effects. The former Soviet Union and other countries have extensively studied REMAs for developing new alloys suitable for aviation and rocket applications. Studies have found that MAs containing 10 % Y can be used at 260 °C. Thus, Mg-Y alloys have been applied in helicopter tail rotor parts and assemblies. Instead of the radioactivity of Th, the element now utilized to increase the heat resistance of MAs is Y, as its heat resistance level can reach up to 370 °C [59,60].

Research on REMAs has come a long way in the last 30 years, with several notable advances and breakthroughs in this field is discussed elsewhere [61–69]. So far researchers have employed different techniques such as vacuum melting, electromagnetic stirring, and inert gas protection melting for the fabrications and analysis of different REMAs. Wang et al. [70] has observed that the YS of Mg-Gd alloys at 200 °C has greatly increased by using the right aging treatment, which in turn, results in improving the heat resistance of the alloys. Liu et al. [71] has studied the in vitro comparative analy-

Table 2
Maximum solubility and binary compounds of RE metals in Mg matrix.

Element symbol (RE)	Atomic number	Eutectic temperature (K)	Solid solution limit (wt.%)	Solid solution limit (at.%)	Coherent compound phase
Sc	21	-	25.9	15.9	MgSc
Y	39	838	12.4	3.35	$Mg_{24}Y_5$
La	57	886	0.79	0.14	$Mg_{12}La$
Ce	58	863	1.6	0.28	$Mg_{12}Ce$
Pr	59	848	1.7	0.31	$Mg_{12}Pr$
Nd	60	821	3.6	0.63	$Mg_{12}Nd$
Pm	61	823	2.9(?)	0.5(?)	?
Sm	62	815	5.8	0.99	$Mg_{41}Sm_5$
Eu	63	844	(≈0)	(≈0)	$Mg_{17}Eu_2$
Gd	64	821	23.5	4.53	Mg_5Gd
Tb	65	832	28.0	4.57	$Mg_{24}Tb_5$
Dy	66	834	32.7	4.83	$Mg_{24}Dy_5$
Ho	67	838	28.0	5.44	$Mg_{24}Ho_5$
Er	68	857	32.7	6.56	$Mg_{24}Er_5$
Tm	69	865	31.8	6.25	$Mg_{24}Tm_5$
Yb	70	782	3.3	0.48	Mg_2Yb
Lu	71	889	41.0	8.80	$Mg_{24}Lu_5$

sis of the Mg-RE based alloys. They have analysed that Gd based Mg alloys exhibits good precipitation hardening, which is supported by the reduction of solubility limit of Gd in Mg from 23.49 % at 548 °C to 3 % at 200 °C. The hardening through ageing enhances the mechanical properties of the alloys by restricting the dislocations. In case of Gd based MAs hardening through aging process mainly depends on the size, number, orientation and plane of the precipitates. And, it has been observed that precipitates with diamond shaped plays a critical role in improving the strength of these alloys [72]. The appearance of the γ'' and β' precipitates during ageing process by suitable addition of alloying element further enhances the strength of the alloy. Same thing has been observed by Zhang et al. [73], when they were studying the effect of Ag on the Mg-Gd based alloy. So, remarkable improvement has been observed in the kinetics and hardness of Mg-Gd based alloys with Ag as compared to those without Ag. The improvement in the characteristics has been attributed to the formation of γ'' and β' precipitate phases which has been verified from TEM images as depicted in Fig. 3. Apart from the occurrence sequential precipitation on prismatic plain of α-Mg matrix, unique sequential precipitation was observed on base plain also. The observed base plane sequential pattern was found to possess the hcp structures γ'', γ', γ which corresponds to the precipitates $Mg_{70}Gd_{15}Zn_{15}$, Mg-GdZn, and $Mg_{12}GdZn$, respectively.

Zhang et al. [74,75] has prepared Mg-Gd alloys using vacuum melting technology and found that the oxidation could be reduced along with improving the micro-homogeneity of the alloy by controlling the gas atmosphere during the melting process. Amberger et al. [76] has also studied the creep resistance and HT strength of Mg-Gd alloys at 200 °C. Through the nanoindentation process they have clearly observed that intermetallic metallic phases are responsible for enhancement in the creep resistance of the MAs. Tian et al. [77] has recently reported a study, in which without altering any constituent in the WE54 alloy, they have developed Mg-5Y-2.5Nd-1.5Gd-0.5Zr alloy by adding Gd to the composition. As per the study, the alloy has outperformed the conventional WE54 and WE43 MAs in terms of mechanical parameters, including TS (295 MPa), YS (216 MPa), and elongation (up to 8.9 % under peak aging conditions at 225 °C). Thus, by carefully manipulating the alloy's composition, scientists have created a number of novel REMAs. Some of the REMAs developed so far and their properties are presented in Table 3 [45].

Table 3
Properties of commonly used magnesium alloys.

REMAs number plate	Capability
Mg-Ce	Improved strength and HT stability. T_{max} = 2509 °C
Mg-Y	Good casting, age-hardening and high-temperature creep resistance temperature creep resistance
Mg-Nd	Higher HT strength and room temperature strength than magnesium alloys strength
Mg-Gd	Greatly enhanced creep resistance than other alloys
Mg-RE-Al	Higher mechanical properties than Mg-Al alloys properties
Mg-RE-Zr	HT strength and creep resistance
Mg-RE-Zn	High casting performance instead of EK30A alloy flame retardant good flame-retardant effect
Mg-RE-Ag	Good tensile properties and creep resistance
Mg-RE-Zn-Zr	Heat-resistant, high-strength casting alloys

3.3. Long-period stacking ordered (LPSO) phase in REMA

LPSO phases are the unique types of honey comb like 3D structures found in MAs which usually remain present at the grain boundaries [78]. In general, these phases exist in both stacking and chemical ordered arrangements [78–82]. In REMAs (Mg-M-RE systems), four type of LPSO structural

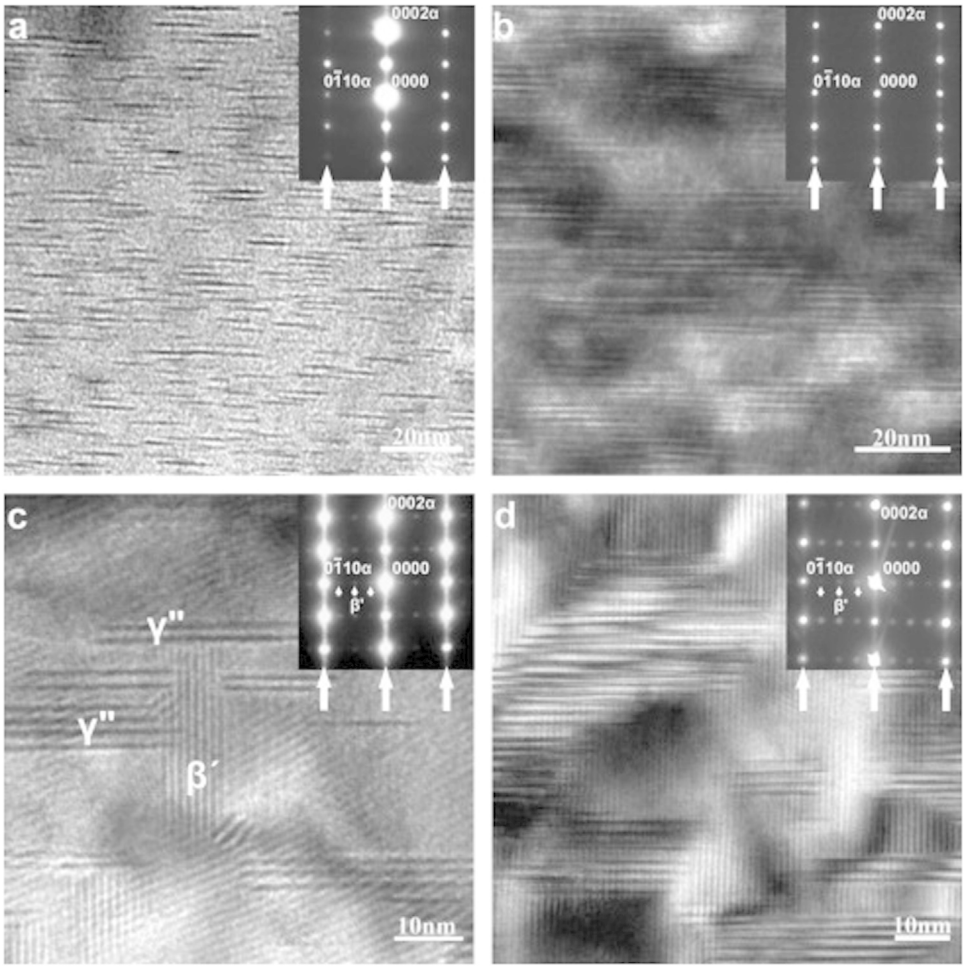

Fig. 3. TEM micrographs of the GQ162K alloy aged at 200 °C for different time periods (a) 20 mins, (b) 8 h, (c) 32 h, and (d) 600 h, along with the SAED patterns. Reproduced with permission from Elsevier [73].

phases have been identified based on the stacking arrangement. These structures are being designated as 10H, 18R, 14H and 24R, among which the designation 18R represents the LPSO phase which has been designated wrongly earlier as 6H [79,83]. However, Mi et al. [84] while studying Mg-Co-Y alloy came across three more new LPSO structure and have been designated as 15R, 12H, and 21R. Every LPSO structure has its unique stacking arrangement. The arrangement corresponding to every LSPO structure is presented in Table 4 [81,84,85]. In the designation, the layers tagged with prime represents the places mainly occupied by M/RE elements [86].

From the Table 4, it is evident that in case of LPSO structures 10H, 18R, and 24R, two layers are occupied by the heavier atoms, with 1–4 layers of Mg sandwiched between the building block atomic layers. On the other hand, in case of structures 15R, 12H, and 21R only one layer is occupied by the heavier atoms, with 2–4 layers of Mg sandwiched between the building block atomic layers. The characteristics of these LPSO structures is governed by the electronic structure of element M present in the configuration of REMA alloys. Apart from these two LPSO structures, the in-plane arrangement of solute atoms is also of great significance. The characteristic of in-plane that is ordered and disordered are very crucial in MAs, as they play a major role in stability and development of LPSO structures. These in-plane characteristics provide us insights about the range of composition variation for a particular LPSO structure [87]. Zhu et al. [80] while studying the ternary Mg-Zn-Y REMA, has found that the presence of in-place ordering of Zn and Y in two back-to-back atomic planes corresponds to 18R and 14H. On behalf

Table 4
Possible sequence of stacking for different LPSO phases in different REMAs.

S.no	LPSO	Stacking sequence (Along c-axis)
01	10H	AB′C′ACAC′B′AB
02	12H	AB′CBCBCB′ABAB
03	14H	AB′C′ACACAC′B′ABAB
04	15R	AB′CBC BC′ACA CA′BAB
05	18R	AB′C′ACACA′B′CBCBC′A′BAB
06	21R	AB′CBCBC BC′ACACA CA′BABAB
07	24R	AB′C′ACACACA′B′CBCBCBC′A′BABAB

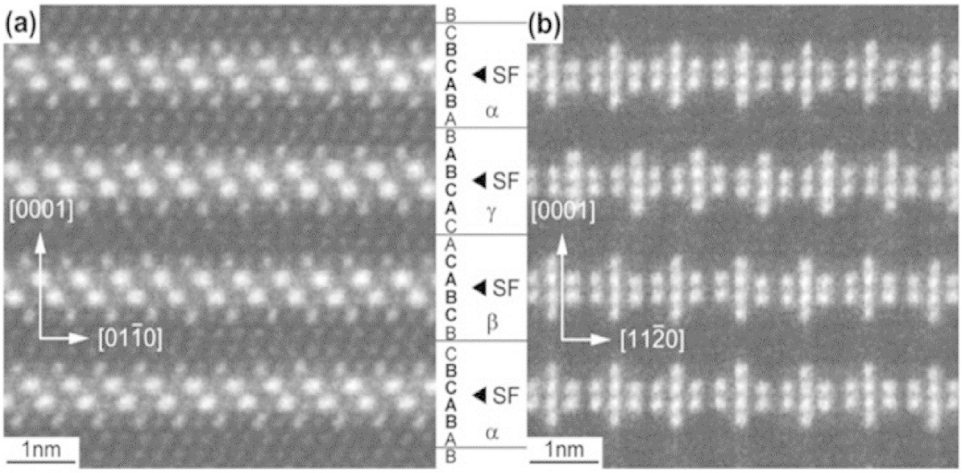

Fig. 4. High resolution TEM image corresponding to the Mg-Al-Gd alloy recorded along two different directions (a) [2–1–10] (b) [1–100]. Reproduced with permission from Elsevier [88].

of the arrangement, they came up with a model based on the ordered configuration of Zn and Y atoms. Also, there are high chances that the streaks from the LSPO structures (18R and 14H) in the composition may belong to the disordered configuration rather than expected long-range structure.

In the REMA Mg-Al-Gd, Yokobayashi et al. [88] have reported the in-plane ordering of the Gd and Al in the atomic planes of LSPO phases. The richness of the atomic planes in Gd and Al facilitates in understanding the crystal structure of developed LPSO structures. The existence of long range ordering of Gd/Al atoms in the planes is clearly evident from the STEM images as depicted in Fig. 4a and b [80]. From the images it is evident that in the enriched portions M/RE atoms are present in four back-to-back planes rather than two as proposed in the model. In case of Mg-Zn-Y ($Mg_{85}Zn_6Y_9$) alloys, a short range weak LPSO phase of L12-type was clearly evident [89]. Theoretical simulations have also been applied for analyzing these ordered and disorder LPSO structures in REMA [87]. In this regard, Kimizuka et al. [87] has applied the DFT calculation for understating the ordered TM_6RE_8 LPSO structure in REMAs like Mg-Al-Gd and Mg-Zn-Y. Moreover, it has been reported by the Yamasaki et al. [90] that the 10H LPSO generated in Mg-Zn-Y alloys when calcinated at 773 K is similar to that of the Mg-Al-Gd alloy. Therefore, heat treatment enhances spot visibility in SAED patterns, indicating improved ordering of the LPSO structure in Mg-Zn-Y alloys. High-resolution STEM confirms the highest in-plane order for the 20H-LPSO phase. However, in-plane LPSO structures in Mg-Co-Y alloys remain unclear, and no literature reports exist on over-diffusion or weak streaks in 15R, 12H, or 21R LPSO structures within the planes [84].

4. Role of rare-earth elements in MAs

RE elements are widely used across different sectors due to their unique properties. While traditionally prominent in ferrous metals, growing understanding of their role in alloys and mechanical behavior has extended their use to non-ferrous metals. Notably, under heat treatments, RE elements enhance casting, strengthen materials, and improve alloy quality, leading to a continuously expanding range of applications [91–95]. Research into developing RE elements for HT applications has recently been a priority, specifically in the MAs [96–104]. Research has shown that the impact of RE elements on MAs becomes more noticeable as the atomic number increases. Elements like La, Ce, Ce-rich mixed RE, Pr, and Nd exhibit the most noticeable impacts. The growing significance of RE elements in materials research and engineering is demonstrated by their integration into MAs, which considerably enhances a range of physical and chemical properties [105–108]. Some of these properties which gets improved significantly by the addition of RE elements [109–113] are briefly discussed as:

4.1. Removal of oxidation inclusions

A wide variety of oxidation inclusions at times occurs in MAs as they are being manufactured. These inclusions typically exist in the form of flakes, particles, or aggregates within the alloy's matrix or at grain boundaries, which can lead to fatigue crack initiation and reduced mechanical properties and corrosion resistance [114–118]. Due to magnesium's highly reactive chemical nature, it has a strong affinity for oxygen, readily forming stable oxide: magnesium oxide (MgO) at elevated temperatures. Consequently, oxidation inclusions predominantly exist in MAs as MgO. During the metal melting process, the oxidation behavior is mainly controlled by the oxide film, and according to the Pilling Bedworth ratio (α) for densification of the oxide film, with $\alpha(Mg) < 1$, the oxide film of Mg is usually porous and lacks protective properties. In contrast, RE metals have an α value greater than one, capable of forming a protective denser oxide film that effectively slows down the oxidation rate of the metal melt. In addi-

tion, RE elements are more reactive with oxygen than Mg; therefore, when these elements are added to molten MAs, RE oxides are produced [117]. This process assists in the removal of oxidation inclusions, thereby enhances the purity and performance of MAs. The frequent and general reactions are as:

$$3MgO+2[RE] = RE_2O_3+3Mg(l)$$

$$4[RE]+3O_2 = 2[RE]_2O_3$$

$$2MgO(s) = 2Mg(l)+O_2\uparrow \text{ (High temperature)}$$

4.2. Hydrogen removal

MAs are susceptible to casting flaws, including porosity, pinholes, and shrinkage, when they melt, because the alloy may absorb hydrogen from atmospheric moisture during reaction. For this reason, lowering the capability of hydrogen absorption capability in MA melt's is essential. The incorporation of RE elements promotes the reaction with water vapor and hydrogen in the Mg melt, forming RE-hydrides and RE-oxides, which effectively decreases the hydrogen content in the alloy melt [58,62–64]. This dehydrogenation process can be represented by the following reactions:

$$H_2O(g)+Mg(l) = MgO(s)+2[H]$$

$$[RE]+2[H] = [RE]H_2$$

$$2[RE]+3MgO = [RE]_2O_3+3Mg(l)$$

Through this reaction, RE elements aid in the removal of hydrogen from the MA melt, thereby improving the quality and performance of the final product.

4.3. Interaction with fluxes

During the melting of MAs, fluxes are commonly used to cover and refine the alloy, preventing the formation of oxides and inclusions. Yet, if fluxes are used improperly, they may introduce flux inclusions, which can affect the alloy's performance. Thermodynamic calculations indicate that all RE elements can react with fluxes in the melt form and thereby reduces interaction of MAs with fluxes. Among the RE elements, La has the strongest reactivity, whereas Y is relatively less reactive. The reaction between common fluxes is mainly composed of $MgCl_2$, and the reaction with RE elements is represented as follows:

$$2[RE]+3MgCl_2 = 2[RE]Cl_3(l)+3Mg$$

This reaction consumes the flux's RE elements, altering the alloy's ultimate composition and qualities.

4.4. Strengthening

Binary alloys of Mg combined with RE elements typically exhibit poor tensile performance at room temperature, which does not meet the requirements for structural applications. This defect is mainly due to the large size of the alloy grains, which directly affects its mechanical properties. A number of MA compositions using RE elements have been developed as a result of this problem's amelioration after it was discovered that Zr can efficiently refine Mg grains. Adding RE elements to cast MAs doesn't do much to improve their tensile properties at room temperature, but it does a great job in increasing their creep strength and tensile performance at HTs. This is especially true for Mg-Al alloys that have a low Al content. There have been a lot of recent findings from studies investigating how heavy RE elements, such as Gd and Nd, affect the characteristics of MAs. Research has shown that by controlling the rate of precipitation and the percentage of volume occupied by precipitated phases, these RE elements enhance the characteristics of MAs. Due to elemental interaction, the solubility of RE element in MAs decreases and their effects on the kinetics of precipitation from supersaturated solid solutions can impart additional strengthening effects when two or more of these elements are added to these alloys at the same time. MAs with RE elements exhibit a reduced solidification temperature range, a decreased risk of weld cracking, and enhanced casting densities [119].

4.5. Improving corrosion resistance

Mg has a low standard electrode potential, and the naturally formed surface oxide film is not dense and has poor protective properties, making Mg highly susceptible to corrosion in natural environments [65–67,120]. Both conventional elements like Al, Mn, Zn, Ca, and RE elements like Gd, Nd, Y, Ce, Dy, as well as elements like Zr and B, have certain effects on the corrosion resistance of MAs.

As per the reported research, the addition of RE element tends to improve corrosion resistance, optimize microstructure, and purify MA grains within a limited range [121,122]. In this regard, it has been observed that the incorporation of Nd into MAs, for instance, results in enhancing the alloys' corrosion and equilibrium potential, refining the grains and in turn making the alloys more resistant to corrosion. Different studies are present in the literature which report the effects of RE elements La, Ce, and Y on the microstructure and mechanical properties of AZ91 MAs. It has been observed that La, Ce, and Y can refine the microstructure of MAs, which is important for improving the corrosion resistance of AZ91 MAs [69,70,72,123]. In this line, Song et al. [124] found that when the content of Nd is not greater than 1.0 mass %, the incorporation of Nd also improves the corrosion resistance of AZ91 MAs. The resistance was optimal when the Nd content is 1.0 mass %, with a corrosion rate of 0.28 $mg{\cdot}cm^{-2}{\cdot}d^{-1}$. Mordike et al. [65] and Azzeddin et al. [125] has also analyzed the corrosion resistance of various cast MAs (including Mg-Sc, Mg-Gd Mg-Sc-Mn, Mg-Sc-Ce-

Mn, Mg-Cd-Sc-Mn, Mg-Y-Mn, Mg-Sc-Mn) and found that RE elements notably tend to increase the corrosion resistance of MAs. Kumar et al. [126] has also reported the effects of RE elements on the corrosion resistance of Mg-Zn alloys. The results have revealed that the incorporation of RE elements like Nd, Y, Gd in Mg-Zn alloys at a 2% mass ratio enhance the alloys' corrosion resistance to varying degrees. As a result of this improvement, the material's impedance is enhanced, making electromagnetic transmission more challenging. Moreover, the corrosion potential shifts towards more positive values, the corrosion current decreases, and consequently, the corrosion rate slows down. Among different RE elements, it has been observed that Y, and Gd have noteworthy effects on enhancing the corrosion resistance of MAs.

Likewise, Meng et al. [127] and Sun et al. [128] has observed that the incorporation of Sr to the Mg-Zn-Ca alloy also impacts its corrosion resistance. For analyzing the impact, they have employed different electrochemical methods, such as electrochemical impedance spectroscopy and potentiodynamic polarization, in conjunction with the hydrogen collection method to evaluate the corrosion performance. It has been observed that the incorporation of Sr to the Mg-Zn-Ca alloy drastically decreases its corrosion resistance. This was mainly because a higher number of secondary phase particles precipitated, leads to the generation of more micro-galvanic couples. The films experienced a reduction in compactness with extended exposure, resulting in the formation of a corrosive product layer on the surface of the samples, which subsequently improved their corrosion resistance.

5. RE integration and boosting of MAs

5.1. Plastic deformation in MAs

Hexagonal close-packed Mg and its alloys possess only two independent slip systems which can readily get activated at room temperature. It contradicts with the von Mises and Taylor criteria for maintaining uniform plastic deformation, that requires at least five independent slip systems [129–131]. The basal slip in Mg is more likely to occur at room temperature, but the critical shear stress (CRSS) for the pyramidal <c + a> slip is much higher than that for basal slip, making it difficult to achieve non-basal slip and thereby affecting the room temperature ductility of Mg [132,133].

The incorporation of alloying elements, that is RE elements Y and Ce, tends to efficiently enhance the plasticity and ductility of Mg. Wu et al. [134] found that the ductility of Mg-Y alloys mainly relies on the number of activated pyramidal <c + a> slips. Meanwhile, Chino et al. [135] confirmed that solid solution strengthening element Y can promote cross-slip and prevent the decomposition of unstable <c + a> slips, thereby improving the ductility of Mg. In addition, Zheng et al. [136] examined that the integration of Ce results in activation of prismatic and pyramidal slip, thus enhancing the plasticity of Mg. Regarding Sm, an important RE element comparatively low in cost, tends to effectively improve the properties of MAs due to its similar atomic size and electronegativity to Mg. Studies have shown that the incorporation of Sm promotes the precipitation response and solid solution strengthening, thereby results in enhancing the mechanical properties of alloys. Guan et al. [137] has observed that the Mg-3Sm-0.5Zn-0.4Zr alloy exhibits brilliant mechanical properties, due to the development of a large number of fine plate-like precipitates at the grain boundaries attributed to the incorporation of Sm. Hu et al. [138] has reported that the incorporation of Sm in MAs leads to the formation of fine and stable spherical nanoscale precipitates within the matrix, thereby enhancing the performance of the ZK60 alloy. Furthermore, they have found that the mechanical properties of the Mg-9Li-5Al-0.4Sm alloy were improved, primarily due to the grain refinement and precipitation strengthening of Sm particles promoted by the addition of Al. Similarly, Zhou et al. [139] has reported that the incorporation of Sm has made it easier for Mg-1Sm to activate pyramidal slip compared to pure Mg, as is evident from Fig. 5.

In addition to the experimental approach, the impact of incorporating the RE ion into MAs has been investigated through various theoretical simulations, including first-principles calculations. Through simulation researchers have calculated the generalized stacking fault energy of MAs and have optimized the crystal structures [140]. In this process, they have optimized the structural parameters and employed the Perdew-Burke-Ernzerh of generalized gradient approximation along with suitable ion-electron interaction potentials.

Gaun et al. [141] while employing the simulation, primarily constructed a supercell containing 144 atoms, and sampled the Brillouin zones of three different slip systems using a k-mesh grid generated by the Monkhorste-Pack method. The calculation results revealed that the GSFE of the basal [0001] <11> slip system is 143.2 mJ/m^2. To understand role of Sm in Mg alloys, they doped the supercell with 0.69 wt.% of Sm atoms and calculated its GSFE. This analysis aids in understanding how Sm affects the plastic behavior of MAs and provides theoretical support for the microstructural design and mechanical property optimization of the alloys. Zhou et al. [139] has also performed the phase and structural study via XRD, morphology via SEM backscattering and TEM for Mg-xSm alloy, as shown in Fig. 6. Through thermodynamic calculations using Thermo-Calc software and CCMg5 database, it has been found that in regions with higher Mg content, the α-Mg phase and $Mg_{41}Sm_5$ phase coexist. It has been observed that at temperature of about 530 °C, 1% Sm is completely dissolved in the Mg-matrix. The XRD pattern indicates that the Mg-1Sm alloy is predominantly composed of the α-Mg phase, similar to pure Mg, indicating that the addition of Sm did not form new intermetallic compounds. The SEM image and EDS spectrum shows that Sm is uniformly distributed in the Mg-matrix without any segregation or secondary phases. These findings suggest that Sm exists as solute atoms in the Mg-lattice, influencing the microstructure and phase composition of the alloy, which facilitates twinning and slip. In the Fig. 6d–f, many <c + a> dislocations were observed to appear in the early stages of deformation under 5% strain, indicating that the solid solution strengthening attained by Sm

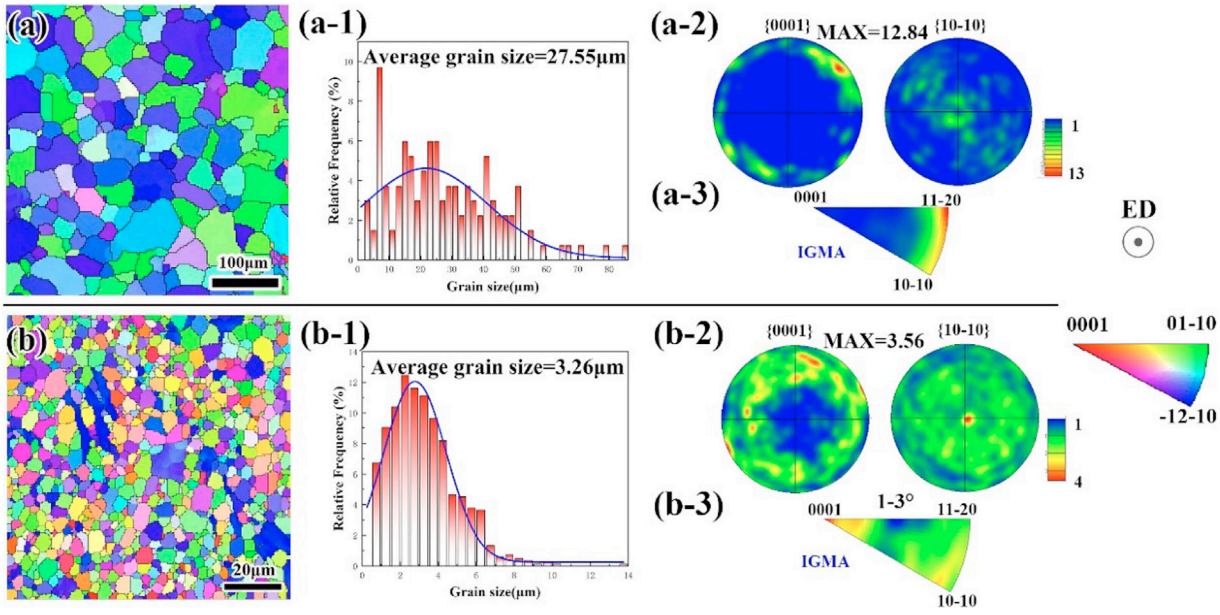

Fig. 5. EBSD micrographs, grain size distribution histograms, pole figures, and IGMA maps of the compressed Mg-*x*Sm alloys: (a) to (a-3) pure Mg alloy, (b) to (b-3) Mg-1 wt.% Sm alloy. Reproduced with permission from Elsevier [139].

is beneficial for the deformation of Mg. The incorporation of Sm easily triggers more pyramidal and basal slip, thus adapting the c-axis strain. As the strain rises to 15 % (Fig. 6g-i), an enormous number of <c + a> slips, and dislocations were observed. Therefore, the pyramidal <c + a> dislocations plays an important role in the tensile deformation process, making twinning and slip more likely to occur in terms of structure and phase composition [139].

The incorporation of RE element Y meaningfully promotes the activation of non-basal slip systems in Mg-Y alloys, especially the prismatic and pyramidal slip systems, which markedly enhances the ductility of the alloy. In a study reported by Chen et al. [142] they have analyzed 100 activated slip bands in 82 Mg-Y grains and 48 activated slip bands in 48 AZ31 grains using high-resolution digital image correlation (DIC) technology. The study found that although the tensile deformation of Mg-Y alloys is still predominantly basal slip, the addition of Y suggestively increases the activation of non-basal slip systems. This phenomenon was attributed to the decrease in the CRSS difference between basal and non-basal slip systems.

During the tensile deformation of Mg-Y alloys, an increased activation of non-basal slip systems was observed, contributing to enhanced ductility. Fig. 7a, b illustrates the identification of slip traces in the Mg-Y alloy, while Fig. 7c summarizes the statistical distribution of activated slip systems. At a tensile strain of 5 %, the activation ratio of non-basal slip systems reaches approximately 31 %.

The phenomenon of non-basal slip activation increasing with strain has also been verified by other researchers. In contrast, in AZ31 alloys, the activation ratio of non-basal slip at 5 % tensile strain is only 7 %, which is significantly less than that of Mg-Y alloys. The deformation mode of AZ31 alloys is primarily dominated by basal slip.

In addition to this, the incorporation of elements such as Al and Zn into MAs leads to an increase in stacking fault energy (SFE). A stacking fault is a type of defect in the crystal structure, and the elevation of its energy barrier implies that the movement of dislocations within the crystal becomes more difficult, thereby increasing the activation energy for the transition from basal plane slip to non-basal plane slip [143].

This increases the difficulty of activating pyramidal slip; hence, Mg-Zn and Mg-Al series alloys often require processing at higher temperatures. However, the incorporation of RE elements, and sometimes calcium, reduces the width of the dislocation core. This facilitates the cross-slip of a-type dislocations from the basal to the pyramidal planes, thereby enhancing the ductility of the MAs. Furthermore, the introduction of alloying elements causes distortion in the lattice structure of MAs. By adjusting the alloy elements, the axial ratio (i.e., the c/a lattice ratio) of the MA can be modified, which regulates the processability of using these alloys at different temperatures. For example, adding elements such as lithium (Li) and indium (In) to MAs can lower the axial ratio, increase the lattice symmetry, and thereby reduces the CRSS for specific slip systems, as illustrated in the Fig. 8 [143]. This allows the activation of multiple slip systems in the MAs even at lower temperatures, thereby demonstrating good ductility.

5.2. Improvement of mechanical properties

RE elements exhibit unique properties due to their distinctive electronic configurations, particularly the distribution of electrons in their outer shell orbits [144]. In MAs, the strengthening effect of RE elements is principally serious. This is mainly attributed to the fact that some of the RE ele-

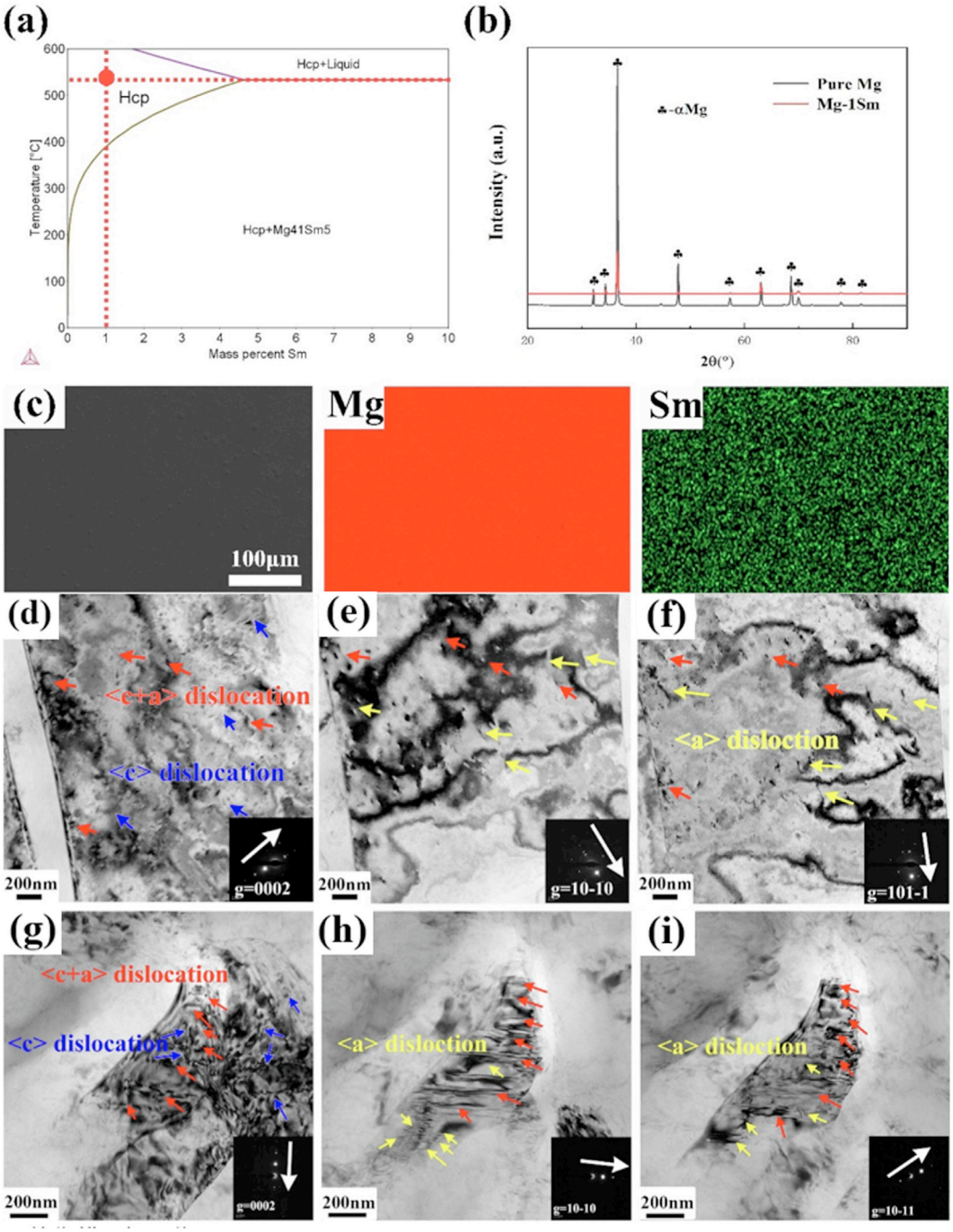

Fig. 6. (a) Phase diagram of the Mg-*x*Sm alloy, (b) XRD pattern of the SS Mg-*x*Sm alloys ($x = 0$, 1 wt.%), (c) SEM image and corresponding EDS spectrum of the Mg-1Sm alloy. Transmission electron microscopy images of Mg-1 wt.% Sm (d-f) deformed to 5 % and (g–i) 15 %, with different g-values. Reproduced with permission from Elsevier [139].

ments have a similar atomic radius to Mg and exhibit a large solubility in it. During aging, dispersed strengthening phases are formed in the alloy, which provide intense aging hardening effects, thus enabling the alloy to exhibit excellent solute and precipitation strengthening characteristics [97,145,146]. Fig. 9 shows the solubility of RE elements in solid Mg as a function of atomic number. This plot illustrates how the solubility of RE elements in a host metal varies with the atomic number of the solute element at different temperatures, providing insights into the thermodynamics of alloy formation [147].

The vertical axis indicates the solubility limit in atomic percent, which shows the maximum concentration of the RE element that can be dissolved in the host lattice. The horizontal axis represents the atomic number of RE elements, starting from La to Lu including Yttrium which is often associated with RE due to its chemical similarity. The plot lines correspond to different temperatures (300 °C, 400 °C, and 500 °C),

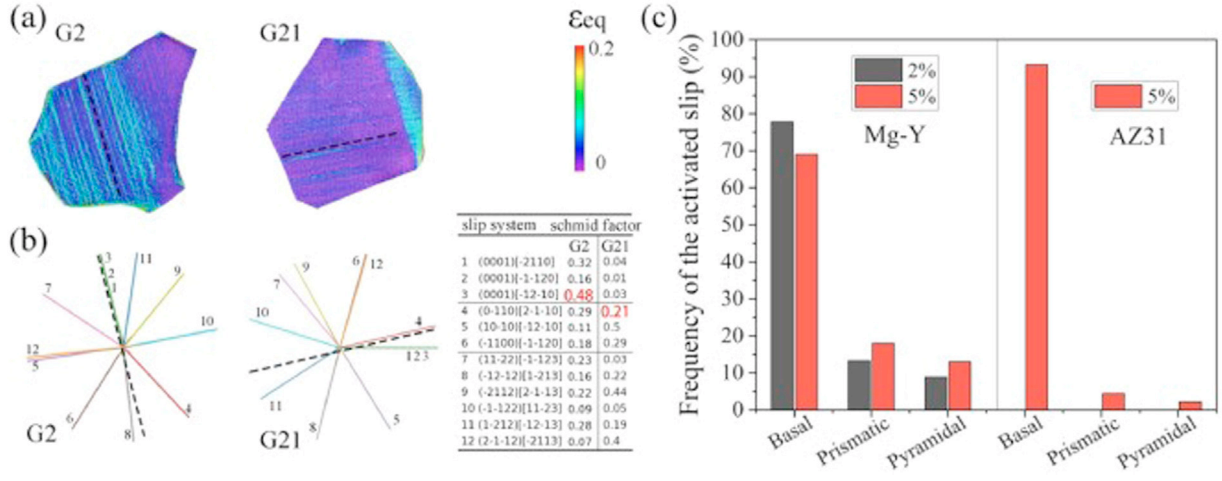

Fig. 7. Detection of active slip modes: (a) Display of slip bands in the strain mapping of Mg-Y alloy, (b) Recognition of the active slip systems using the criterion of best fit between the calculated and observed slip paths, (c) Statistical analysis of the slip modes activated following the tensile deformation of Mg-Y and AZ31 alloy. Reproduced with permission from Elsevier [142].

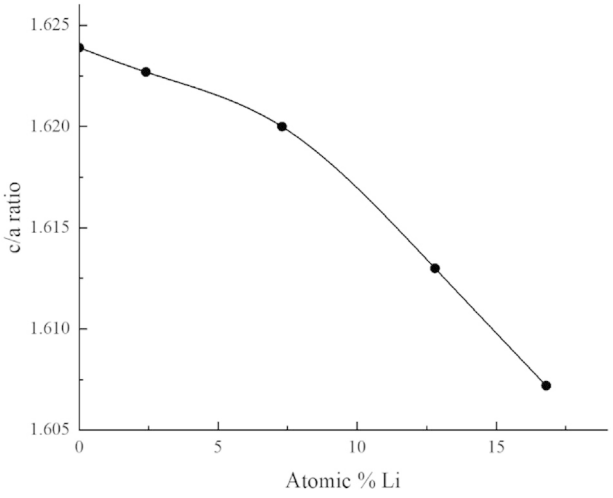

Fig. 8. Effect of the addition of Li elements on the c/a ratio of magnesium alloys. Reproduced with permission from Springer Nature [143].

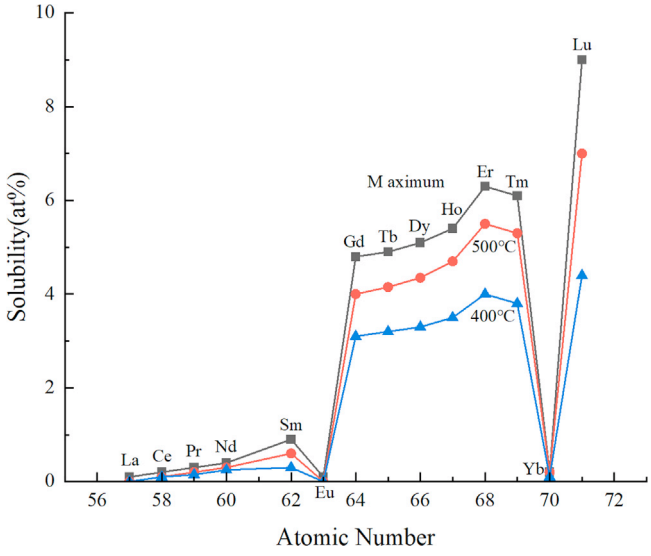

Fig. 9. Variation of solid solubility of RE elements in solid magnesium with atomic number. Reproduced with permission from Springer Nature [147].

showing that the solubility of most RE elements increases with temperature. A noticeable trough in the solubility is observed around Eu (atomic number 63), which indicates that Eu has a consequential lower solubility in comparison to its neighboring elements. The solubility peaks begin with Y and end with Lu, suggesting that these elements have the highest solubility in the host metal at elevated temperatures. The sharp increase in solubility at higher atomic numbers suggests that heavier RE elements may form more soluble alloys at the given temperatures. The increased solubility with temperature is consistent with the expectation that solute diffusion and lattice spacing generally increase with temperature, allowing more atoms to be added into the host lattice. The reduced solubility of Eu might be related to its electronic structure or atomic radius, which may not fit as easily into the host lattice as other RE elements. The higher solubility of Lu could be explained by their specific atomic radii and electronic structures, which might make them more compatible with the host lattice, especially at HTs. This plot can be used in the development of new alloy compositions, as it indicates which RE elements are more likely to form solid solution at given temperatures and which might lead to the formation of secondary phases. The graph provides valuable data for the design and processing of REMAs.

The incorporation of RE elements is a key strategy for strengthening MAs, as it effectively enhances the mechanical properties of the material [98–100]. This strengthening mechanism typically involves the combined addition of RE elements, especially the combination of Y and Nd which is very common and technically mature in MA strengthening [101,102]. For instance, in the WE series MAs (including WE43 and WE54) which are the prominent alloys. Al-

though WE54 alloy has high strength, its low plasticity limits its applications. Therefore, to broaden the scope of applications, WE43 alloy with fewer RE elements was developed, which provides better mechanical performance while maintaining lower production costs, making it one of the widely used MA in industry.

Using Y and Nd composite materials, Xie et al. [148] has examined the effects of RE elements on the mechanical characteristics of Mg-6Al alloy at both room temperature and HT. According to the findings, the alloy's plasticity, YS, and TS gets considerably improved as the Y and Nd content increased (from 0 to 1.8 % by mass). Wu et al. [149] investigated the impact of lanthanide elements like Ce, Nd, Y, and combination of Y+Nd on the mechanical characteristics of MAs. It has been observed that MAs mechanical characteristics gets enhanced by distributing the intermediate phases Mg-Ce and Mg-Nd, which are produced by Ce and Nd with Mg, along grain boundaries. Son et al. [150] has investigated the impact of Sm on the characteristics of Mg-5Al-3Ca MAs. The alloy's grains were refined once Sm was added, and the amount of grain refinement also got increased with the increase in the concentration of Sm, according to the experiment. The alloy's TS and YS were optimal at Sm concentration of 2 %, which has been attributed to the formation of Al_2Sm phase at grain boundaries. This phase being both evenly distributed and mechanically stable, tends to greatly improves the alloy's mechanical characteristics. Employing the double-stage ageing treatment and deformation processing, Zhang et al. [151] has studied the effects of Sm incorporation on ZM6 alloy. They observed that the incorporation of Sm tends to change the alloy's ageing precipitation behavior, making the alloy stronger and thereby opening up new possibilities for its use in lightweight structural components for aerospace and other industries. The effect on the mechanical properties of MAs with varying contents of RE element Y has also been explored to great extent. The main phase in the as-cast AZ91 alloy without Y treatment is the continuous eutectic phase $Mg_{17}Al_{12}$. Although, with the incorporation of Y, momentous changes occur in the nature of the precipitates: when the Y content is only 0.3 % (by weight), no Y precipitates are detected in the alloy; when the Y content is in the range of 0.6–0.9 % (by weight), a new Al_2Y phase begins to form, and the growth morphology of the $Mg_{17}Al_{12}$ phase also changes; when the Y content is increased to 1.2 % (by weight), the Al_2Y phase becomes rougher, while the $Mg_{17}Al_{12}$ phase transforms into a structure resembling cotton [98]. Fig. 10a depicts the relationship in-between the Y content and the strength of the AZ91 alloy. From the plot, it is evident that the AZ91-Y MA containing RE element Y has higher strength than the AZ91 alloy without Y under different temperature conditions. At room temperature and at an effective temperature of 200 °C, both the YS and TS of the alloy increase with the increase in Y content, reaching a peak between 0.6 % and 0.9 % with Y content. When the Y content exceeds 0.9 %, the alloy strength begins to decline.

Similarly, addition of the Y to AZ91D alloy extruded at 300 °C was found to suggestively enhance the alloy strength, especially when the Y content was 2 % (by weight), the alloy was found to exhibits the best mechanical properties. This enhancement effect was attributed to two reasons: first, the stress on the Mg-matrix can be effectively transmitted to the Al_2Y phase, thereby tends to increase the overall strength of alloy; second, the Al_2Y phase hinders the dislocations, prompting more dislocations to accumulate around it, thereby enhancing the dislocation strengthening effect [109]. In comparison with the AZ91 alloy, the Mg-12.55Al-3.33Zn-0.58Ca-1Nd alloy has a higher TS, reaching 481 MPa, however the elongation length was limited to 5 % only [110]. Upon analyzing the effect of Gd on the Mg-2Al-1Zn performance, it was discovered that the Mg-2Al-1Zn-4Gd alloy has excellent thermal stability, as shown by its greatest YS and TS at both room temperature and at an elevated temperature of 200 °C [152]. Yang et al. [153] used first principal investigations for studying the different alloys. As per the studies, although AM60Z, AM60B, AM50A, and AM20 MAs are known for their excellent fluidity and toughness at room temperature, together with their relatively low strength. RE elements like Ce and Y may be added to these alloys to make them stronger. In their study they have analyzed the effects of Ce on the Mg-5Al-0.3Mn alloy. The estimated results depict that the elongation is (8 %), YS (64 MPa), and TS (158 MPa) of the Mg-5Al-0.3Mn alloy devoid of Ce are all rather low. Nevertheless, the alloy's tensile characteristics are much enhanced as the Ce level increases. The alloy's TS, YS, and elongation achieve their maximum values at 1.5 % Ce, with enhancements of 28.5 %, 37.5 %, and 150 %, respectively. However, the tensile strength of the alloy starts to decrease as the Ce % keeps going up. Thus, Ce improves the mechanical characteristics of MAs till the optimum concentration, but too much of it is harmful. The $Al_{11}Ce_3$ phase is formed at the alloy's grain boundaries when Ce is added. This phase enhances the mechanical characteristics of the alloy by effectively preventing the movement of dislocations and the sliding of grain borders [154]. The mechanical characteristics of the Mg-5Al-0.3Mn-1.5Ce alloy are improved when Ce is added because it refines the β-$Mg_{17}Al_{12}$ phase and reduces its volume percentage. Elements Y, tends to increase the microhardness and tensile strength of Mg-6Al-0.3Mn-xY alloys (where x = 0, 0.3 %, 0.6 %, or 0.9 % by weight), according to studies [155]. Fig. 10b shows that the elongation increases from 11.8 % to 12.6 % as the Y content increases from 0 % to 0.9 % (by weight). Equally, Fig. 10c shows that the rolled alloy's TS and YS increase from 293 MPa and 221 MPa to 303 MPa and 255 MPa, respectively, along with the increase in elongation from 10.3 % to 17.1 %. As the Y content goes from 0 to 0.9 % (by weight), the as-cast alloy's TS and YS goes from 179 MPa and 56 MPa to 192 MPa and 62 MPa, respectively. The existence of the stable phase of Al_2Y with high-melting point of 1758 K is responsible for the alloy's improved microhardness and tensile characteristics. Al_2Y tends to improves the microhardness and tensile characteristics of the alloy by preventing dislocation movement and grain boundary sliding during hot rolling. As the degree of deformation rises, more pressure is required because the alloy's dislocation density increases during defor-

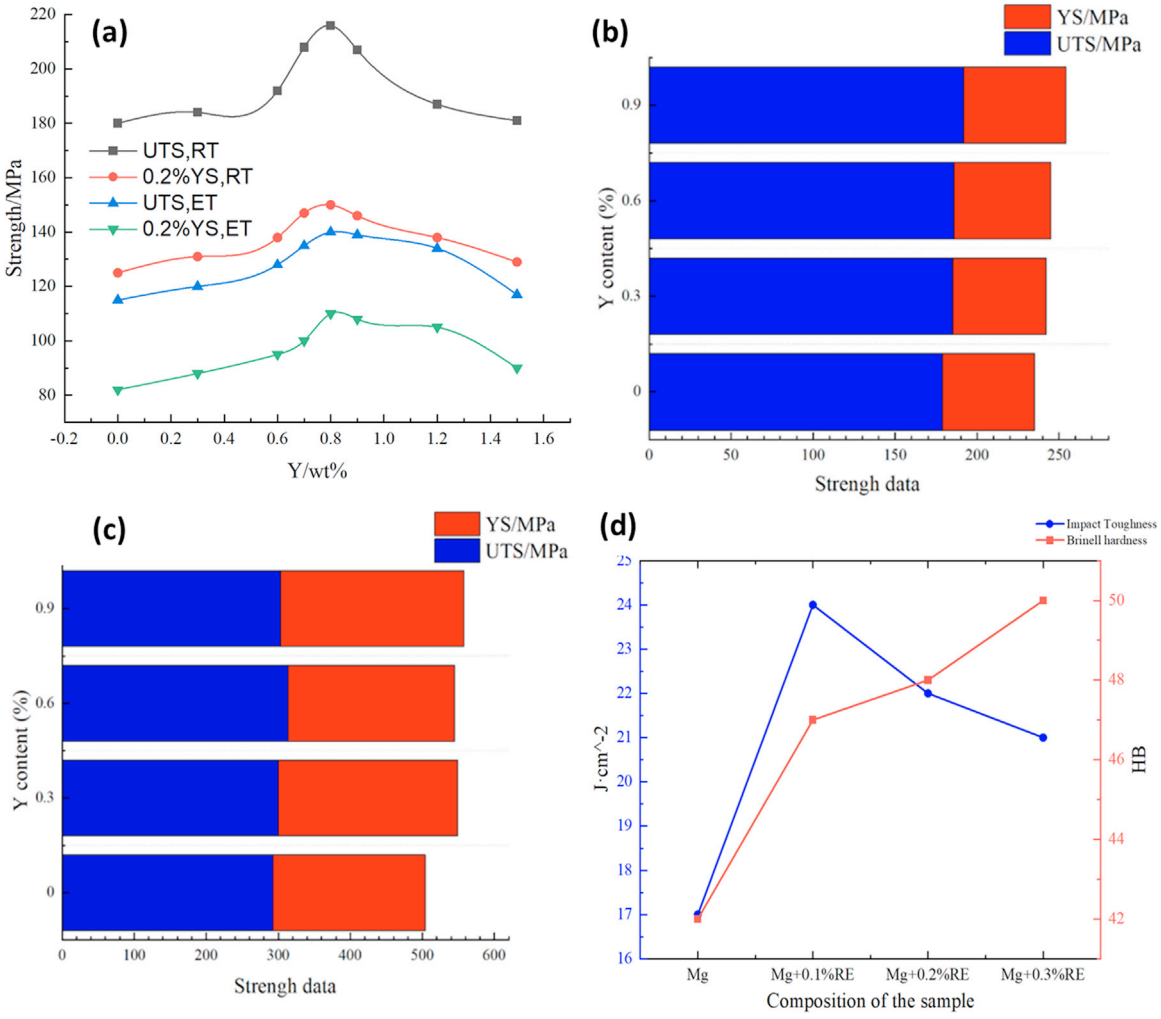

Fig. 10. (a) Effect of Y incorporation on the strength of AZ91 alloy (b) Tensile and yield strengths of cast alloys (c) Tensile and yield strengths of alloys in the rolled state (d) Mechanical properties of Mg-RE alloy. Reproduced with permission from Springer Nature [98].

mation, creating more obstruction between dislocations. The alloy's YS and other mechanical property indices gets further enhanced by the inclusion of the Y element and hot rolling treatment, which refine the grains. According to the findings, it is possible to efficiently improve the mechanical characteristics of metal materials by controlling the alloy composition and heat treatment techniques that would suit the needs of individual engineering applications [155]. Zhang et al. [156] has reported the impact on toughness and hardness of Mg-RE alloys with varying amounts of mixed RE elements by measuring their mechanical properties. The alterations to the alloys' microstructure were studied using metallographic microanalysis methods. Fig. 10d shows the experimental findings demonstrating that when the concentration of mixed RE elements rises, the impact toughness of Mg-RE alloys first increases and then eventually declines. At RE percentage of 0.1 %, the alloy reaches its maximum impact toughness of 24 J/cm^2, which is 41 % more than pure Mg. Similarly, the alloy's hardness rises from 42 HB to 50 HB, a 19 % increase, as the concentration of RE element increases.

Thus, the mechanical qualities of MAs, such as YS and TS, are greatly enhanced by including RE elements. This is because these elements are soluble in metals to a certain extent and tend to improve the mechanical characteristics of materials via processing steps, including grain refining, dispersion strengthening, solid solution strengthening, and ageing precipitation strengthening, and other properties. Table 5 lists the mechanical properties of some alloys containing Y along with their characteristics such as YS, TS, and elongation limits [103,104,106–108]. Y has been often added to MAs to enhance their mechanical characteristics. The tests were carried out under different temperatures and circumstances. The table lists alloys with varying amounts of Y and other elements like Sn, Gd, and Zn. The "Condition" column refers to the physical state of the alloy, such as "Extruded state," "Extrusion-T5," "Cast state," "ECAP." and "Rolled state," which reflect the manufacturing process and subsequent heat treatments that alloys have undergone. The "Temperature" column distinguishes between room temperature (25 °C) and high temperature (250 °C) testing conditions,

Table 5
Mechanical properties and strengthening mechanism of some Y-containing MAs.

Alloy	Condition	Temperature (°C)	YS/MPa	UTS/MPa	EL (%)
Mg-0.5Sn-0.3Y	Extruded state	25°C	141	288	30.3
Mg-0.5Sn-2Y	Extruded state	25°C	132	299	-
Mg-0.5Sn-2Y	Extruded state	250°C	110	213	-
Mg-0.5Sn-3.5Y	Extruded state	25°C	165	297	-
Mg-0.5Sn-3.5Y	Extruded state	250°C	151	223	-
Mg-14Gd-2Y-1Zn-0.5Mn	Extrusion-T5	25°C	448	520	3.5
Mg-14Gd-2Y-1Zn-0.5Mn	Extrusion-T5	250°C	322	344	18.8
Mg-2Y-3Gd-2Nd-0.5Zn-0.5Zr	Extrusion-T5	25°C	198	281.7	11.1
Mg-2Y-3Gd-2Nd-0.5Zn-0.5Zr	Extrusion-T5	250°C	171.6	216.7	16.1
Mg-4Gd-1Y-1Zn-0.5Ca-1Zr	Cast state	25°C	93.1	204.2	12.5
Mg-4Gd-3Y-1Zn-0.5Ca-1Zr	Cast state	25°C	104.6	212.6	10.1
Mg-4Gd-5Y-1Zn-0.5Ca-1Zr	Cast state	25°C	112.7	215.3	8.4
Mg-10Gd-0.2Zn-1Y-0.4Zr	Extrusion-T5	25°C	233	370	4.8
Mg-5Y	ECAP	25°C	273.9	306.4	23.9
Mg-9.8Y-6.6Ni	Extruded state	25°C	502	542	4.5
Mg-3.7Y-2.5Ni	Extruded state	25°C	390	415	9.2
Mg-6.7Y-4.3Ni	Extruded state	25°C	465	510	7.2
Mg-4Li-3Al-0.5Y	Extruded state	25°C	-	529	22.8
Mg-4Li-3Al-1.5Y	Extruded state	25°C	-	248	27.1
Mg-5Li-3Al-2Zn-0.8Sn-1.2Y	Cast state	25°C	166.2	228.6	14.8
Mg-8Li-1Al-0.6Y-0.6Ce	Rolled state	25°C	-	278.7	15.0
Mg-9Li-3Al-2Y	Extruded state	25°C	187	239	43.8

which are crucial to considerate the alloy's performance in different working environments.

A general trend of decreasing YS and ultimate TS is observed as the testing temperature increases from 25 °C to 250 °C, indicating a typical reduction in mechanical strength at elevated temperatures. However, certain alloys, such as Mg-14Gd-2Y-1Zn-0.5Mn, retain considerable strength at high temperatures, suggesting the presence of effective heat-resistant alloying elements and beneficial microstructural characteristics. The elongation varies meaningfully across different alloys, suggesting different levels of ductility which is a critical property for various applications were flexibility and toughness are required [157]. Alloys like Mg-9Li-3Al-3Sn-1Y exhibit exceptional ductility at room temperature (EL = 43.8 %), which could be advantageous for different applications. This study's evidence shows that Y and other elements affect the mechanical characteristics of MAs [158]. Solid-solution strengthening, grain refinement, and precipitation hardening are just a few of the strengthening mechanisms that might result from certain components and manufacturing procedures like extrusion and heat treatment. Metal alloys behave as expected at HTs, where thermal activation may cause atomic mobility to rise and deformation resistance to decrease. This explains why mechanical characteristics fluctuate with variation in temperature.

Thus, from the above discussion it is evident that the inclusion of mixed RE elements mainly causes the alloy matrix structure to be refined and secondary phases to be formed, which in turn increases impact toughness and hardness. On the other hand, if the alloy has too many secondary phases, its impact toughness can go down after an initial spike. This research lends strong credence to the idea that MAs characteristics may be optimally optimized.

5.3. High-temperature performance of MAs

Researchers have investigated a number of alloying procedures for improving the high-temperature performance of MAs, one of which is the incorporation of RE elements (Gd, Ce, etc.). The addition of RE elements to MAs tends to improves their high-temperature performance in a number of ways [133,159–161] such as:

a) Grain boundary strengthening:- Compounds formed by RE elements often form precipitate at grain boundaries, which effectively hinder grain boundary slip, thereby increasing the HT strength and plasticity of the material [113,162].
b) Grain refinement:- RE elements aid grain refining, increasing the material's YS and toughness [163–167].
c) Pinning effect:- Precipitated phases formed by RE elements can pin dislocations, preventing their movement, thereby maintaining the strength of the material at HTs.

Apart from that, the intermetallic compounds such as Al_2Gd and $Al_{11}RE_3$ are formed when RE react with Al in MAs. These compounds enhance the HT strength of MAs because their thermal stability is often better than that of other phases [134,168,169]. This stability allows the compounds to stay stable even when heated to very HTs. In addition, RE elements may strengthen the bond between the oxide layer and the alloy matrix, thereby preserving the oxide layer's integrity, decrease oxide shedding, and increase interface integrity. By preventing oxide development, RE element segregation at oxide grain boundaries tend to increase surface oxide particle production, decrease microcracks in the oxide film, and reduce the likelihood of oxide film peeling [170]. Wei et al. [171] have reported that adding an appro-

priate amount of Gd to the AZ81 MA results in the formation of Al_2Gd grain phase. These phases possess much higher thermochemical stability than the $MgAl_2$ phase and can maintain more strength at HTs. They tend to improve the mechanical properties of AZ81 at HTs by effectively inhibiting dislocation movement and grain boundary slip in these alloys. Similarly, Mahmudi et al. [172] have observed that the addition of RE element like Ce results in the formation of rod-like precipitates of $Al_{11}RE_3$ in the microstructure, as a result of which $Mg_{17}Al_{12}$ phase gradually decreases and becomes finer. Due to its higher melting point compared to the $Mg_{17}Al_{12}$ phase and its distribution at grain boundaries, the $Al_{11}RE_3$ precipitate improves the HT strength of the MA by preventing grain boundary slip at HTs. Thus, the MAs with RE elements added have a better chance of succeeding in HT applications due to improved performance by creating stable intermetallic compounds, strengthening of grain boundaries, refinement of grains, and the pinning effect.

5.4. Creep resistance of MAs

The use of RE elements in MAs is essential for augmenting the characteristics of these alloys. The high solubility of these elements in MAs enhances the microstructure, resulting in improved performance at both room temperature and HTs. As the temperature drops, the solubility of RE elements reduces considerably, allowing them to readily form precipitates during the ageing process of the alloy. This ultimately augments the strength of the alloy. It has been reported that incorporating small amount of Y into AM50 MA tends to successfully enhance the structural grains of the alloy and thereby greatly enhance its TS and YS at both room temperature and HT (150 °C). This development effectively increases the resistance of AM50 MAs to deformation under constant stress, known as creep resistance [173,174]. Akin to, the incorporation of RE elements like Y and Gd results in the development of short-range ordered structures that cause dislocation hardening and increase the alloy's creep resistance. This strengthening effect persists even at HTs. The Gd element in the Mg-18Gd alloy creates precipitates mostly of Mg_7Gd or Mg_5Gd, which greatly aid in the ageing hardening process because of their dense distribution [175]. The pre-aging treatment in the Mg-2.5Nd binary alloy produces huge, high-density precipitates that effectively impede dislocation movement and increase the alloy's creep resistance [176]. Zhuo et al. [177] has examined AZ61 alloy and found that the RE element Ce is present in it as Al_4Ce compound in blocky and rod-like shapes. The structural confirmation was observed while analyzing the effects of Ce on the microstructure and HT performance of Mg-Al alloys (like AZ61). The developed structural units apart from being insoluble in the alloy matrix, have high melting temperatures, with small amount getting separated at grain boundaries. Apart from that, Ce also tends to enhance the quality of Mg-Al alloys by smoothing out their matrix grains and decreasing the amount of β-$Mg_{17}Al_{12}$ phase in the alloy. β-$Mg_{17}Al_{12}$ phase is a primary factor affecting the HT performance of MAs alloys. This is because the β-phase has a low melting point (approximately 300 °C) and poor thermal stability. At lower temperatures, the β-phase is prone to discontinuous precipitation in the α-saturated solid solutions near grain boundaries where it grows and softens easily at HTs, leading to increased grain boundary diffusion and thereby weakening the resistance to grain boundary slip. Therefore, the addition of Ce suggestively improves the HT creep resistance of MAs alloys. It has been observed that in the cast based REMAs, steady-state creep rate initially increases and then decreases with change in grain size, indicating the presence of an optimal grain size range where the creep rate is the lowest. Both too small and too large grain sizes lead to increased creep rates. At 523 K, for the ZM6 alloy, as the grain size decreases, the EL, TS, and creep resistance are all improved. This is mainly because during creep, as the grain size reduces, the strain produced by grain boundary slip accounts for an increasing proportion of the total strain, thereby enhancing the overall EL and TS of the material [178,179]. Geng et al. [180] has reported that in the similar way Gd also results in the formation of precipitates mainly composed of Mg_7Gd or Mg_5Gd after being incorporated in MAs. These tightly packed precipitates exhibit noteworthy strengthening effects during aging. Li et al. [181] has reported the effect of Nd incorporation in the MAs. They have reported that after the pre-aging treatment the creep behavior of the Mg-2.5Nd binary alloy possess high-density of precipitates that effectively prevents dislocation movement, thereby increasing the alloy's resistance to creep deformation.

From the above discussion it has been observed that during creep deformation, the alloy's properties are affected by the complex interaction of grain size. Although the Hall-Petch formula suggests that the strength of a material is inversely proportional to grain size, at HTs. Grain boundary softening leads to high-density grain boundaries in small grains, which thereby affects the strength of material. Therefore, the impact of grain size on performance is not simple but plays an active role in both strengthening and softening effects.

5.5. Thermal conductivity of MAs

RE elements in MAs typically exist either in solid solutes or as intermetallic compounds. For solid solution REMA, Chen et al. [182] have experimentally measured the thermal conductivity of Mg-11Y-5Gd-2Zn-0.5Zr (mass fraction, %) alloy and found that by incorporating high content of RE elements, the thermal conductivity of the alloy decreases from 158 W/(m·K) for pure Mg to only about 23 W/(m·K). This phenomenon indicates that RE elements like Gd and Y greatly reduce the thermal conductivity of MAs. The decrease was found to occur because of their high solubility in Mg, with solubility limit of 4.53 % and 3.35 % (mole fraction), respectively [132]. The substitution of RE atoms for Mg atoms produces severe lattice distortion, disrupting the original lattice arrangement of the Mg matrix. This greatly obstructs the movement of electrons and phonons, which are scattering sources, thereby reducing their average free path which notably lowers the thermal conductivity of the MAs

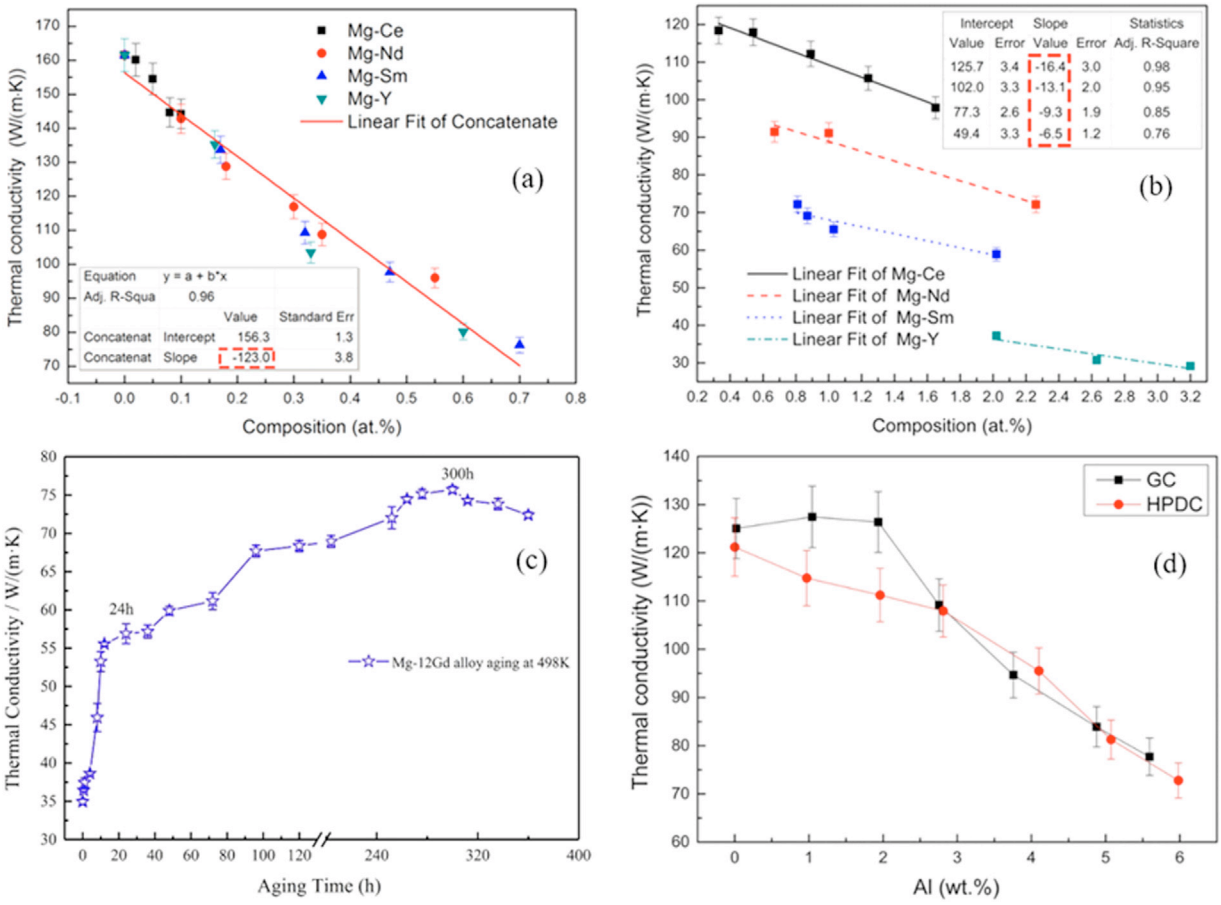

Fig. 11. Effect of RE elements on thermal conductivity: (a) SS state, (b) Intermetallic state, (c) Variation of thermal conductivity variation of solution Mg-12Gd alloy with aging time, and (d) Variation of thermal conductivity of Mg-4Ce-*x*Al-0.5Mn alloy with Al content increasing in GC and HPDC condition. Reproduced with permission from (a, b) Elsevier [184] (c) Elsevier [183] (d) Springer Nature [185].

[153,154]. The degree of lattice distortion in Mg strongly depends on the type of alloying element and increases with the element content. Zhong et al. [183] has reported the impact of Gd, Ce, Nd, and Y elements on the thermal conductivity of MAs and found that in addition to the solute atom content, the size difference of RE atoms, their valence, and the stability of sub-electron layers also affect the thermal conductivity (Fig. 11c) [159]. According to the Linde rule, the higher the valence of the solute atom, greater will be the thermal resistance of the alloy, with the thermal resistance increment proportional to the square of the valence of the solute atom. Additionally, rise in the number of empty orbitals in the valence electron layer of the solute atom makes it easier to capture conduction electrons, which reduces the concentration of free electrons in the alloy and thus lowering the thermal conductivity [133]. When RE elements tend to form the intermetallic compounds within MAs, the mismatch of their lattice constants with the Mg matrix lattice causes lattice distortion at the interface, serves as an effective center for electron and phonon scattering. In this way, it has been observed that as compared to solute atoms, intermetallic compounds have a relatively smaller impact on the thermal conductivity of the alloy.

Fig. 11a–b shows a statistical comparison of the thermal conductivity of MAs with RE elements presented as solid-solutes, and intermetallic compounds. It is evident that introducing 1.0 % (molar ratio) of RE elements into MAs can significantly affect the thermal conductivity characteristics. If the RE elements are present as solute atoms, the resulting decrease in thermal conductivity reach 123 W/(m·K); in contrast, when the RE elements are present as intermetallic compounds, the decrease in thermal conductivity is suggestively reduced, ranging only between 6.5 and 16.4 W/(m·K). Hence, optimizing the technique and composition that will directly led to the development of intermetallic compounds instead of solute RE elements in MAs is an excellent way to increase their thermal conductivity [184]. Su et al. [185] have analyzed the effects of adding different Al concentration on the thermal conductivity of the Mg-4Ce-*x*Al-0.5Mn (mass fraction, %) system alloys, and the observed variation is depicted in Fig. 11d. It has been observed that within the range of 0 to 2.0 % (mass fraction) of Al added, the thermal conductivity of the alloy remains stable, at the level of 126 W/(m·K). This has been attributed to the fact that the added Al elements mainly forms either of the Al_2Ce, $Al_{10}Ce_2Mn_7$, and $Al_{11}Ce_3$ phases. Interestingly, when the amount of Al

added is further increased, the excess Al element begins to dissolve in the alloy matrix, leading to a gradual decrease in thermal conductivity of the alloy. Furthermore, Yamasaki et al. [186] has reported that the transition metals incorporation in REMAs also tends to enhance the interaction in between the elements and the matrix that result in the generation of long-range ordered phases, which are advantageous for enhancing the alloy's thermal conductivity properties. From the above discussion, it is evident that REs as solid-solutes in MAs have less impact on their thermal conductivity behavior as compared to the ones resulting in the formation of intermetallic compounds. Thus, developing REMAs with high thermal conductivity, certain light RE elements like Ce and La will be ideal candidates because they are less soluble in Mg and are more likely to form intermetallic compounds.

6. Strengthening mechanisms of REMAs

The above discussion has clearly favored the fact that incorporation of the RE in the MAs remarkably led improvement in different characteristic features including their strengthening. There are different ways through which the incorporation of REs led to strengthening of MAs, some of the prominent ways are discussed below:

6.1. Solid solution strengthening

The process of strengthening involves adding solute elements to the metallic matrix of an alloy in order to increase its strength and hardness. The interaction of solute atoms with the dislocations disrupts the alloy lattice which is the key to this strengthening. Solute atoms having different atomic radii and elastic moduli from the matrix, tends to create local stress fields in the alloy that hinder the movement of dislocations, making slip more difficult and thereby strengthening the alloy [121,181,187,188].

According to the Hume-Rothey principle, the solubility of solute atoms in the solvent is affected by the difference in their atomic radius. When the atomic radius difference exceeds 15 %, the solubility is usually low; the solubility is higher when the difference is less than 15 %. A stronger solid solution is produced when there is a large disparity between the elastic modulus and valence electron number, as well as when the solubility of the solute atoms in the solvent is high. Since the atomic size of RE metals is similar to that of Mg, the atomic radius difference between most of RE metals and Mg atoms is within 15 %, which enables these metals to produce significant solid solution strengthening effects in MAs [122,189]. Liu et al. [179,190] have studied the solid solution strengthening effect of WE43 alloy. They have reported that the alloy acquired with fine grain strengthening and solid solution strengthening has substantially showed the improved mechanical properties. Zhang et al. [191] have observed that the incorporation of 1.5 % Sm. into the Mg-10Y alloy not only enhances the alloy matrix but also the $Mg_{24}Y_5$ phase in the alloy. These microstructural improvement results in enhancing the mechanical properties at Hats' He et al. [192] has analyzed the enhancement in the ductility through extrusion temperature and variation of atomic ratios in Mg-*y*Nd-*z*Zn-*x*Zr alloy microstructures. It has been observed that modification in the texture plays an important role in enhancing the strength and ductility of the alloy. The increment in ductility has been attributed to grain refinement. It is the solubility of RE elements in Mg that plays an important role in the enhancing the characteristic features MAs [193]. The maximum solid solution percentage of RE elements in Mg is given in Table 2.

The table lists the elements in ascending order of atomic number, providing the electron configuration for each. The eutectic temperature is the lowest temperature at which a mixture of substances will melt or solidify, and the maximum solid solution is the highest concentration at which the element will dissolve in Mg. Eutectic temperatures are included, indicating the temperature at which the solubility limit is determined. The data shows a general trend where certain RE elements have very low solubility in Mg (e.g., La, Ce, Pry, Nd), as indicated by their atomic percent values. Conversely, elements like Gd, Tb, Dy, and others toward the end of the series show pointedly higher solubility. The table also includes the electron configuration of each element, which can affect solubility due to the size and valency of the element.

Among all the RE elements, Y has a solid solution capability of the order of 3.35 % and a mid-range eutectic temperature of 565 °C. The eutectic temperature generally increases with the atomic number, except for Eu, which has a solubility of 0 %, indicating no solid solution formation with Mg. Lu shows the highest solubility capability of the order of 8.8 %, coupled with the highest eutectic temperature, suggesting a strong interaction with Mg. The fact that RE elements have different maximum solid solution percentages indicates that atomic size, electron configuration, and valency are major variables in deciding how well an element dissolves in Mg. The tabulated solubility and eutectic temperature values thus provide a basic insight into the design of REMAs. Materials scientists aiming to optimize alloy composition for enhancing qualities, including strength, ductility, and temperature resistance, will find these insights crucial.

When RE elements dissolve into the MA matrix, they enhance the interatomic binding force, cause lattice distortion, thereby slowing down the rate of atomic diffusion and hindering dislocation movement. This way they help in achieving strengthening of the alloy matrix and thereby improving their mechanical properties. Solid-solution strengthening effect of heavy RE elements is generally better as compared to that of light RE elements, but light RE element is more easily enriched at the solid-liquid interface, forming high-melting intermetallic phases. Therefore, the combination of light and heavy RE elements tends to achieve the optimal effect of RE elements. Furthermore, the impact of RE elements on MAs in solid-solution strengthening has shown that heavy RE elements substantially tend to strengthen the alloys.

6.2. Precipitation hardening

Precipitation hardening is a mechanism that enhances the YS of a material by forming fine precipitates within the alloy that hinder the movement of dislocations [194]. This is one of the most effective strengthening methods in MAs. As discussed, that RE elements possess high solubility in MAs, but as the temperature decreases their solubility considerably decreases [195,196]. For example, when the temperature drops to about 200 °C, the solubility of RE metals can decrease up to one-tenth of their maximum solubility. The decrease in solubility results in the development of stable precipitates inside the alloy. These precipitates effectively stop dislocations from moving, which increases the alloy's YS. The solubility limits and types of precipitate phases for some commonly used RE elements in MAs are shown Table 2 [197]. The size, number, morphology, and distribution of precipitates all play a crucial role in hardening of MAs. More the number of precipitates with smaller sizes, more dispersed distributions, resulting in better strengthening effects. The hardening impact is also affected by the orientation relationship among the precipitate phases and the matrix. The strongest strengthening effects are provided by coherent relationships [198–200].

The interaction between precipitate phases and slip dislocations enhances the YS of the alloy by reducing the occurrence of slip dislocations in the microstructure. Currently, there are two main mechanisms for precipitation hardening: the Orowan mechanism [201,202] and the Friedel mechanism [197,203]. The difference between these two mechanisms lies in the fact that in the primary mechanism, the secondary phase particles are treated as invariable mass points [204]. When dislocations encounter these mass points, they will move around them, and the movement is governed by the equation [201,205]:

$$\Delta\tau = \frac{Gb}{2\pi\lambda\sqrt{-\nu}} \ln\frac{d_p}{r_0}$$

Where: $\Delta\tau$ is the increased CRSS, G is the shear modulus of the matrix, b is the Burgers vector of dislocation slip, ν is Poisson's ratio, λ is the effective distance between secondary phase particles, d_p is the average diameter of the secondary phase particles, and r_0 is the length of the dislocation core. In Friedel mechanism the dislocations cut through secondary phase particles and move forward. The interaction mechanism between dislocations and secondary phase particles that cut through includes: modulus strengthening, interface strengthening, order strengthening, coherent strengthening, and stacking fault strengthening. The change in strength due to this interaction is represented by the Friedel relationship equation [197,203]:

$$\Delta\tau = \left(\frac{2}{b\sqrt{\Gamma}}\right)\left(\frac{1}{L_p}\right)\left(\frac{F}{2}\right)^{\frac{3}{2}}$$

Studies have shown that MAs can achieve very high precipitation hardening effects through appropriate selection of alloying elements and heat treatment processes. Jia et al. [194] reported that after the incorporation of alloying element in Mg-4Y-1.6Nd-1Sm-0.5Zr alloy. It was found to exhibit precipitation hardening due to the formation of excessive number of precipitates in its microstructure, which existed in the form of needles and particles. These microstructures being fine in size, were dispersed evenly, which thereby notably improved the mechanical properties of the alloy. Jiu et al. [206] has reported that due to the presence of microstructural Mg-RE phases in Mg-4Y-2Nd-1Gd-0.4Zr alloy, considerable precipitation hardening was observed after solution ageing. These precipitates greatly improved the alloy's mechanical characteristics since they were small, scattered, and varied in kind. Due to low diffusivity of RE metals and their precipitate phases in Mg, the MAs shows a strong thermal stability [207,208].

Thus to achieve the optimal precipitation hardening effect, the ideal alloying elements should possess the characteristics, that is: should have a high solubility in MAs and experience a rapid decrease in solubility as temperature decreases, enabling the formation of supersaturated solid solutes during solution treatment; they should have a slow diffusion rate in MAs to inhibit the formation of coarse precipitates during aging; the precipitated phases formed should contain high amount of Mg, which helps to precipitate more phases during aging and reduces the amount of alloying elements required. Apart from these, the precipitated phases should possess high melting point. Also, the number of precipitated phases can be increased through multicomponent alloying or the formation of various secondary phases containing multiple alloying elements.

6.3. Dispersion strengthening

Dispersion strengthening is an effective mechanism for enhancing the strength and heat resistance of metallic materials. Intermetallic compounds with high melting points and strong HT stability can be formed in MAs by adding alloying and trace metals [100,182,209–211]. Compounds with poor matrix solubility tend to be dispersed as microscopic particles either within or on the edges of grains. At HTs, these fine alloy phases can impede the sliding of grain boundaries through a pinning effect and simultaneously inhibit the movement of dislocations, thereby enhancing the mechanical properties of the matrix as well. Moreover, in REMAs some eutectic phases with high melting points and thermal mechanical stability are formed during solidification, which further increases the HT performance of these alloys. Plastic forming techniques can refine these eutectic phases by improving their shape, making them more evenly distributed in the matrix, thus achieving better reinforcement effects [184,212]. Compared to precipitation hardening, dispersion strengthened alloys have particles with higher melting points and characteristics of being insoluble in the matrix, thus exhibiting better thermodynamic stability. At room temperature, both precipitated phases and dispersed particles hinder dislocation slip, thereby strengthening the alloy. Still, at HTs, precipitated phases tend to become coarse and lose their strengthening effect, causing material softening. However, the uniformly distributed fine particles can still effectively impede dislocation movement, maintaining the HT mechanical properties of the alloy. To ensure

that such alloys maintain structural and performance stability at HTs, it is important that the interface bond between the particles and the metallic matrix is strong. If the interface bond is poor, the bond between the matrix and particles may crack during plastic deformation, thereby weakening the overall toughness of the alloy. Therefore, while developing and manufacturing this dispersion strengthened alloys, it is necessary to comprehensively consider the alloy formulation, heat treatment steps, and forming processes for achieving the excellent overall performance.

6.4. Grain refinement

Grain refining is a process that decreases the grain size of metal MAs, which improves their mechanical properties [213]. Incorporating this strengthening process into MAs greatly enhances their properties. Some of the benefits of MA grain refining are as follows:

- ❖ The solubility of RE element such as Ce, Y, Sc in α-Mg determines the amount of RE needed to refine the grains in MAs. Materials' strength and flexibility gets improved by adding RE elements, which in turn notably reduce grain size. Solute segregation and nucleation site provision are the primary mechanisms that accomplish this. Because of solute segregation, the alloy composition is supercooled, and the RE elements that are rich at the solid-liquid interface can prevent dendrite growth, which in turn prevents grain growth [167].
- ❖ The addition of RE elements provides new nucleation sites, thereby promoting the formation of fine equiaxed grains.
- ❖ An enormous number of Mg-RE phases on the grain boundaries further control grain growth, not only by limiting the growth of grains at the source but also making already grown grains smaller. This dual strategy notably improves the performance of MAs.

In particular, different research studies have concluded that the RE element Gd greatly improve the grain refinement of ZK MAs by converting the $MgZn_2$ phase into uniformly fine granular particles [214]. Many studies have tested the effects of different Gd contents on alloy microstructure, hardness, and room temperature tensile mechanical properties. When the Gd content is 1.6%, the alloy performance reaches its optimal level. It has been reported that with the increase in Gd content, as-cast microstructure of the alloy grains gets refined, and the Mg-Zn-Gd phase at the grain boundaries gradually increases, forming a continuous network-like distribution; the hardness value first increases significantly, then gradually decreases, and then increases again. But, at the room temperature tensile mechanical properties remains relatively unchanged [215–217]. Pucun et al. [100] has reported that the addition of Nd element in Mg-12.55Al-3.33Zn-0.58Ca alloy has notably improved its microstructure by transforming them into fine equiaxed grains with a maximum grain size not exceeding 5 μm. Apart from that, the incorporation of Nd has efficiently enhanced the YS and TS of the alloy. The effect of

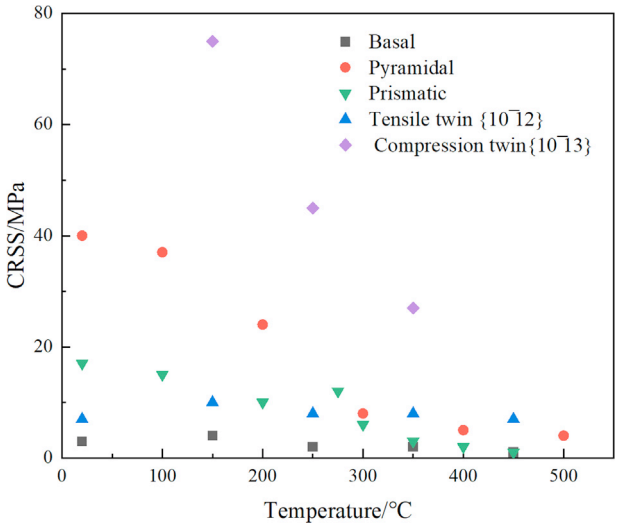

Fig. 12. Critical shear stress (CRSS) for basal and non-basal slip of magnesium at different temperatures. Reproduced with permission from Elsevier [132].

Zr on refining the different properties of MAs has also been explored. Su et al. [184] have studied the refining effects of dissolved or undissolved Zr elements in the Mg-Nd-Zn-Zr alloy. It has been observed that Zr in both the cases tends to refine the grains. However, Zr being costly as compared to Al, thus preferential effect of Al on Mg-RE alloys has been studied mostly. Liu et al. [210] has analyzed the effect of Al on the Mg-RE alloy and have observed that incorporation of Al tends to reduce the solute content in the α-Mg melt, thereby resulting in a lower grain growth restriction factor (Q value).

Thus, grain refinement plays a crucial function in MAs, as depicted by these experimental results. To top it all off, some elements can refine grains by acting as heterogeneous nucleation sites. The metallurgical quality and mechanical qualities of the original castings are greatly enhanced through grain refining, which not only reduces grain size but also alters the type, shape, and distribution of secondary-phase particles.

7. Deformation mechanism of REMAs

7.1. Slip systems in REMAs

In pure Mg with hcp crystal structure, the main slip system at room temperature is the basal slip, but due to presence of only two independent slip-systems in the basal slip system it does not meet the Von-Mises yield criterion, so five independent slip systems are needed to achieve uniform plastic deformation of polycrystalline materials. The CRSS values corresponding to the basal and non-basal slips for Mg along with the twinning at 1% plastic strain at varying temperatures are depicted in Fig. 12 [133,134]. A system with only basal slip is considered to be the simplest possible system. Lower CRSS value in the basal slip system makes it most active for deformation process at HTs (over 300 °C). The strain hardening effects of the prismatic and secondary pyramidal slip

systems are found to be modest within this temperature range. It is more challenging to activate the non-basal slip system during deformation because it requires a substantially greater CRSS as compared to the basal slip system.

However, since the basal <a> slip system can only accommodate strain along the basal plane and cannot achieve deformation along the c-axis, this results in significant anisotropy in the material's deformation behavior. Such anisotropy further limits the plastic deformation capacity of MAs. Prism and pyramidal slips, which are not part of the basic slip system, become active when RE elements are added, mostly because of their unique valence electron shell structure. In order to enhance the plastic deformation capacity and formability of MAs, mainly at ambient temperature, where substrate slip is insufficient, this activation is crucial. Liu et al. [169] has conducted an in-depth study on pure Mg and MAs containing 0.8 % Y (mass fraction), exploring their texture and mechanical properties. It has been observed that the addition of a trace amount of Y to MAs remarkably reduce the texture strength by 18.2 %, as compared to 13.3 % in pure Mg, thus, result in a random distribution of textures. Furthermore, when containing 0.8 % Y (mass fraction), the MAs were found to exhibit an almost 20 % increase in EL, whereas the EL of pure Mg was less than 5 %. This suggests that the incorporation of Y significantly increases the plastic deformation capability of MAs. Panda et al. [218] has experimentally investigated the texture and mechanical performance of rolled pure Mg and MAs containing 0.2 % Ce (mass fraction). They have reported that the addition of a trace amount of light Ce greatly reduced the texture strength of the MAs by roughly 4.7 %. Meanwhile, the formability of the MAs was greatly improved. This change was attributed to the activation of multiple non-basal slip systems during deformation due to the presence of Ce, thereby promoting uniform plastic deformation of the material. Similarly, it has been reported by Wu et al. [134] that MA with 3 % Y (mass fraction) exhibits an excellent plastic deformation capabilities. The enhancement was attributed to the fact that during the deformation process, a multiple number of <a+c> dislocations on the cone surfaces are activated, which contributes to the uniformity of deformation. Furthermore, the addition of Y tends to affects the SFE on various slip planes. The variation in SFE results in changing the activation resistance of slip systems and thereby encouraging non-basal dislocations to become more active. The deformation process of Mg-Y alloys was examined by Li et al. [154] using the crystal plasticity finite element method. They observed that the material's plasticity was greatly improved due to the broad activation of the prismatic slip and primary cone slip systems. The light RE element, that is Ce plays an important role in weakening the texture of MAs. In addition to this, RE elements also have a significant impact on the ease of activation of slip systems i.e., CRSS and the regulation of slip mechanisms during deformation. Jang et al. [219] has employed the molecular dynamics simulations to explore the effect of varying Y content on the stress-strain relationship and CRSS of Mg-Y alloys. Fig. 13 depicts the CRSS ratios for different slip systems in MAs containing 1 % Y as follows: prismatic slip system ($CRSS_{pri}$): basal slip system ($CRSS_{basal}$): non-basal pyramidal <a+c> slip system ($CRSS_{pyrII<a+c>}$) = 1.1:1.0:1.8. When the Y content increases to 3 %, the CRSS ratio gets decreased to 1.1:0.8:1.0, notably lower than that of pure Mg (22:1:276). This finding reveals that the incorporation of Y not only enhances the CRSS of different slip systems in the alloy but also reduces the ratio differences between different slip systems, promoting the activation and initiation of non-basal slip systems during plastic deformation. Subsequently, using 3D X-ray diffraction technology, Wang et al. [161] has studied the deformation mechanisms and CRSS of slip systems in MAs enriched with 3 % and 5 % of Y. The studies have revealed that in MAs with 3 % Y content, the non-basal to basal slip CRSS ratio was $CRSS_{pri}$: $CRSS_{basal}$:$CRSS_{pyrII<a+c>}$= 3.0:1.0:3.2. But, for MAs with 5 % Y content, the $CRSS_{prism}/CRSS_{basal}$ and $CRSS_{pyr<a>}/CRSS_{basal}$ ratios were nearly 1.8–2.7 and 1.6–1.8, respectively. This finding emphasizes the effectiveness of Y element in reducing the CRSS ratio among non-basal and basal slip systems, thereby enhancing the material's ability for uniform plastic deformation.

RE elements not only adjust the slip system CRSS ratios but also promote dislocation cross-slip, expanding the pathways for dislocation movement, thereby improving the plastic deformation capability of MAs. Sandlöbes et al. [133] has observed through TEM that the addition of RE element Y facilitate cross-slip of <c+a> dislocations between primary and secondary pyramidal planes. Nitol et al. [220] has utilized density functional theory (DFT) for evaluating the effect of different alloying elements on the cross-slip energy barriers between primary and secondary pyramidal planes, and the comparative results are depicted in Fig. 14a. Among the diifferent RE elements Y, Ce, Er, Gd, and Nd has notably reduced the cross-slip energy barriers, thereby effectively promoting the cross-slip of <c+a> dislocations and improving the material's plastic deformation capability. Using the first principle calculations, Liu et al. [221] has obtained the electronic work function of the Mg matrix after the incorporation of different solute atoms and predicted the basal-prismatic cross-slip capability of the alloys. Fig. 14b illustrates the relationship between the basal-prismatic cross-slip softening ratio and the electronic work function after the incorporation of alloying elements.

Alloying elements with larger ratios, located in the upper left region of the figure, notably reduce the stress required for basal-prismatic cross-slip. This area is mostly composed of RE elements, as can be seen in the graphic. The RE element La promotes basal-prismatic cross-slip more than any of the others.

Deng et al. [222] has subjected Mg-8Gd-4Y-Zn MAs sheets to rolling treatment. The results indicate that simple rolling twins are not sufficient to fully promote plastic deformation in the alloy. Instead, the main function of twins is to provide the Mg matrix with crystal orientations favorable for slip. Also, it has been observed that the CRSS required to activate non-basal slip system is lowered due to incorporation of RE element. The alloy's propensity to

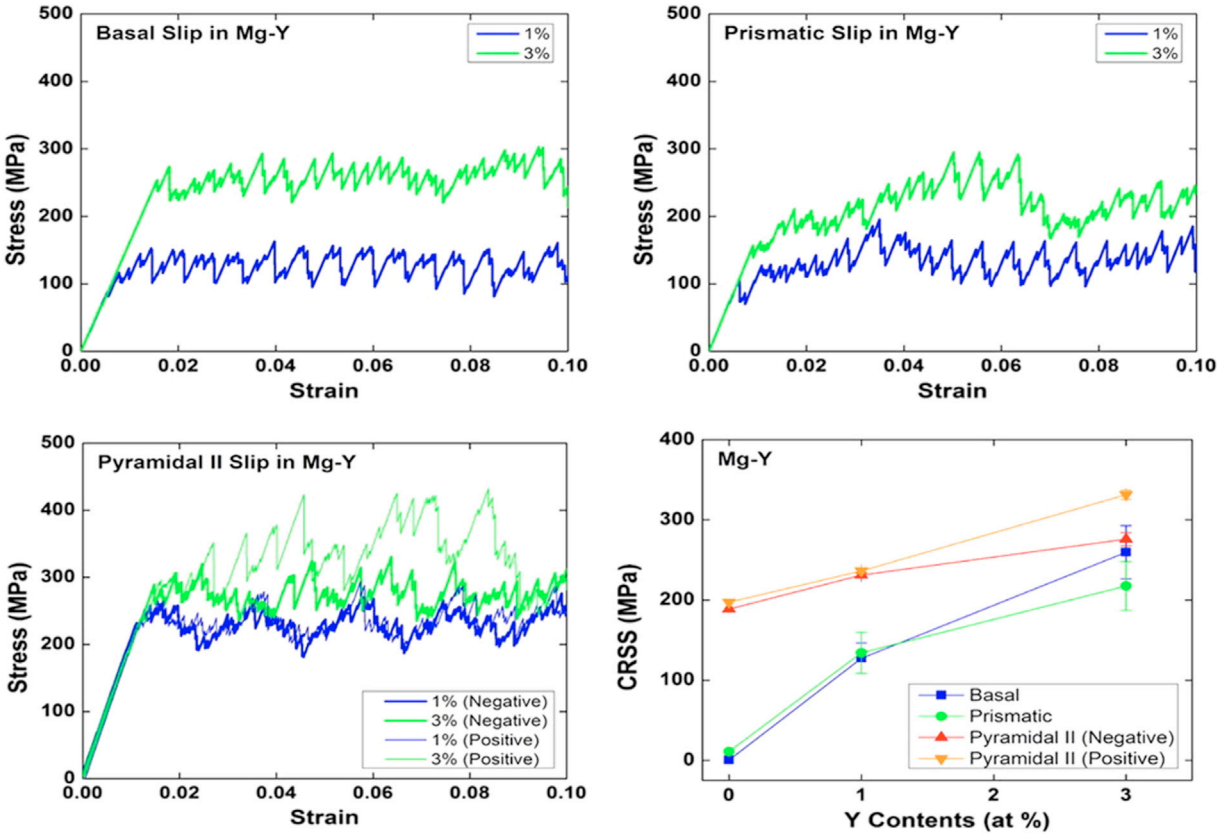

Fig. 13. (a-c) Simulated stress−strain curves \and (d) CRSS of Mg-Y alloys on basal, prismatic, and pyramidal II planes, at 0 K. Reproduced with permission from Elsevier [155].

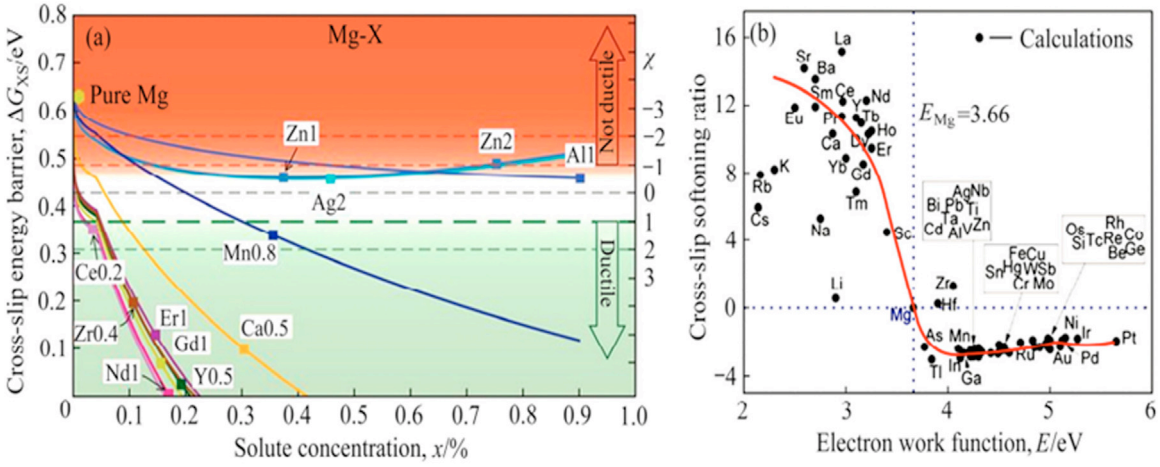

Fig. 14. (a) Predicted pyramidal II–I cross-slip activation energy barrier for binary magnesium alloys as a function of solute concentration c for the same solutes, taking into account solute variations and ductility index c. When c > 1, the ductility conditions are good. At extremely low concentrations, RE solutes obtain c > 1; Mn is somewhat effective, while Zr and Ca are also quite efficient. Nearly similar Zn and Ag do not attain ideal conditions for ductility because their c < 0. Reproduced with permission from Science [134]. (b) Effect of different alloying elements on the cross-slip energy barriers of primary and secondary cones. Reproduced with permission from Elsevier [169].

fracture during rolling was lessened by the non-basal slip activation, which efficiently coordinated strain along the c-axis. For investigating the plastic and facture mechanism REMAs sheets were synthesized via cross rolling method. While comparing the fracture mechanism and plastic deformation for conventional and cross rolling's it has been found that the later has a significant effect on slip activations with small Schmid factor. It was found that the MAs developed via cross-rolling possess both basal and non-basal slips as it tends to reduce the CRSS of non-basal slip. Fig. 15 illustrates how non-basal slip systems are activated [170].

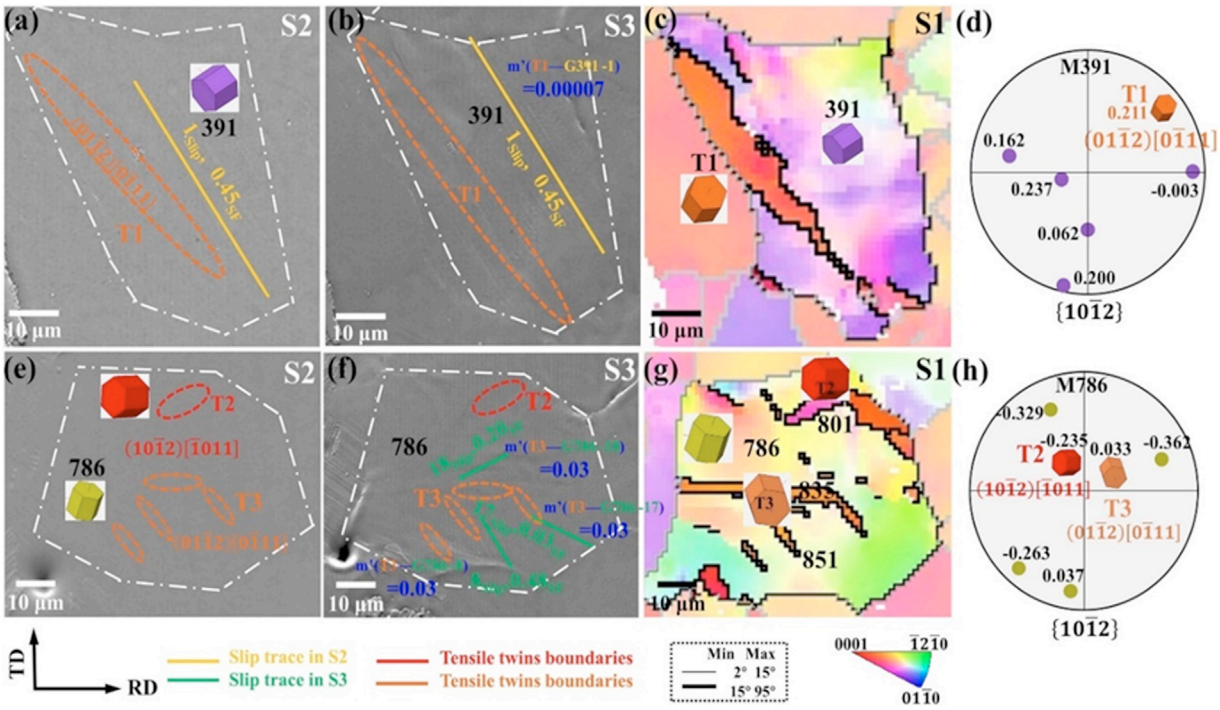

Fig. 15. Processes by which slip systems close to tensile twins are activated in conventionally rolled sheets: (a, b, e, f) SEM images; (c, g) IPF map of the selected area in S1; (d, h) [101–1] pole figures of the selected grains. Reproduced with permission from Elsevier [170].

7.2. Recrystallization behavior in REMAs

Recrystallization is a key to microstructural change during the plastic deformation of metallic materials, encompassing both dynamic and static recrystallization. For traditional Mg-Zn and Mg-Al alloy systems, the influence of dynamic recrystallization (DRX) on texture after hot deformation is typically not pronounced [167]. Studies have shown that even when numerous fine equiaxed grains are generated during deformation, these grains tend to maintain the same orientation as the original parent grains, leading to the formation of a pronounced deformation texture in subsequent deformation [223]. The scenario, however, alters the structure of REMAs. Hantzsche et al. [163] has also studies the deformation mechanism of MAs. They have found that during the deformation process, RE elements facilitated the appearance of secondary and compression twins and thereby serve as nucleation sites for recrystallization, thus weakening the texture, as illustrated in Fig. 16.

7.2.1. Static Recrystallization

MAs undergo a dramatic transformation in texture upon doping with RE elements like Gd and Nd. The correct concentration of RE elements added to AZ80 MAs improves the material's isotropy by weakening the basal texture and thereby encourages the creation of non-basal textures [224]. In case of Mg-Al alloys, RE element when added during casting of a material causes the dendritic structure to vanish and the lamellar $Mg_{17}Al_{12}$ phase composition at grain boundaries to increase. After homogenization treatment, the grain size is notably reduced. Predominantly when 2% of RE elements (Gd, Nd) are added, the precipitated phases not only hinder the growth of recrystallized grains but also contribute to fine-grain strengthening through the particle-stimulated nucleation mechanism, which remarkably improves the alloy's YS [37]. During the annealing process of MAs, grain boundaries, twins, shear bands, and secondary-phase particles al provide nucleation sites for recrystallization. Therefore, nucleation sites, stored energy, and the migration ability of grain boundaries are key factors affecting static recrystallization. Recrystallized grains with noticeable orientation differences may occur as a result of the increased lattice distortion energy brought about by adding RE components, which in turn facilitate static recovery.

7.2.2. Dynamic recrystallization

DRX plays a crucial role in the microstructural changes of REMAs, especially when they undergo HT processing. The alloy's mechanical properties are greatly influenced by its impact on grain refinement, texture alteration, and interaction with other microstructural features. During the DRX process in MAs, RE elements act as nucleating agents which facilitates the initiation of DRX [225,226]. RE elements, due to their high melting points and chemical stability, remain stable at grain or sub-grain boundaries during the thermal processing of the alloy, thus providing the necessary initial sites for recrystallization. For instance, the addition of a certain number of RE elements can lower the starting temperature and the critical strain required for DRX of the alloy, allowing it to occur at lower temperatures and smaller strains. MAs with RE

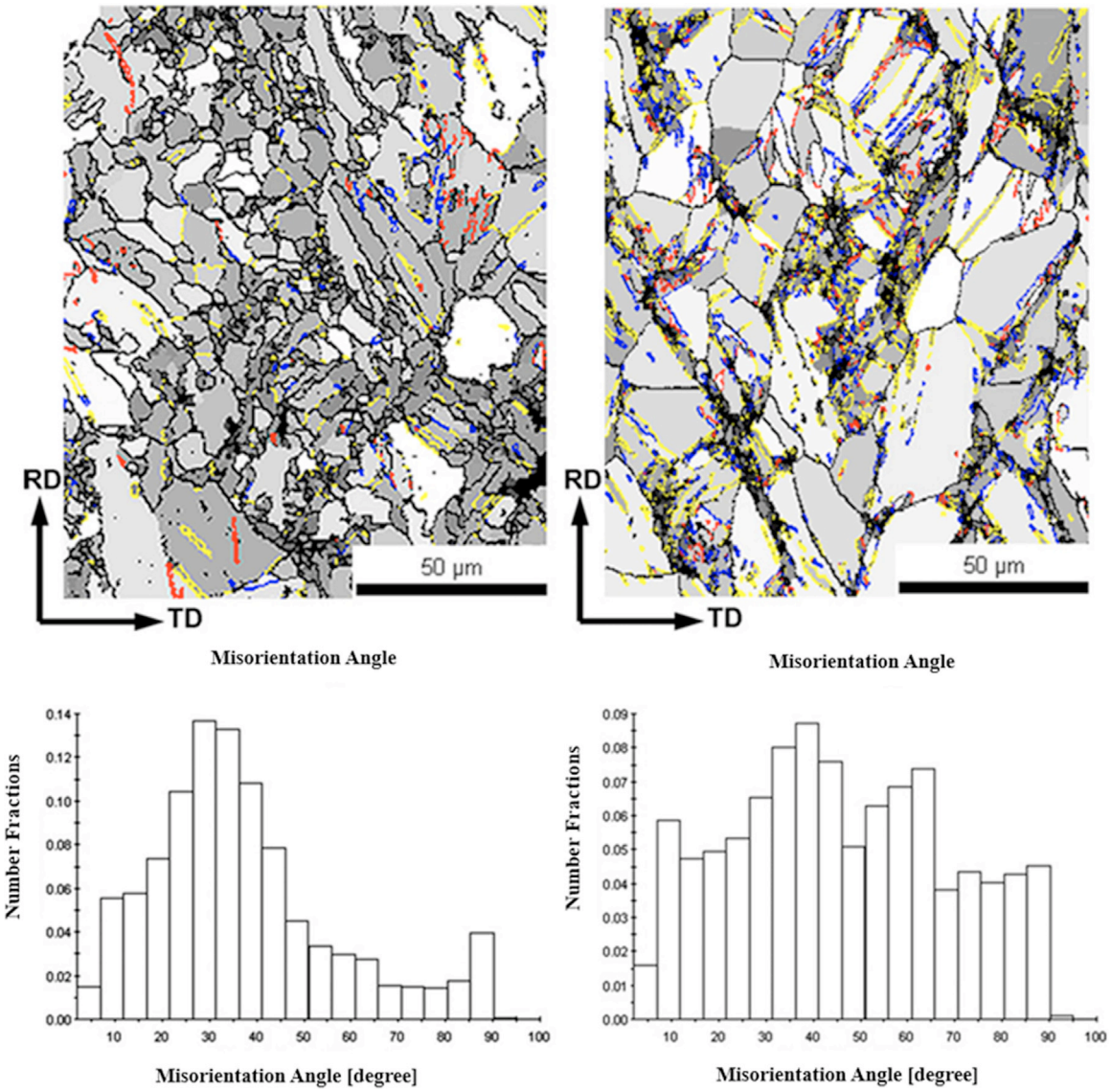

Fig. 16. EBSD antipodal plots (red: [10–12] stretching twins, blue: [10–13] compression Li crystals, yellow: [10–11]/[10–12] and [10–13]/[10–12] twin crystals) and neighboring orientation difference plots: (a), (c) MgNd0.01; (b), (d)MgNd0.04203. Reproduced with permission from Elsevier [163].

elements have better isotropy and deformation ability because of unique ""RE-texture," which is distinct from the conventional basal texture. Furthermore, the incorporation of these elements affects the selection of recrystallization nucleation sites, tending to occur on specific crystal planes and orientations, thereby adjusting the type and strength of the texture [227,228]. Reducing residual stresses, refining the microstructure, and improving the alloy's mechanical characteristics are all goals of DRX. The behavior of RE elements during DRX is of great importance in the superplastic deformation process of MAs [229–231]. Under certain strain rate and temperature conditions, DRX initially refine the coarse-grained REMAs, thereby enhancing their super-plasticity. Simultaneously, the enhanced super-plasticity is a result of the quick diffusion channels provided by the numerous high-angle grain boundaries that are formed during DRX. Zhang et al. [225] has reported that the incorporation of the RE elements like Ce, Y tends to reduce the intensity of the basal texture in AZ321 sheet materials. They also enhance the nucleation directions for DRX in grains, thus boosting the performance of REMAs. Li et al. [226] have analyzed that the incorporation of Ce in the Mg-Al-Zn alloys promotes the formation of numerous small-sized DRX grains during deformation, which greatly improves the alloy's plastic deformation capabilities.

Stanford et al. [227] has observed that the grains formed during DRX exhibit a clear regularity in their crystallographic orientations, tending to grow and align in directions similar to the original deformed grains. In the 0001-pole shown in Fig. 17, the orientations of the DRX grains are roughly centered around those of the original deformed grains. This phenomenon has been observed consistently in several samples which is in agreement with earlier observation on the textural behavior of conventional MAs like AZ31 and REMAs during deformation.

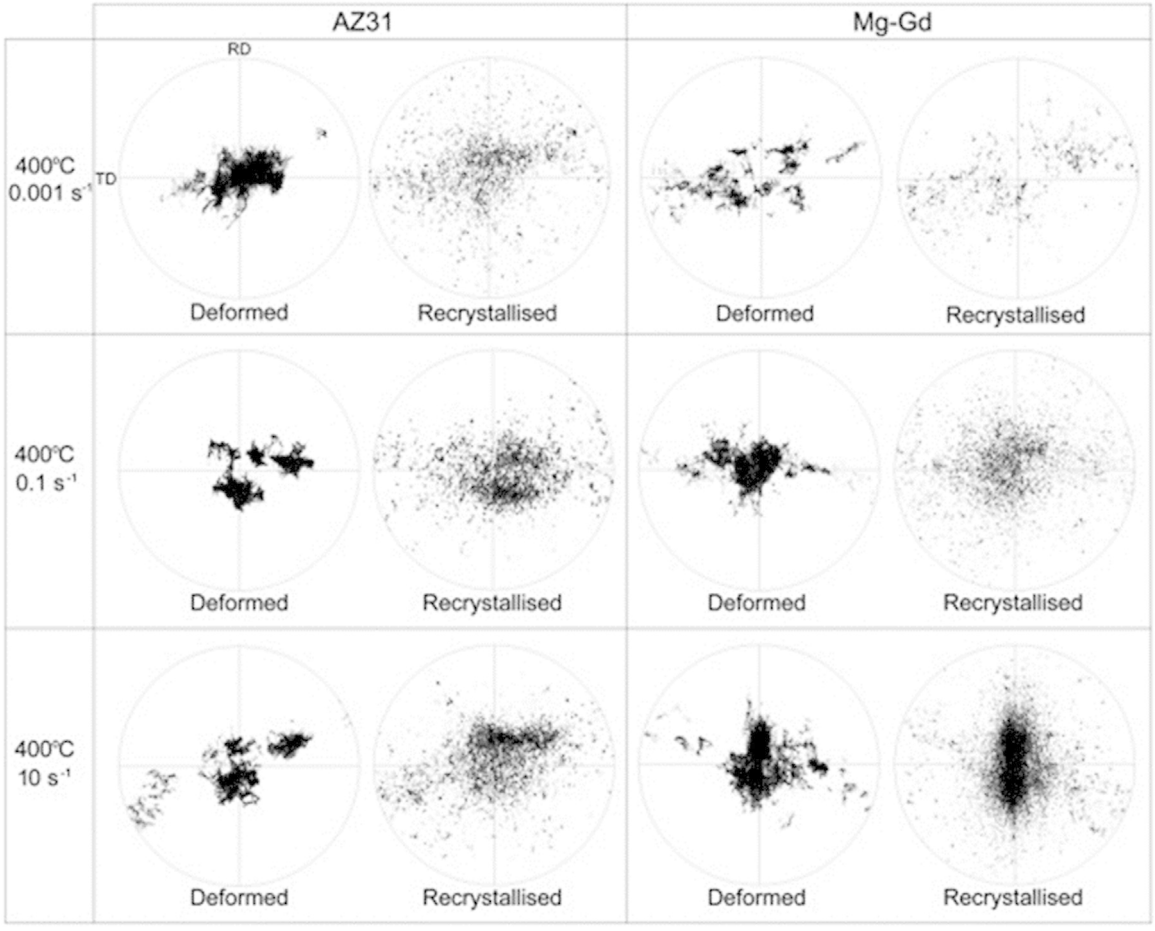

Fig. 17. As-deformed and dynamically recrystallized textures, for materials deformed at 400 °C long with the strain rates were assessed using EBSD. Each distorted and recrystallized section of the textures is represented by a 0001-pole figure. Reproduced with permission from Elsevier [227].

These investigations suggest that plastic deformation leads to the development of a distinct crystal orientation distribution in the alloy. As a result, DRX grains arise with comparable orientation features. This similarity reflects the stability of crystal orientations during recrystallization as well as the combined action of deformation and recrystallization mechanisms. Furthermore, it has been found that DRX typically occurs through two primary mechanisms: continuous DRX (cDRX) and discontinuous DRX (dDRX). It involves the gradual evolution of sub-grains within deformed grains, resulting in the development of new grains with low dislocation density. On the other hand, dDRX is characterized by nucleation and growth of new strain-free grains at the expense of the deformed matrix. The presence of RE elements affects the activation energy of DRX and the relative advantage of cDRX or dDRX mechanisms. DRX plays a crucial role in refining the grain size of REMAs. Compared to the original deformed grains, the new grains formed during DRX are typically smaller and more equiaxed. According to the Hall-Petch relationship, the refinement of grain size directly contributes to the improvement of the alloy's YS and hardness. Additionally, the uniform grain size distribution achieved via DRX enhances the overall toughness and mechanical property uniformity of the alloy. DRX also leads to noteworthy changes in the texture of REMAs. During thermal deformation, the development of DRX can disrupt the strong basal texture typically associated with MAs, resulting in a more random texture. This modification of texture is beneficial for improving the ductility and isotropy of mechanical properties, as it allows for more uniform deformation behavior under multi-axial loading. The interaction of DRX with other microstructural features, such as LPSO phases, precipitates, and existing dislocations, is crucial for determining the total performance of the alloy. For instance, the presence of LPSO phases can hinder grain growth during DRX, resulting in a finer and more stable grain structure. Comprehending and managing the DRX process is crucial for maximizing the efficiency of REMAs, enabling their use in high-performance sectors that demand materials with outstanding strength, malleability, and resistance to heat.

7.3. Texture properties of REMAs

The MAs undergo changes in their crystal structure and textural development upon addition of RE elements. The mechanical qualities of a material get greatly affected by its texture, which relies on the arrangement of grains. From the different studies it has been observed that RE elements gets

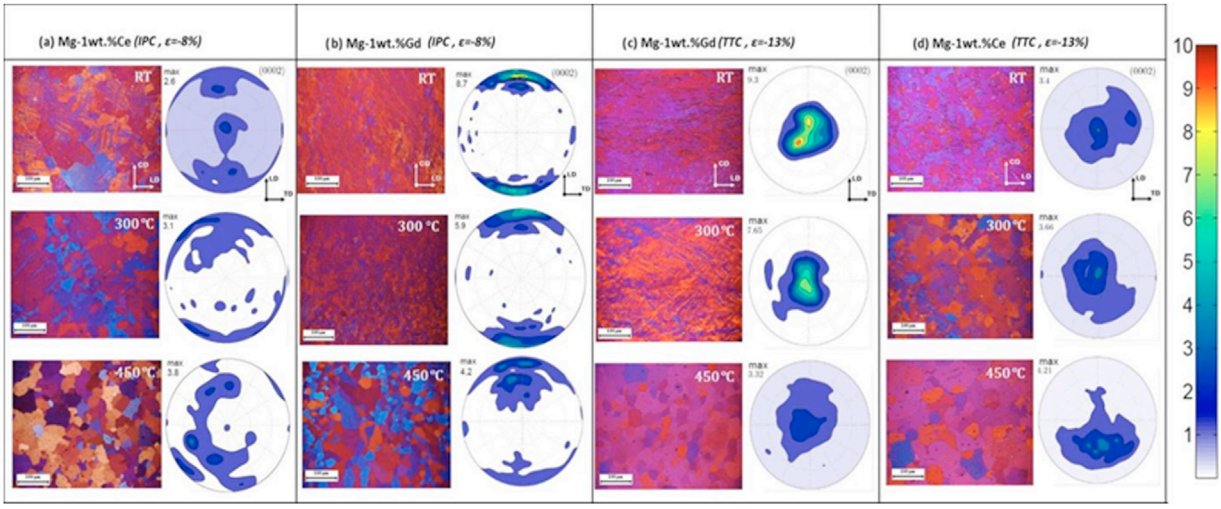

Fig. 18. Block weave and microstructure of Mg-1Ce in IPC (a), Mg-1Gd in IPC (b), Mg-1Gd in TTC and (d) Mg-1Ce in TTC. Reproduced with permission from Elsevier [232].

dilute in Mg matrix, and thereby affects the MAs textures [228].

The effects of RE elements are mainly manifested in three aspects: adjusting SFE, fixing grain boundaries, and changing the axis ratio (c/a). SFE affects the generation and propagation of dislocations within the crystal. In MAs, a lower SFE leads to wider dislocations, making it difficult for partial dislocations to aggregate into full dislocations. Therefore, reducing the basal SFE decreases the likelihood of basal cross-slip, while increasing the likelihood of pyramidal cross-slip. To illustrate the point, MAs can have their flexibility increased by adding RE metals like Y, which decreases the activation energy for basal external shear modes and increases the activity of pyramidal dislocations. Further it is well-known that when MAs undergo recrystallization, their crystal structure changes, which thereby has a direct effect on the deformation texture. Typically, MAs develop a strong basal texture after recrystallization, but certain compositions of MAs can develop a weak basal texture or even eliminate the basal texture completely, forming non-basal textures under specific conditions. This change is closely related to the added elements, especially RE elements. RE elements are considered to be important in regulating the recrystallization texture of MAs, with this specific recrystallization texture previously referred to as the "RE-texture."

In the same line, recent studies have found that different types of RE elements and their concentrations notably influence the formation of recrystallization textures. Fig. 18 shows that block weave and microstructure of REMAs containing RE elements Ce, and Gd. These components promote the creation of various recrystallization patterns. Different RE elements produce significantly different types of textures in MAs under the same external conditions [232]. According to studies reported by Hantzsche et al. [163] alloy deformation texture can be effectively reduced during annealing by adding elements like Y, Nd, and Ce. Furthermore, the addition of Gd and Dy elements not only reduces the basal texture but also promotes the formation of annular non-basal textures when the annealing temperature is increased, demonstrating excellent texture control capabilities [233]. Thus, the recrystallization texture in binary REMAs is directly related to the type of RE element chosen. It can be inferred that by precisely controlling the type of RE element added, the recrystallization process of MAs can be effectively manipulated, and their texture characteristics can be optimized. Moreover, lower diffusivity of RE elements causes them to accumulate near grain boundaries and dislocations, thereby impeding dislocation movement and inducing solute drag effects. This mechanism hinders the activation of basal slip mechanisms, increasing the CRSS required for basal slip. This in turn weakens the texture and enhances the plastic forming performance of the material [132]. Sandlöbes et al. [234] have experimentally proven that when Y is added to Mg to form Mg-Y alloys, it aids in activating non-basal shear deformation modes, thereby substantially reducing the I1 type SFE. This change makes the slip of <c+a> dislocations more active, introducing an additional pyramidal slip mechanism into Mg-Y alloys, ultimately improving the plasticity of Mg alloys. In summary, the addition of Y enhances the plasticity of Mg alloys because Y promotes different types of dislocation slip within the alloy, thus increasing the deformation capacity of the material.

RE elements, due to their high solubility in Mg, promote the formation of nanoscale precipitates during deformation, which hinder dislocation motion [107,241–243]. Additionally, RE additions reduce the axial ratio of Mg alloys, facilitating the activation of non-basal slip systems. This axial ratio reduction alters deformation modes and recrystallization behavior, leading to texture weakening and improved plasticity.

8. Applications of REMAs

REMAs are the most wonderful materials governed by different mechanisms. Owing to their special characteristic features they are being used in different technological domains

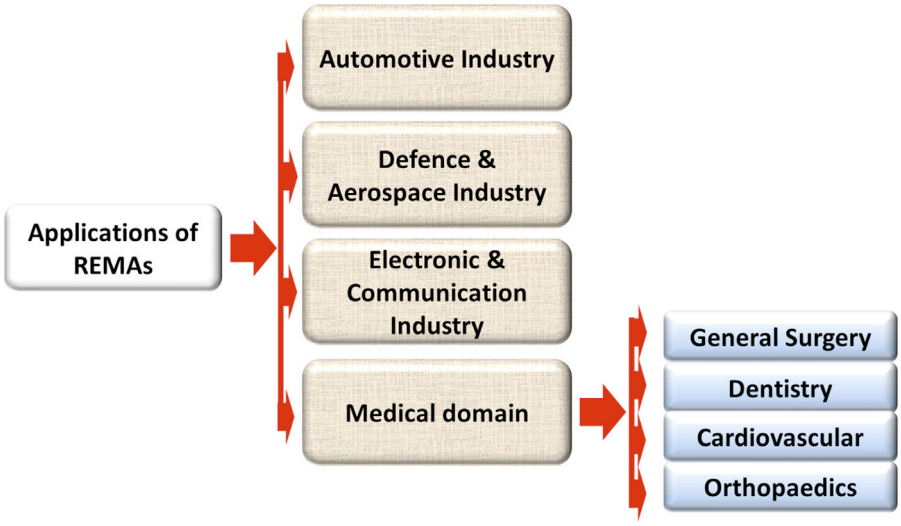

Fig. 19. Pictorial representation depicting the application of REMAs in different fields.

Table 6
The approximate mechanical property intervals of the alloys.

Alloy number plate	TS range	YS interval	Elongation range
AM60B	240-300	90-160	5-15 %
AZ91X	250-350	90-160	5-15 %
MB26	300-420	120-240	5-15 %
AM20	160-260	40-120	5-15 %
AM50	210-310	90-160	5-15 %

for different purposes. The main application fields of REMAs are shown in Fig. 19 followed by a brief discussion about each one of them.

8.1. Automotive industry

The automobile industry has made extensive use of REMAs owing to their high strength and low weight, especially in the production of vital parts such as engine cylinder heads, transmission housings, and engine housings. Several well-known automotive manufacturers, including Ford, General Motors, Daimler Chrysler, Mercedes-Benz, Volkswagen, Toyota, and Fiat-Alfa Romeo, have already begun to use RE die-cast MAs for reducing the component weight and improving performance. Table 6 shows the range of mechanical properties for some of these alloys. From the data in the table, it is clear that these alloys have good mechanical properties, with their higher strengths supporting their use in their respective areas of expertise.

In modern automotive manufacturing, the application of REMAs is gaining increasing attention, mostly in the pursuit of lightweighting to achieve energy savings and reduced emissions. Taking Toyota Motor Corporation as an example, the company has integrated the airbag into the steering wheel design and replaced traditional steel and Al materials with AM60B die-cast MAs, successfully achieving 45 % and 15 % weight reduction while reducing vibrations in the steering system. Similarly, V6 engine heads which earlier was fabricated with JDM1 alloys using low pressure and cast process is now being prepared with REMAs through tile pouring technique as shown in Fig. 20a and b [235,236]. These heads are being employed in car for testing on the road sites. Also because of the good casting and ductility of the JDM1 alloy, fabricated via cast and flowing technology are now being used in car wheels (Fig. 20c) [235].

Also, Chery Automobile Company and Changchun Institute of Applied Chemistry collaborated to develop high-performance REMAs that substantially improved the alloy's heat and creep resistances. They also achieved mass production of MAs die-castings at a rate of 1500 tons per year, establishing the largest industrial base for REMAs in China, used for manufacturing key components such as engine cylinder heads. Dongfeng Technology Brake System Company and Likon Group have separately established MA die-casting production lines with annual capacities of 630 tons and 3000 tons, respectively. Chang'an Automobile further promotes the application of REMAs, by mastering the reconstruction design technology of vehicles and components after replacing traditional materials with these alloys. This achievement includes the industrial development of multiple components such as power trains, seat frames, steering wheel frames, wheels, and spare tire racks. The current developed MA materials include new RE die-cast MAs (AZ91X), high-strength REMAs (Mg-Gd-Y), and high-toughness REMAs (MB26). These materials are not only used domestically but also internationally. Therewithal these some other REMA series such as AE, WE, and OE have also been developed. Globally, the automotive industries in North America, Europe, Japan, and South Korea have begun to extensively use REMAs, primarily replacing cast iron, Al, plastic, and stamped welded parts, especially in the application of die-castings. The use of MAs in automotive die-casting in North America is growing at an annual rate of 15 %. Chinese Academy of Sciences and institutions such as FAW have successfully developed over 60 types of MA based automotive components, covering key areas such as in-

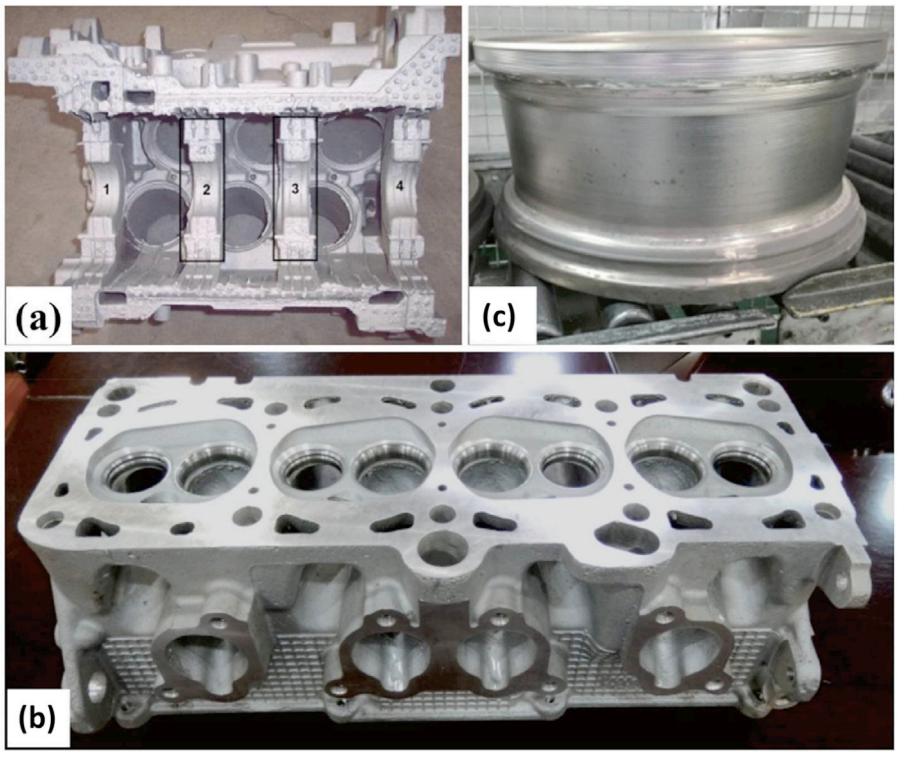

Fig. 20. (a) V6 engine block casted via low pressure casted process (b) Engine cylinder head fabricated via tile-pouring method (c) Car wheel fabricated via cast and flow process. Reproduced with permission from Elsevier [235].

strument panels, seat frames, steering wheels and columns, engine cylinder heads, and transmission housings.

Automotive lightweighting is not only an effective way to improve energy efficiency and reduce emissions but is also crucial for enhancing vehicle safety and comfort. With the increasing demand for safety devices and advanced interiors in the automotive industry, the application of light-structured materials becomes more widespread. For instance, Mercedes-Benz uses die-cast MAs from the AM20 and AM50 series as seat frame materials, successfully reducing weight and substantially decreasing vibrations, thus improving the riding experience. Currently, the average use of MAs per vehicle abroad has reached 40 kg. With the progress in REMA technology and reduction in manufacturing costs, the application of MAs in automobiles is increasing continuously and is expected to reach up to 150 kg, and which will result in weight reduction of 10–15 % for the vehicles, reduction in fuel consumption by 6–10 %, and CO_2 emission reduction of about 5 g/km.

8.2. Defense and aerospace fields

High-performance light metal materials play a significant role in aerospace and defense construction [237–239]. REMAs, with their excellent casting and machining properties, are suitable for manufacturing large, complex, thin-walled structural components which are commonly used in the shells of aerospace power system components. Considering that aerospace engine components operating under HTs and high vibrations for long periods, REMAs acts as unique materials for component fabrication which requires high-strength heat-resistance. Using the JDM1 and JDM2 alloys researchers have developed different types of weapons for missiles and along with components for radars as shown in Fig. 21 [235].

Table 7
Room temperature mechanical properties of cast REMA materials for aero-engine components.

Alloy Number Plate	Preparation process	UTS/MPa	YS/MPa	EL%
QE22	Metal mold casting-T6	199	274	13.0
WE25	Metal mold casting-T6	198	282	11.1
WE33	Metal mold casting-T6	188	275	11.7
WE34	Metal mold casting-T6	189	272	13.2
WE43	Sand casting-T6	198	247	4.0
EV31	Metal mold casting-T6	170	280	5.0
EV33	Sand casting-T6	220	308	4.1
ZE41	Metal mold casting-T6	153	245	13.4
ZM6	Sand casting-T6	130	220	5.5

In this regard, Table 7 shows a comparison of the mechanical properties of commonly used REMAs in aerospace engine components, and also lists the mechanical property data of newly developed REMAs based on WE43, EV31, and other series alloys. Although the YS and EL of QE22 alloy are outstanding, however, its cost is not advantageous due to the presence of 2 % Ag element. With a TS beyond 280 MPa and outstanding mechanical qualities, WE43 is now the market leader among REMAs.

Fig. 21. Different spherical parts (a-c) missile shells (d-g) components for radars, fabricated JDM1 and JDM2 alloys. Reproduced with permission from Elsevier [235].

REMAs are being studied more and more for use in aerospace applications due to their desirable mechanical properties at HTs and good strength-to-weight ratios. From the tabular data (Table 7), we can see the mechanical properties at room temperature compared for a number of REMAs. According to the results, the casting process and RE elements are two most important factors in deciding how well MAs mechanically function. Selecting suitable materials for aero-engine components requires a comparative study of room-temperature mechanical characteristics. As the choice of alloy and manufacturing process directly impacts the performance and reliability of these components in service. In the field of aerospace, weight has a fundamental impact on economic efficiency and performance optimization. For example, the MD600N helicopter's transmission system utilized REMAs, successfully reduced the structural weight and meaningfully improved the rotor efficiency. In China's space missions, the Shenzhou series manned spacecraft achieved weight savings of about 13 kg by applying an electrical box developed from the MB26 MA, reflecting the potential of MAs in weight-sensitive applications [240]. Materials for aerospace and defense equipment must operate under a variety of complex conditions, such as vibration, dust, corrosion, and HTs. In these harsh environments, REMAs such as WE43 and WE54 are used in key components like aerospace engine gearboxes and helicopter transmission systems for their excellent performance. Various types of Chinese fighter jets, bombers, helicopters, transporters, shipborne radars, surface-to-air missile systems, launch vehicles, artificial satellites, and manned spacecraft widely employ these alloy components. It is noteworthy that Shanghai Jiao Tong University used a coating transfer precision casting technique combined with the low-RE JDM1 casting MA to successfully prepare a lightweight missile's cabin and engine casting, meeting high internal sur-

face finish requirements [241]. Similarly, by combining low-pressure casting technology with the high-RE JDM2 casting MA, a helicopter tail gearbox and missile casing were developed, demonstrating MAs application prospects and optimization potential in aerospace structural materials. The use of REMAs in aircraft vehicles is anticipated to grow in the next years as manufacturing prices for these alloys are reduced and new technology is developed.

8.3. Electronics and communications field

In today's technological world, 3C (computers, communications, consumer electronics) products are constantly striving for lighter, thinner, and smaller design concepts, driving the widespread application of REMAs in this field [188,242–244]. Traditionally, the casings of 3C products often use plastic materials such as polycarbonate (PC), acrylonitrile-butadiene-styrene (ABS) copolymers, and PC/ABS alloys, which are lightweight but poor in electromagnetic shielding performance, often requiring subsequent treatments to improve their performance. Also, REMAs offer unique advantages in electronic devices, especially for laptop computers, smartphones, cameras, and their casings due to their lightweight, attractive appearance, excellent electromagnetic shielding effects, effective thermal dissipation, corrosion resistance, and high specific strength and stiffness [244–246]. The touch sensation provided by REMAs also offers a more comfortable experience for consumers. Global electronic brands such as Lenovo, Dell, Apple, Toshiba, Panasonic, and Sony have adopted RE die-cast MAs in many of their flagship products, pointedly enhancing the structural integrity of products while effectively reducing potential electromagnetic radiation exposure to users' health. Among various REMAs, AZ91D has become the mainstream choice in the market due to its wide range performance advantages.

As technology advances and cost-effectiveness continues to improve, REMAs are expected to play an even more critical role in future 3C product design, a trend closely tied to the increasing global focus on green manufacturing and sustainable development. Increased progress towards 3C product lightweighting, performance optimization, and environmental friendliness is anticipated as a result of ongoing research and development of REMAs.

8.4. Healthcare sector

REMAs play a crucial role in the medical field, providing advanced materials that are lightweight yet strong, biocompatible, and capable of withstanding sterilization processes, making them ideal for surgical instruments, implants, and other medical devices [207,247]. Some of the prominent application of REMAs in medical field are briefly discussed below:

8.4.1. Orthopedic applications

In the field of orthopedic implants, emerging REMAs materials are gradually becoming the focus of research, as they offer a series of significant advantages over traditional medical metal materials such as stainless steel, cobalt-based alloys, and titanium alloys [208,248,249]. REMAs implants are designed to be gradually absorbed by the body following the completion of bone repair. This advantageous feature eliminates the necessity for patients to undergo secondary removal surgery, thereby suggestively alleviating both discomfort and financial burden throughout the treatment process [214,255,256]. The physical properties of these alloys, remarkably their congruent density and elastic modulus relative to human bone, contribute to the reduction of stress shielding and facilitate accelerated bone healing. As a fixation material in the early stages of fracture management, these alloys provide essential mechanical support to promote fracture healing while minimizing the risk of stress shielding due to their comparable mechanical properties to human bone. This demonstrates their excellent biocompatibility and positions them as a promising innovation in the field of orthopedics [250,251].

For the treatment of bone defects, bone repair materials play a critical role and form an important branch of orthopedic implant devices, and thus have remained a hotspot in bone repair research. An ideal artificial bone should not only replace the missing bone but also degrade gradually in vivo while promoting the growth of bone cells, ultimately achieving self-repair of the bone. Although existing porous bone tissue engineering materials, such as bio-ceramics and polylactic acid, have certain clinical application potential, their mechanical properties are still not ideal [252,253]. Porous REMAs, as an innovative biodegradable material, not only meets the requirements for mechanical properties but also its inherited bioactivity promotes cell differentiation and proliferation, as well as angiogenesis, thus providing a potential strategy for the repair of bone defects. Kraus et al. [254] have analyzed the responsive growth of bone and tissue in Mg alloys with and without RE elements that is WZ21 and ZX50. Both of these advanced alloys were found to exhibit distinctly different degradation behaviors. The primary sample, containing 2 wt.% of Y, demonstrated a linear degradation pattern following implantation, with minimal loss of pin volume. In contrast, ZX50 sample, which lacks a RE element, exhibited a rapid degradation rate leading to complete loss of pin volume within a short period. Furthermore, it was noted that corrosion effects are more pronounced in this latter sample, as gas generation occurs within a brief timeframe. The overall degradation trends over time are illustrated in Fig. 22.

The biodegradable properties of MAs lead to significant degradation rates, which consequently restrict their application in medical devices. Several factors influence the degradation behavior of MAs. Notably, their low standard electrode potential and chemical reactivity make them susceptible to corrosion in biological environments. As well, the corrosion layers that form on the surface of the MAs can be adversely affected by chloride ions under harsh environmental conditions, resulting in the development of porous structures [255]. The degradation process generates hydrogen gas, which can lead to the breakdown of corrosion layers and consequently fails to protect the MAs from degradation. As a result, the

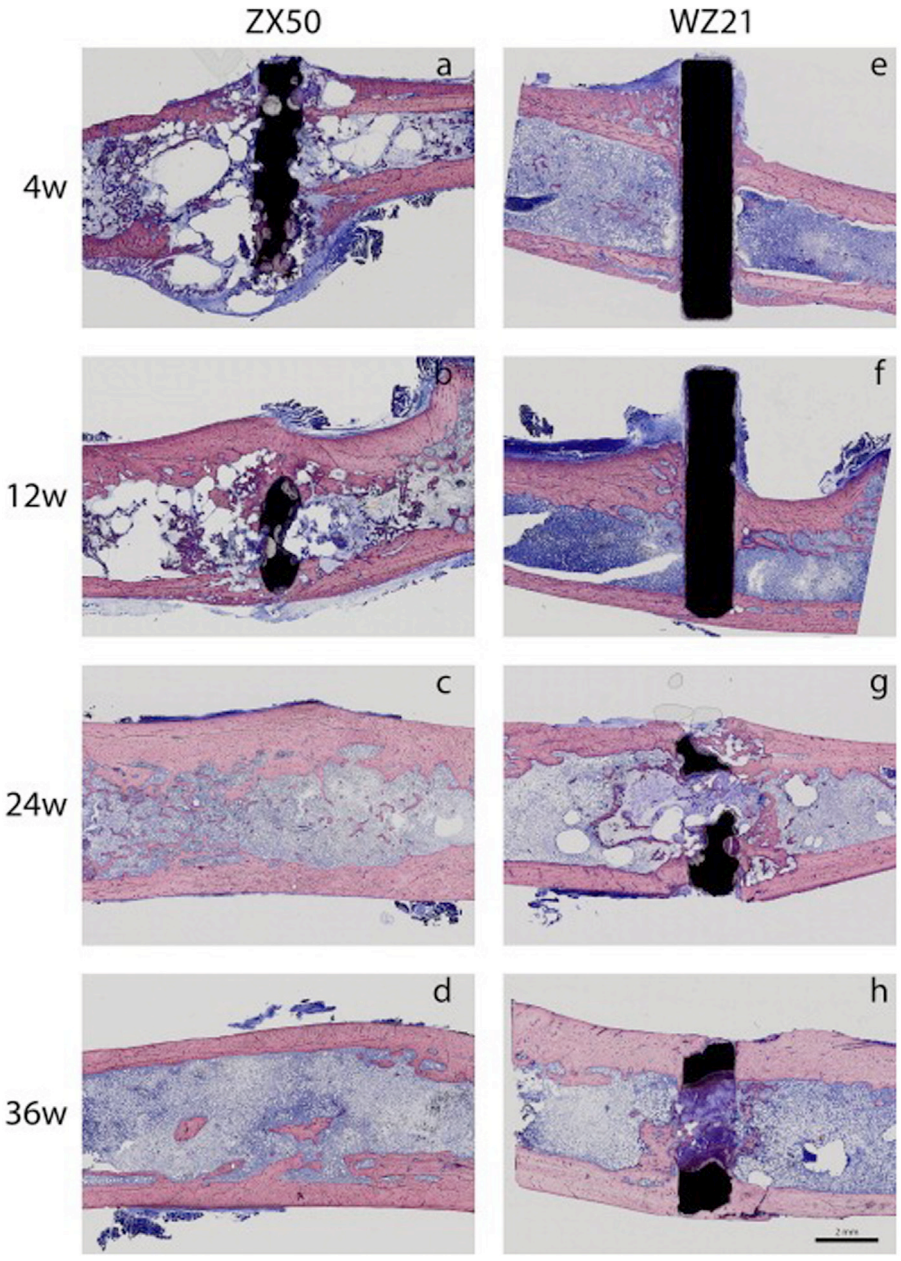

Fig. 22. Thin slides of (a–d) ZX50, (e–h) WZ21 (e–h) pins stained with Levai–Laczko provides insights into their interaction with surrounding tissue. WZ21 highlights the positive attributes of magnesium alloys, demonstrating their ability to promote new bone formation around the implant. Reproduced with permission from Elsevier [254].

use of MAs in implants has been limited, as their mechanical properties tend to deteriorate before the bone can accommodate the actual load. However, the integration of RE elements into MAs has addressed many of these challenges, leading to momentous improvements that have facilitated the use of REMAs as bio-implants in recent times. These enhancements are primarily driven by three mechanisms: the mitigation of corrosion, changes in the types of phases, and variations in the arrangement and volume fractions, alongside the maintenance of an intact protective corrosion coating layer [255]. Some of the REMAs along with their improvement mechanism are presented in Table 8.

Therewithal this researchers have explored the biocompatibility of REMAs in different animal bodies and found that it is better as compared to the other biomaterials [250]. Of course, further exploration needs to be done for evaluating the short and long-term uses of these materials.

8.4.2. Cardiovascular and general surgery applications

Owing to their good controllability of mechanical properties and corrosion kinetics under physiological conditions, REMAs have shown significant advantages in vascular dilatation applications [267]. The utilization of these materials not only facilitates vascular dilation but also substan-

Table 8
Mechanism of improving the degradation behavior in REMAs by the incorporation of different rare-earth elements.

REMA	Improvement mechanism	Ref.
Mg-Dy	Trapping of the impurities from the intermetallic compounds.	[256]
Mg-Gd	Development of protective oxide film on the surface of REMA.	[257]
Mg-Sc	Results in the formation of Sc_2O_3 on the REMA surface.	[258]
Mg-Sc-Y	Results in the formation of two oxide films that is Sc_2O_3 and Y_2O_3 on the surface.	[259]
Mg-Nd	Generate a strong oxide film on the matrix surface.	[260]
Mg-Al-Ce	Intends to change the change the phase.	[261]
WZ21	Alterative in the volume fraction and phase change.	[159]
WE43	Alterative in the volume fraction and phase change as well as development of oxide film.	[262]
AZ61	Reduces the $Al_{12}Y$ phase to $Mg_{17}Al_{12}$ phase at the grain boundaries.	[263]
Mg-Zn-Zr-Nd	Suppression of galvanization among the secondary phases by Nd.	[264]
Mg-Zr-Sr-Sc	Development of protective layer of Sc_2O_3.	[265]
Mg-Zn-Y-Zr	Inhibition of the secondary phase generations.	[266]

tially minimizes the complications commonly associated with long-term implantations. Additionally, the biodegradability of these alloys facilitates repeated interventional treatments at the same lesion site. In the same line, the negative charge characteristics of the REMA surface reduce the risk of acute thrombosis, thereby decreasing the incidence of stent thrombosis [268,269]. In the field of hepatobiliary surgery, biliary stricture is a common and frequently occurring problem that poses a challenge to surgeons [270]. The advancement of endoscopic and interventional radiological techniques has led to biliary stent drainage becoming the primary treatment for biliary strictures. This method is widely acknowledged for its minimally invasive nature, convenience, effectiveness in achieving drainage, and reduced treatment costs [250].

Currently, commonly used biliary stents in clinical practice include metal stents and plastic stents, each with their own advantages [271] but their inherent limitations have also led to many defects, which limit their more extensive application. Against this backdrop, biodegradable stents, especially REMAs stents, have received increasing attention due to their ability to degrade in vivo and their excellent mechanical support performance. The superior mechanical properties of these alloy stents provide temporary support for the biliary tract, whereas their biocompatibility and biodegradability reduce the risks and complications associated with long-term implantation [272].

A study reported by May et al. [273] carried out on 48 patients suffering from malleolar factures. On performing the surgery 23 among them were treated with RE based Mg alloys screws and remaining were treated with conventional screws (Ti based). Taking a follow up after one year, it was found that REMAs based screws are better as compared to the Ti ones as no secondary surgery for their removal was needed. Likewise, Aktan et al. [274] have reported a study on a general surgery where in REMA screws has been used for the fixation of osteochondral fragment in distal humerus facture. Apart from that, the lateral column of the facture has been stabilized by the Ti column plate, both of them were separated as shown in Fig. 23. Therefore, it has been noted that a small amount of gas was generated around the screw, which results in minor surface reduction.

Apart from these, there are lot of studies carried out by different researches mentioning better results of REMAs over other conventional materials, thereby signifying their importance in our day-to-day life.

8.4.3. Dental applications

REMAs, due to their similarity to human bone cortical density, exhibit excellent biomechanical compatibility in the field of dental implants. Additionally, they promote the deposition of calcium and phosphorus and the growth of cortical bone, indicating great potential for application in the field of oral implantology.

Currently, researchers have begun to explore the application of REMAs in various branches of dentistry, including oral surgery, oral implantation, oral medicine, orthodontics, and tissue engineering scaffolds. For example, the development of absorbable REMA repair systems for oral guided bone and tissue regeneration, as well as porous REMA dental implants. At the same time, RE-Mg and its alloys are also considered as potential materials for inlays, crown restorations, and removable partial dentures, as well as for potential applications in orthodontics. But, most of these studies are still in the preliminary stage. In the field of hepatobiliary surgery, biliary stricture is a common and challenging disease to treat. With the development of endoscopic and interventional radiological techniques, biliary stent drainage has become the main treatment for biliary stricture, widely recognized for its minimally invasive, convenient, effective, and low-cost characteristics [250].

Bioresorbable materials developed using MAs have proved to be highly useful for guided bone regeneration (GBR). These materials are now widely used in maxillofacial surgeries [275]. When jaw bones are removed due to conditions such as periodontitis, infected teeth, tumors, cysts, or other abnormalities, it leads to various challenges, including disfigurement. To address bone deformities and promote osteogenesis, GBR, which involves bone scaffolds and bio-membranes, has proved to be incredibly beneficial. The bio-membranes serve as a barrier between the hard and soft tissues, creating space for osteoprogenitor cells and preventing soft tissues from interfering with the osteogenesis process [276]. Because Mg-based bioresorbable membranes are biodegrad-

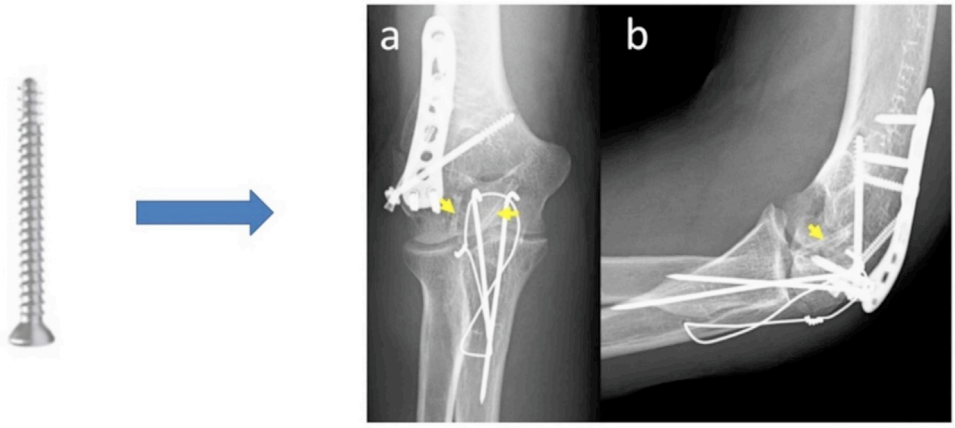

Fig. 23. Post operated X-ray images of (a) anteroposterior, (b) lateral-elbow, with yellow marked designated REMA based screws. Reproduced with permission from Cureus [274].

able, they eliminate the need for a second surgery, unlike non-bioresorbable options. In cases of alveolar sockets or substantial bone defects, these membranes help preserve the space needed for osteogenesis and bone height due to the mechanical properties of MAs [277]. Guo et al. [278] developed a composite material by combining MAs with reinforced block mineralized collagen (MC) for rebuilding the alveolar bone, specifically targeting the buccal canine plate. To compare the effectiveness, both the composite and MC implants were placed in the mandibular buccal plate, and bone regeneration was assessed over a period of 12 to 24 weeks. In the 12-week period, both implants showed similar progress with only minimal differences. However, after 24 weeks, while both implants demonstrated comparable bone growth and overall volume, the bone formed with the composite was found to be denser than the bone formed with MC alone. This analysis clearly indicates that incorporating MA into the MC enhances the restoration of alveolar ridges, particularly in the buccal bone area. Wang et al. [279] studied the impact of osteogenesis on mandibular canine defects using magnesium-silver (Mg-Sr) MA. After the removal of the second and third premolars, the corresponding MA was placed on the mandibular buccal fracture of the canines. The progress of the MC and MA scaffolds was compared. The results showed that both the volume and thickness of the bone were greater in the MA group compared to the MC group. These findings suggest that MA scaffolds have superior osteogenic capabilities when used in canine mandibular lesions. In another study by Lee et al. [280] a comparison was made regarding stress-bearing capabilities in sagittal split ramus mandible osteotomy using biodegradable MA and titanium screws. The load-bearing tests concluded that MA-based screws could withstand more stress than titanium screws, reducing the negative impact on the stability of the sagittal split ramus. Therewithal that, the flexibility of MAs is also an advantage, allowing for easy modification of membranes to fit complex bone defect shapes [281,282]. Furthermore, the antibacterial properties of MAs decrease the chance of bone resorption as well as bacterial infections [283].

9. Challenges and prospects

The incorporation of RE elements in magnesium alloys shows considerable promise; however, it also introduces several challenges due to the complex physical and chemical behaviors of these elements. Five key challenges in incorporating rare-earth elements into MAs are pointed below

a) REEs tend to segregate during solidification, leading to inhomogeneous microstructures that can negatively affect mechanical properties and corrosion resistance.
b) REEs are expensive and geopolitically sensitive materials. Their high cost and limited global supply constrain the large-scale application of RE-containing magnesium alloys.
c) The addition of REEs can lead to the formation of intermetallic compounds that may improve strength but reduce ductility and formability, complicating processing steps like extrusion, rolling, or forging.
d) REEs often form complex intermetallic phases (e.g., $Mg_{12}RE$, Mg_3RE) whose stability and morphology depend on precise alloying and processing conditions. These phases influence mechanical properties and corrosion resistance in non-trivial ways.
e) Recycling RE-containing magnesium alloys is difficult due to the complexity of separating REEs from magnesium, potentially increasing environmental burden and reducing sustainability.

10. Conclusion

This review provides a comprehensive analysis of metal alloys with a focus on the influence of REEs on key performance characteristics such as mechanical strength, formability, and thermal conductivity. Special emphasis is placed on the role of RE-induced intermetallic compounds, which seriously enhance high-temperature strength and oxide scale adherence. In addition, the grain refinement effects of REEs contribute to improved mechanical strength and ductility. The impact of REEs on deformation mechanisms is particularly

notable and descried with proper citations. They reduce texture strength, activate non-basal slip systems, and promote uniform plastic deformation, thereby enhancing formability. Our review also highlights how RE incorporation facilitate dislocation cross-slip by reducing the critical resolved shear stress ratio between basal and non-basal systems, as demonstrated using various models and datasets. Although a slight reduction in thermal conductivity is observed with RE incorporation, this can be mitigated through careful alloy design and processing optimization. However, the detailed mechanisms of RE-induced deformation and their microscopic behavior in MAs require further investigation. We recommend future research to integrate both experimental and theoretical approaches, including molecular dynamics simulations, to deepen understanding. Key future directions include optimizing processing and heat treatment parameters to improve plastic deformation, hot workability, and superplasticity. Environmental considerations such as the selection of eco-friendly alloying elements, life cycle impact analysis, and microstructural optimization will also be critical for the sustainable development of RE-containing alloys.

Declaration of competing interest

The authors declare that they have no known competing financial interests or personal relationships that could have appeared to influence the work reported in this paper.

CRediT authorship contribution statement

Zhiqi Zhu: Writing – original draft, Visualization, Validation, Software, Resources, Methodology, Investigation, Conceptualization. **Irfan Ayoub:** Writing – original draft, Validation, Software, Resources, Investigation, Formal analysis, Data curation. **Jie He:** Writing – review & editing, Writing – original draft, Software, Investigation, Funding acquisition, Formal analysis, Data curation. **Jingran Yang:** Visualization, Validation, Methodology, Investigation, Formal analysis. **HanDong Zhang:** Visualization, Validation, Supervision, Software, Methodology, Formal analysis. **Zhiqin Zhu:** Writing – review & editing, Writing – original draft, Visualization, Validation, Software, Project administration, Methodology, Investigation. **Qi Hao:** Writing – review & editing, Writing – original draft, Visualization, Investigation, Data curation. **Ziming Cai:** Supervision, Methodology, Investigation, Data curation. **Oluwafunmilola Ola:** Writing – review & editing, Writing – original draft, Resources, Funding acquisition, Formal analysis, Data curation. **Santosh K. Tiwari:** Writing – review & editing, Supervision, Project administration, Conceptualization.

Acknowledgment

SKT and OO sincerely appreciate the support of the SPARC project (P3808) and UKIERI-4 Strand 1 Institutional Research & Mobility Partnerships Grant (45580615 UKIERI-SPARC/01/18) under the Indo-UK scheme. Additionally, SKT extends heartfelt gratitude to Nitte University for providing the research grant (grant no. NUFR-23–070), which has significantly facilitated our research endeavors.

References

[1] S.V.S. Prasad, S.B. Prasad, K. Verma, R.K. Mishra, V. Kumar, S. Singh, J. Magnes. Alloy. 10 (2022) 1–61, doi:10.1016/j.jma.2021.05.012.
[2] K.U. Kainer, F. von Buch, The current state of technology and potential for further development of magnesium applications, in: Magnesium—Alloy Technology, John Wiley & Sons, Ltd, 2003, pp. 1–22, doi:10.1002/3527602046.ch1.
[3] N.A. Agha, R. Willumeit-Römer, D. Laipple, B. Luthringer, F. Feyerabend, PLoS One 11 (2016) e0157874, doi:10.1371/journal.pone.0157874.
[4] J. Wang, J. Xu, W. Liu, Y. Li, L. Qin, Sci. Rep. 6 (2016) 1–10, doi:10.1038/srep26341.
[5] J.C. Fariñas, I. Rucandio, M.S. Pomares-Alfonso, M.E. Villanueva-Tagle, M.T. Larrea, Talanta 154 (2016) 53–62, doi:10.1016/j.talanta.2016.03.047.
[6] Y. Zhang, X. Xu, Shape Mem. Superelast. 6 (2020) 374–386, doi:10.1007/S40830-020-00303-0/FIGURES/5.
[7] A.A. Luo, A.K. Sachdev, Adv. Wrought Magnes. Alloy. (2012) 393–426, doi:10.1533/9780857093844.3.393.
[8] Michael M. Avedesian, Hugh Baker, De Gruyter (2011), doi:10.1515/corrrev.2000.18.6.499.
[9] N. Hort, Y. Huong, K.U. Kainer, Adv. Eng. Mater. 8 (2006) 235–240, doi:10.1002/adem.200500202.
[10] B. Jahani, K. Meester, X. Wang, A. Brooks, Biomed. Sci. Instrum. 52 (2022) https://onlinelibrary.wiley.com/doi/full/10.1002/advs.201902443.
[11] N.T. Kirkland, I. Kolbeinsson, T. Woodfield, G.J. Dias, M.P. Staiger, Mater. Sci. Eng. B 176 (2011) 1666–1672, doi:10.1016/J.MSEB.2011.04.006.
[12] M.P. Staiger, I. Kolbeinsson, N.T. Kirkland, T. Nguyen, G. Dias, T.B.F. Woodfield, Mater. Lett. 64 (2010) 2572–2574, doi:10.1016/J.MATLET.2010.08.049.
[13] B.L. Mordike, T. Ebert, Mater. Sci. Eng. A 302 (2001) 37–45, doi:10.1016/S0921-5093(00)01351-4.
[14] J.L. Wang, J.K. Xu, C. Hopkins, D.H.K. Chow, L. Qin, Adv. Sci. 7 (2020) 1902443, doi:10.1002/ADVS.201902443.
[15] M. Esmaily, J.E. Svensson, S. Fajardo, N. Birbilis, G.S. Frankel, S. Virtanen, R. Arrabal, S. Thomas, L.G. Johansson, Prog. Mater. Sci. 89 (2017) 92–193, doi:10.1016/J.PMATSCI.2017.04.011.
[16] J. Song, J. She, D. Chen, F. Pan, J. Magnes. Alloy. 8 (2020) 1–41, doi:10.1016/j.jma.2020.02.003.
[17] B. Li, K. Zhang, G. Shi, K. Wang, Y. Li, X. Li, M. Ma, J. Yuan, J. Rare Earths 39 (2021) 600–608, doi:10.1016/j.jre.2021.01.012.
[18] J. Bohlen, F. Chmelík, P. Dobroň, F. Kaiser, D. Letzig, P. Lukáč, K.U. Kainer, J. Alloys. Compd. 378 (2004) 207–213, doi:10.1016/j.jallcom.2003.10.102.
[19] Z.H. Chen, W.J. Xia, Y.Q. Cheng, D.F. Fu, Zhongguo Youse Jinshu Xuebao/Chinese J. Nonferrous Met. 15 (2005) 1–11.
[20] A. Jäger, P. Lukáč, V. Gärtnerová, J. Bohlen, K.U. Kainer, J. Alloys. Compd. 378 (2004) 184–187, doi:10.1016/j.jallcom.2003.11.173.
[21] Z. Chen, Z. Li, J. Chen, P. Kallem, F. Banat, H. Qiu, J. Environ. Chem. Eng. 10 (2022) 107104, doi:10.1016/j.jece.2021.107104.
[22] B.K. Mokoena, L.S. Mokhahlane, S. Clarke, Int. J. Coal. Geol. 259 (2022) 104037, doi:10.1016/j.coal.2022.104037.
[23] J.H. Kim, B.O. Lee, C.B. Lee, S.H. Jee, Y.S. Yoon, J. Rare Earths 30 (2012) 599–603, doi:10.1016/S1002-0721(12)60097-0.
[24] J. Tan, S. Ramakrishna, Appl. Sci. 11 (2021) 6861, doi:10.3390/app11156861.

[25] G. wei CHANG, S.ying CHEN, ZHOU C, X.dong YUE, Y. hui QI, Trans. Nonferrous Met. Soc. China (English Ed.) 20 (2010) 289–293, doi:10.1016/S1003-6326(09)60136-9.
[26] D.A. Kramer, Magnesium and magnesium alloys, Kirk-Othmer Encyclopedia of Chemical Technology (2000) 1–55.
[27] F. Witte, Acta Biomater. 6 (2010) 1680–1692, doi:10.1016/j.actbio.2010.02.028.
[28] R.J. Fruehan, JOM 37 (1985) 54, doi:10.1007/BF03258642/METRICS.
[29] L.L. Rokhlin, Adv. Light Alloy. Compos. (1998) 443–448, doi:10.1007/978-94-015-9068-6_58.
[30] B.R. Powell, V. Rezhets, M.P. Balogh, R.A. Waldo, JOM 54 (2002) 34–38, doi:10.1007/BF02711864/METRICS.
[31] O. Haruyama, N. Annoshita, N. Nishiyama, H.M. Kimura, A. Inoue, Mater. Sci. Eng. A 375–377 (2004) 288–291, doi:10.1016/J.MSEA.2003.10.041.
[32] A. Imandoust, C.D. Barrett, T. Al-Samman, K.A. Inal, H. El Kadiri, J. Mater. Sci. 521 52 (2016) 1–29 (2016), doi:10.1007/S10853-016-0371-0.
[33] T. Zhang, W. Wang, J. Liu, L. Wang, Y. Tang, K. Wang, Front. Bioeng. Biotechnol. 10 (2022) 953344, doi:10.3389/FBIOE.2022.953344/XML/NLM.
[34] L. Shi, S. Chen, F. Zheng, M. Liu, H. Yang, B. Zhang, Colloids Surfaces A Physicochem. Eng. Asp. 658 (2023) 130664, doi:10.1016/J.COLSURFA.2022.130664.
[35] P. Kumar Rout, S. Roy, D. Rathore, Today Proc. 115 (2024) 24–30, doi:10.1016/J.MATPR.2023.06.341.
[36] J. Xu, T. Zhang, X. Li, Research on the process, energy consumption and carbon emissions of different magnesium refining processes, Materials 16 (9) (2023) 3340.
[37] S. Tekumalla, S. Seetharaman, A. Almajid, M. Gupta, Metals. (Basel) 5 (2014) 1–39, doi:10.3390/met5010001.
[38] Y. Huang, W. Gan, K.U. Kainer, N. Hort, J. Magnes. Alloy. 2 (2014) 1–7, doi:10.1016/J.JMA.2014.01.005.
[39] N. Stanford, D. Atwell, A. Beer, C. Davies, M.R. Barnett, Scr. Mater. 59 (2008) 772–775, doi:10.1016/J.SCRIPTAMAT.2008.06.008.
[40] T.L. Chia, M.A. Easton, S.M. Zhu, M.A. Gibson, N. Birbilis, J.F. Nie, Intermetallics. (Barking) 17 (2009) 481–490, doi:10.1016/J.INTERMET.2008.12.009.
[41] L. Gao, R.S. Chen, E.H. Han, J. Alloys. Compd. 472 (2009) 234–240, doi:10.1016/J.JALLCOM.2008.04.049.
[42] Z. Lü, J. Zhou, Z. Sun, R. Chen, Effect of rare earth elements on the structures and mechanical properties of magnesium alloys, Chinese Sci. Bull. 58 (7) (2013) 816–820.
[43] C. Wei, C. Xu, W. Fu, Z. Yi, Z. Li, A. Shi, C. Fan, G. Kuang, Yanshi Xuebao/Acta Petrol. Sin. 38 (2022) 455–471, doi:10.18654/1000-0569/2022.02.10.
[44] H. Liu, Y. Zhang, Y. Luan, H. Yu, D. Li, Metals. (Basel) 10 (2020) 1–13, doi:10.3390/met10101376.
[45] J. Liu, H. Yu, C. Chen, F. Weng, J. Dai, Opt. Lasers. Eng. 93 (2017) 195–210, doi:10.1016/j.optlaseng.2017.02.007.
[46] L. Zhan, Y. zhi Le, Z. jun Feng, Y. chun Lou, M. Ruan, H. wen Li, China Foundry 17 (2020) 212–218, doi:10.1007/s41230-020-9070-1.
[47] H. Xie, G. Wu, X. Zhang, W. Liu, W. Ding, Mater. Charact. 175 (2021) 111076, doi:10.1016/j.matchar.2021.111076.
[48] S.C. Jin, J.U. Lee, J. Go, H. Yu, S.H. Park, J. Magnes. Alloy. 10 (2022) 850–861, doi:10.1016/j.jma.2021.04.015.
[49] Y. Zhang, X. Xu, Appl. Phys. a Mater. Sci. Process. 126 (2020) 1–12, doi:10.1007/S00339-020-03503-8/TABLES/3.
[50] A. Incesu, A. Gungor, J. Mater. Sci. Mater. Med. 31 (2020) 1–12, doi:10.1007/S10856-020-06468-5/FIGURES/10.
[51] M. Gupta, S.N.M. Ling, Magnesium, magnesium alloys, and magnesium composites, John Wiley & Sons, 2011.
[52] C.O. Muga, Z.W. Zhang, Adv. Mater. Sci. Eng. 2016 (2016), doi:10.1155/2016/1078187.
[53] H. Dieringa, N. Hort, D. Letzig, J. Bohlen, D. Höche, C. Blawert, M. Zheludkevich, K.U. Kainer, Solid solution strengthening behaviors in binary mg-y single phase alloys, in: Minerals, Metals & Materials Series, Springer, Cham, 2018, pp. 3–14, doi:10.1007/978-3-319-72332-7_1.
[54] A. Biesiekierski, Y. Li, C. Wen, A. Biesiekierski, Y. Li, C. Wen, Adv. Mater. 32 (2020) 1901715, doi:10.1002/ADMA.201901715.
[55] A. Saccone, S. Delfino, D. Macció, R. Ferro, J. Phase Equilibria 14 (1993) 280–287, doi:10.1007/BF02668225.
[56] L.L. Rokhlin, Research progress in preparation and purification of rare earth metals, in: Magnesium Alloy Contain Rare Earth Met, CRC Press, 2020, pp. 28–29, doi:10.1201/9781482265163-8.
[57] Y.M. Kim, C.D. Yim, H.S. Kim, B.S. You, Scr. Mater. 65 (2011) 958–961, doi:10.1016/j.scriptamat.2011.08.019.
[58] Y. Fan, G. Wu, H. Gao, G. Li, C. Zhai, J. Mater. Sci. 41 (2006) 5409–5416, doi:10.1007/s10853-006-0256-8.
[59] A. Gloria, R. Montanari, M. Richetta, A. Varone, Metals. (Basel) 9 (2019) 662, doi:10.3390/met9060662.
[60] L.A. Dobrzański, G.E. Totten, M. Bamberger, The importance of magnesium and its alloys in modern technology and methods of shaping their structure and properties, in: Magnesium and its alloys, CRC Press, 2019, pp. 1–28.
[61] H. Yi, Q. Wang, H. Cao, J. Mater. Res. Technol. 20 (2022) 627–649, doi:10.1016/j.jmrt.2022.07.083.
[62] Y. Fan, G. Wu, C. Zhai, Mater. Sci. Eng. A 433 (2006) 208–215, doi:10.1016/j.msea.2006.06.109.
[63] X. Song, Y. Hu, J. Tian, Y. Wang, Z. Yan, Int. J. Met. 18 (2024) 292–302, doi:10.1007/s40962-023-00997-9.
[64] T. Zhang, G. Meng, Y. Shao, Z. Cui, F. Wang, Corros. Sci. 53 (2011) 2934–2942, doi:10.1016/j.corsci.2011.05.035.
[65] B.L. Mordike, J. Mater. Process. Technol. 117 (2001) 391–394, doi:10.1016/S0924-0136(01)00793-2.
[66] N. Birbilis, M.A. Easton, A.D. Sudholz, S.M. Zhu, M.A. Gibson, Corros. Sci. 51 (2009) 683–689, doi:10.1016/j.corsci.2008.12.012.
[67] F. Saidi, O. Ouadah, N. Ameur, ECS. J. Solid. State Sci. Technol. 12 (2023) 103007, doi:10.1149/2162-8777/acff83.
[68] U.C. Rodewald, B. Chevalier, R. Pöttgen, J. Solid. State Chem. 180 (2007) 1720–1736, doi:10.1016/j.jssc.2007.03.007.
[69] S. Zhang, S.E. Saji, Z. Yin, H. Zhang, Y. Du, C.H. Yan, Adv. Mater. 33 (2021) 2005988, doi:10.1002/adma.202005988.
[70] X.Y. Wang, F.F. Wang, K.Y. Wu, X.F. Wang, L. Xiao, Z.Q. Li, Z.Q. Han, Rare Met. 40 (2021) 1–9, doi:10.1007/s12598-019-01355-7.
[71] J. Liu, D. Bian, Y. Zheng, X. Chu, Y. Lin, M. Wang, Z. Lin, M. Li, Y. Zhang, S. Guan, Acta Biomater. 102 (2020) 508–528, doi:10.1016/J.ACTBIO.2019.11.013.
[72] Y. Li, A. Zhang, C. Li, H. Xie, B. Jiang, Z. Dong, P. Jin, F. Pan, J. Mater. Res. Technol. 26 (2023) 2919–2940, doi:10.1016/j.jmrt.2023.08.055.
[73] Y. Zhang, Y. Wu, L. Peng, P. Fu, F. Huang, W. Ding, J. Alloys. Compd. 615 (2014) 703–711, doi:10.1016/J.JALLCOM.2014.07.028.
[74] J.L. Zhang, S. Bin Wang, M.Z. Li, X.G. Liu, B.S. Xu, Mater. Sci. Forum. 546–549 (2007) 195–198, doi:10.4028/www.scientific.net/msf.546-549.195.
[75] T. Wu, K. Zhang, Coatings 13 (2023) 1533, doi:10.3390/coatings13091533.
[76] D. Matschkal-Amberger, P. Tuengerthal, S. Lamm, M. Göken, H.W. Höppel, P. Felfer, Metals. (Basel) 11 (2021) 1727, doi:10.3390/met11111727.
[77] Z. Tian, Q. Yang, K. Guan, J. Meng, Z. Cao, J. Alloys. Compd. 731 (2018) 704–713, doi:10.1016/j.jallcom.2017.09.063.
[78] X. Shao, H. Yang, J.T.M. De Hosson, X. Ma, Microsc. Microanal. 19 (2013) 1575–1580, doi:10.1017/S1431927613012750.
[79] E. Abe, Y. Kawamura, K. Hayashi, A. Inoue, Acta Mater. 50 (2002) 3845–3857, doi:10.1016/S1359-6454(02)00191-X.
[80] Y.M. Zhu, A.J. Morton, J.F. Nie, Acta Mater. 58 (2010) 2936–2947, doi:10.1016/J.ACTAMAT.2010.01.022.
[81] E. Abe, A. Ono, T. Itoi, M. Yamasaki, Y. Kawamura, Philos. Mag. Lett. 91 (2011) 690–696, doi:10.1080/09500839.2011.609149.
[82] Y.M. Zhu, A.J. Morton, J.F. Nie, Acta Mater. 60 (2012) 6562–6572, doi:10.1016/J.ACTAMAT.2012.08.022.

[83] D.H. Ping, K. Hono, Y. Kawamura, A. Inoue, Philos. Mag. Lett. 82 (2002) 543–551, doi:10.1080/0950083021000018652.
[84] S.B. Mi, Q.Q. Jin, Scr. Mater. 68 (2013) 635–638, doi:10.1016/J.SCRIPTAMAT.2012.12.025.
[85] M. Matsuda, S. Ii, Y. Kawamura, Y. Ikuhara, M. Nishida, Mater. Sci. Eng. A 393 (2005) 269–274, doi:10.1016/J.MSEA.2004.10.040.
[86] L. Bi, Natl. Sci. Rev. 4 (2017) 269–282, doi:10.1093/NSR/NWX049.
[87] H. Kimizuka, M. Fronzi, S. Ogata, Scr. Mater. 69 (2013) 594–597, doi:10.1016/J.SCRIPTAMAT.2013.07.003.
[88] H. Yokobayashi, K. Kishida, H. Inui, M. Yamasaki, Y. Kawamura, Acta Mater. 59 (2011) 7287–7299, doi:10.1016/J.ACTAMAT.2011.08.011.
[89] D. Egusa, E. Abe, Acta Mater. 60 (2012) 166–178, doi:10.1016/J.ACTAMAT.2011.09.030.
[90] M. Yamasaki, M. Matsushita, K. Hagihara, H. Izuno, E. Abe, Y. Kawamura, Scr. Mater. 78–79 (2014) 13–16, doi:10.1016/J.SCRIPTAMAT.2014.01.013.
[91] J. Mi, Y. Cao, J. Zhang, C. Chen, D. Li, X. Lin, J. Chen, L. Jiang, Ind. Eng. Chem. Res. 57 (2018) 833–844, doi:10.1021/acs.iecr.7b03443.
[92] C. Weidenthaler, A. Pommerin, M. Felderhoff, W. Sun, C. Wolverton, B. Bogdanović, F. Schüth, J. Am. Chem. Soc. 131 (2009) 16735–16743, doi:10.1021/ja9042565.
[93] T. Zhang, Y. Lv, Z. Zhang, Z. Jia, T.P. Loh, Org. Lett. 25 (2023) 4468–4472, doi:10.1021/acs.orglett.3c01449.
[94] Z. Zhao, X. Teng, G. Zhou, J. Leng, J. Geng, Xiyou Jinshu Cailiao Yu Gongcheng/Rare Met. Mater. Eng. 43 (2014) 791–795, doi:10.1016/s1875-5372(14)60085-0.
[95] F.A. Mirza, D.L. Chen, Fatigue Fract. Eng. Mater. Struct. 37 (2014) 831–853, doi:10.1111/ffe.12198.
[96] F. Zucchi, V. Grassi, A. Frignani, C. Monticelli, G. Trabanelli, J. Appl. Electrochem. 36 (2006) 195–204, doi:10.1007/s10800-005-9053-3.
[97] H. Huang, H. Kato, C. Chen, Z. Wang, G. Yuan, Mater. Lett. 79 (2012) 281–283, doi:10.1016/j.matlet.2012.04.018.
[98] S.R. Wang, P.Q. Guo, L.Y. Yang, Y. Wang, J. Mater. Eng. Perform. 18 (2009) 137–144, doi:10.1007/s11665-008-9255-z.
[99] Z. Zhao, Q. Chen, Y. Wang, D. Shu, Mater. Sci. Eng A 515 (2009) 152–161, doi:10.1016/j.msea.2009.03.030.
[100] B. Pucun, D. Taishang, H. Xiaohu, Z. Chunwang, X. Yongming, Mater. Charact. 61 (2010) 756–760, doi:10.1016/j.matchar.2010.04.009.
[101] G. Wu, X. Tong, R. Jiang, W. Ding, Jinshu Xuebao/Acta Metall. Sin. 58 (2022) 385–399, doi:10.11900/0412.1961.2021.00519.
[102] L. Wang, J. Jiang, T. Yuan, Q. Xie, H. Liu, A. Ma, Met. Mater. Int. 26 (2020) 551–563, doi:10.1007/s12540-019-00410-3.
[103] X. Hou, Z. Cao, L. Wang, S. Xu, S. Kamado, L. Wang, Mater. Sci. Eng. A 528 (2011) 7805–7810, doi:10.1016/j.msea.2011.06.034.
[104] W. Guo, Q. Wang, B. Ye, H. Zhou, J. Alloys. Compd. 552 (2013) 409–417, doi:10.1016/j.jallcom.2012.11.067.
[105] Y. Liu, Z. Zheng, D. Zhu, J. Gao, G. Cao, Cailiao Rechuli Xuebao/Transactions Mater. Heat Treat. 39 (2018) 1–6, doi:10.13289/j.issn.1009-6264.2018-0149.
[106] Q. Li, X. Li, Q. Zhang, J. Chen, Rare Met 29 (2010) 557–560, doi:10.1007/s12598-010-0168-2.
[107] Q.A. Li, W.J. Liu, Z. Chen, Adv. Mater. Res. 881–883 (2014) 1338–1341, doi:10.4028/www.scientific.net/AMR.881-883.1338.
[108] J. Wang, Q.A. Li, X.Y. Chen, W.W. Mei, Cailiao Rechuli Xuebao/Transactions Mater. Heat Treat. 43 (2022) 143–151, doi:10.13289/j.issn.1009-6264.2021-0376.
[109] D. Zuo, H. Ding, M. Zhi, Y. Xu, Z. Zhang, M. Zhang, Materials. (Basel) 17 (2024) 3183, doi:10.3390/ma17133183.
[110] D. Liu, K. Yang, S. Chen, Materials. (Basel) 17 (2024) 68, doi:10.3390/ma17010068.
[111] S. Golmakaniyoon, R. Mahmudi, Mater. Sci. Eng. A 528 (2011) 1668–1677, doi:10.1016/j.msea.2010.10.095.
[112] Z.L. Ning, H.H. Liu, F.Y. Cao, S.T. Wang, J.F. Sun, M. Qian, Mater. Sci. Eng. A 560 (2013) 163–169, doi:10.1016/j.msea.2012.09.052.
[113] J. Wang, L. Luo, Q. Huo, Y. Shi, Z. Xiao, Y. Ye, X. Yang, J. Alloys. Compd. 774 (2019) 1036–1045, doi:10.1016/j.jallcom.2018.10.013.
[114] Z. Esen, E.B. Öcal, A. Akkaya, B. Gürçay, C. Özcan, B.A. Özgümüş, Ö. Duygulu, A.F. Dericioğlu, Corros. Sci. 166 (2020) 108470, doi:10.1016/j.corsci.2020.108470.
[115] S.K. Woo, C. Blawert, K.A. Yasakau, S. Yi, N. Scharnagl, B.C. Suh, Y.M. Kim, B. Sun You, C. Dong Yim, Corros. Sci. 166 (2020) 108451, doi:10.1016/j.corsci.2020.108451.
[116] S.F. Liu, L.G. Kang, H. Han, L.Y. Liu, X.Q. Zou, H.H. Guo, J. Cent. South Univ. Technol. (English Ed.) 13 (2006) 613–617, doi:10.1007/s11771-006-0002-z.
[117] Y. Fan, G. Wu, H. Gao, G. Li, C. Zhai, Jinshu Xuebao/Acta Metall. Sin. 42 (2006) 35–40.
[118] L. Liu, J. Lei, L. Li, J. Zhang, B. Shang, J. He, N. Li, F. Pan, Adv. Mater. Interfaces. 5 (2018) 1800213, doi:10.1002/admi.201800213.
[119] R. Fan, L. Wang, S. Zhao, L. Wang, E. Guo, Materials. (Basel). 16 (2023) 4155, doi:10.3390/ma16114155.
[120] G.L. Song, A. Atrens, J. Magnes. Alloy. 11 (2023) 3948–3991, doi:10.1016/j.jma.2023.08.012.
[121] F. Pan, J. Zhang, H.L. Chen, Y.H. Su, C.L. Kuo, Y.H. Su, S.H. Chen, K.J. Lin, P.H. Hsieh, W.S. Hwang, Materials. (Basel). 9 (2016) 417, doi:10.3390/ma9060417.
[122] Z. Fan, L. Wang, H. Yuan, H. Zhang, Y. Yan, Mater. Lett.. 366 (2024) 136534, doi:10.1016/j.matlet.2024.136534.
[123] Z. Zheng, Z. Dong, B. Jiang, Y. Cheng, A. Zhang, J. Song, T. Li, F. Pan, Scr. Mater. 238 (2024) 115772, doi:10.1016/j.scriptamat.2023.115772.
[124] X.M. Cui, P.C. Bai, X.H. Hou, W. Liu, L.Y. Wang, Chin. Rare Earths 36 (2015) 110–115, doi:10.16533/J.CNKI.151099/TF.201504019.
[125] H. Azzeddine, A. Hanna, A. Dakhouche, L. Rabahi, N. Scharnagl, M. Dopita, F. Brisset, A.L. Helbert, T. Baudin, J. Alloys. Compd. 829 (2020) 154569, doi:10.1016/j.jallcom.2020.154569.
[126] S. Arun Kumar, K.R. Rajesh, J. Jayaraj, K.G. Raghu, A. Srinivasan, J. Mater. Eng. Perform. 32 (2023) 2840–2852, doi:10.1007/S11665-022-07213-5/FIGURES/16.
[127] X. Meng, Z. Jiang, S. Zhu, S. Guan, J. Alloys. Compd. 838 (2020) 155611, doi:10.1016/j.jallcom.2020.155611.
[128] S.J. Sun, S.P. Ju, C.C. Yang, K.C. Chang, I.J. Lee, Sci. Rep. 10 (2020) 1–14, doi:10.1038/s41598-020-58789-8.
[129] B. Yang, C. Shi, X. Ye, J. Teng, R. Lai, Y. Cui, D. Guan, H. Cui, Y. Li, A. Chiba, J. Magnes. Alloy. 11 (2023) 998–1015, doi:10.1016/j.jma.2021.06.008.
[130] K. Wei, R. Hu, D. Yin, L. Xiao, S. Pang, Y. Cao, H. Zhou, Y. Zhao, Y. Zhu, Acta Mater. 206 (2021) 116604, doi:10.1016/j.actamat.2020.116604.
[131] X. Luo, Z. Feng, T. Yu, J. Luo, T. Huang, G. Wu, N. Hansen, X. Huang, Acta Mater. 183 (2020) 398–407, doi:10.1016/j.actamat.2019.11.034.
[132] A. Chapuis, J.H. Driver, Acta Mater. 59 (2011) 1986–1994, doi:10.1016/j.actamat.2010.11.064.
[133] S. Sandlöbes, S. Zaefferer, I. Schestakow, S. Yi, R. Gonzalez-Martinez, Acta Mater. 59 (2011) 429–439, doi:10.1016/j.actamat.2010.08.031.
[134] Z. Wu, R. Ahmad, B. Yin, S. Sandlöbes, W.A. Curtin, Science (1979) 359 (80) (2018) 447–452, doi:10.1126/science.aap8716.
[135] Y. Chino, M. Kado, M. Mabuchi, Acta Mater. 56 (2008) 387–394, doi:10.1016/j.actamat.2007.09.036.
[136] J. Zheng, Q. Wang, Z. Jin, T. Peng, Mater. Sci. Eng. A 527 (2010) 1677–1685, doi:10.1016/j.msea.2009.10.067.
[137] K. Guan, F. Meng, P. Qin, Q. Yang, D. Zhang, B. Li, W. Sun, S. Lv, Y. Huang, N. Hort, J. Meng, J. Mater. Sci. Technol. 35 (2019) 1368–1377, doi:10.1016/j.jmst.2019.01.019.
[138] Z. Hu, Z. Yin, Z. Yin, B. Tang, X. Huang, H. Yan, H. Song, C. Luo, X. Chen, J. Alloys. Compd. 842 (2020) 155836, doi:10.1016/j.jallcom.2020.155836.
[139] S. Zhou, T. Liu, A. Tang, Y. Huang, P. Peng, J. Zhang, N. Hort, R. Willumeit-Römer, F. Pan, Mater. Des. 225 (2023) 111476, doi:10.1016/j.matdes.2022.111476.
[140] Q. Qiu, S. Yue, and J. Song, 2024. First Principles Studies of Stacking Fault Energies in Ternary Magnesium Alloys. arXiv preprint arXiv:2404.00564.

[141] K. Guan, B. Li, Q. Yang, X. Qiu, Z. Tian, D. Zhang, D. Zhang, X. Niu, W. Sun, X. Liu, J. Meng, J. Alloys. Compd. 735 (2018) 1737–1749, doi:10.1016/j.jallcom.2017.11.315.
[142] W. Chen, W. He, B. Jiang, F. Pan, Int. J. Plast. 170 (2023) 103753, doi:10.1016/j.ijplas.2023.103753.
[143] A. Becerra, M. Pekguleryuz, J. Mater. Res. 23 (2008) 3379–3386, doi:10.1557/jmr.2008.0414.
[144] J. Zhou, G.A. Fiete, Phys. Today 73 (2020) 66–67, doi:10.1063/PT.3.4397.
[145] B. Wang, S. Guan, J. Wang, L. Wang, S. Zhu, Mater. Sci. Eng. B 176 (2011) 1673–1678, doi:10.1016/j.mseb.2011.03.015.
[146] Q.F. Wang, H. Li, S.B. Li, Z.H. Wang, W.B. Du, Trans. Nonferrous Met. Soc. China (English Ed.) 21 (2011) 874–879, doi:10.1016/S1003-6326(11)60796-6.
[147] l.l. rokhlin, J. Phase Equilibria 19 (1998) 142–145, doi:10.1361/105497198770342607.
[148] J. chang XIE, Q.an LI, X.qiang WANG, J.hong LI, Trans. Nonferrous Met. Soc. China (English Ed.) 18 (2008) 303–308, doi:10.1016/S1003-6326(08)60053-9.
[149] A. Ru Wu, C.Qing Xia, Mater. Des. 28 (2007) 1963–1967, doi:10.1016/j.matdes.2006.04.023.
[150] H.T. Son, J.S. Lee, D.G. Kim, K. Yoshimi, K. Maruyama, J. Alloys. Compd. 473 (2009) 446–452, doi:10.1016/j.jallcom.2008.06.016.
[151] Y. Zhang, X. Huang, Y. Li, Z. Ma, Y. Ma, Y. Hao, J. Rare Earths 35 (2017) 494–502, doi:10.1016/S1002-0721(17)60939-6.
[152] D. Zhang, H. Zhang, X. Yu, X. Zhang, D. Fan, g, structure evolution and mechanical properties of extruded Mg-12Zn-1.5Er alloy, in: Advanced Materials Research, Trans Tech Publications Ltd, 2011, pp. 500–504, doi:10.4028/www.scientific.net/AMR.284-286.500.
[153] M. Yang, J. Zhou, H. Huang, S. Cao, Q.M. Hu, W. Li, Q. Chen, Y. Qiao, H. Wang, J. Mater. Res. Technol. 26 (2023) 2140–2150, doi:10.1016/j.jmrt.2023.08.048.
[154] W. Li, L. Wang, B. Zhou, C. Liu, X. Zeng, J. Mater. Sci. Technol. 35 (2019) 2200–2206, doi:10.1016/j.jmst.2019.04.030.
[155] K.H. Kim, J.B. Jeon, N.J. Kim, B.J. Lee, Scr. Mater. 108 (2015) 104–108, doi:10.1016/j.scriptamat.2015.06.028.
[156] J. Zhang, D. Tang, H. Zhang, L. Wang, J. Wang, J. Meng, Xiyou Jinshu /Chinese J. Rare Met. 32 (2008) 659–667.
[157] N. Su, Y. Wu, Q. Deng, Z. Chang, Q. Wu, Y. Xue, K. Yang, Q. Chen, L. Peng, Mater. Sci. Eng. A 810 (2021) 141019, doi:10.1016/j.msea.2021.141019.
[158] L.Li Chang, C.Chang Shi, H.Wei Cui, Trans. Nonferrous Met. Soc. China (English Ed.) 28 (2018) 30–35, doi:10.1016/S1003-6326(18)64635-7.
[159] J. Xie, J. Zhang, Z. You, S. Liu, K. Guan, R. Wu, J. Wang, J. Feng, J. Magnes. Alloy. 9 (2021) 41–56, doi:10.1016/j.jma.2020.08.016.
[160] Z. Huang, L. Wang, B. Zhou, T. Fischer, S. Yi, X. Zeng, Scr. Mater. 143 (2018) 44–48, doi:10.1016/j.scriptamat.2017.09.011.
[161] L. Wang, Z. Huang, H. Wang, A. Maldar, S. Yi, J.S. Park, P. Kenesei, E. Lilleodden, X. Zeng, Acta Mater. 155 (2018) 138–152, doi:10.1016/j.actamat.2018.05.065.
[162] K. Li, Q. Huo, Y. Zhang, C. Zhang, W. Huang, Y. Ye, A. Hashimoto, X. Yang, Mater. Sci. Eng. A 771 (2020) 138618, doi:10.1016/j.msea.2019.138618.
[163] K. Hantzsche, J. Bohlen, J. Wendt, K.U. Kainer, S.B. Yi, D. Letzig, Scr. Mater. 63 (2010) 725–730, doi:10.1016/j.scriptamat.2009.12.033.
[164] Q. Zhu, C. Fang, N. Li, L. Meng, Y. Wang, Y. Wu, X. Zhang, Xiyou Jinshu Cailiao Yu Gongcheng/Rare Met. Mater. Eng. 42 (2013) 771–775.
[165] Y. Han, Z. Chen, H. Chen, J. Huang, C. Liu, Metall. Mater. Trans. a Phys. Metall. Mater. Sci. 54 (2023) 4806–4824, doi:10.1007/s11661-023-07203-9.
[166] X. Lin, Z. Chen, J. Shao, J. Xiong, Z. Hu, C. Liu, J. Magnes. Alloy. 11 (2023) 2340–2350, doi:10.1016/j.jma.2021.08.006.
[167] J. Liu, J. Li, Z. Cui, L. Ruan, Jinshu Xuebao/Acta Metall. Sin. 48 (2012) 1510–1519, doi:10.3724/SP.J.1037.2012.00486.
[168] S. Sandlöbes, M. Friák, J. Neugebauer, D. Raabe, Mater. Sci. Eng. A 576 (2013) 61–68, doi:10.1016/j.msea.2013.03.006.
[169] Z.R. Liu, D.Y. Li, Acta Mater. 89 (2015) 225–233, doi:10.1016/j.actamat.2015.01.051.
[170] J. Tian, J. Deng, Y. Zhou, Y. Chang, W. Liang, J. Ma, J. Mater. Res. Technol. 22 (2023) 473–488, doi:10.1016/j.jmrt.2022.11.102.
[171] Z. Wei, Q. Li, H. Kang, Q. Zhang, Appl. Mech. Mater. (2012) 1125–1128, doi:10.4028/www.scientific.net/AMM.117-119.1125.
[172] R. Mahmudi, F. Kabirian, Z. Nematollahi, Mater. Des. 32 (2011) 2583–2589, doi:10.1016/j.matdes.2011.01.040.
[173] B.K. Lee, E.C. Ko, Y.H. Kim, H.S. Yoo, H.T. Son, S.K. Hong, Korean J. Mater. Res. 33 (2023) 393–399, doi:10.3740/MRSK.2023.33.10.393.
[174] S. Zhu, M.A. Easton, T.B. Abbott, M.A. Gibson, J.F. Nie, Adv. Eng. Mater. 18 (2016) 932–937, doi:10.1002/adem.201500545.
[175] L. Gao, J. Zhou, Z.M. Sun, R.S. Chen, E.H. Han, Chinese Sci. Bull. 56 (2011) 1142–1146, doi:10.1007/s11434-010-4061-z.
[176] N. Mo, I. McCarroll, Q. Tan, A. Ceguerra, J. Cairney, H. Dieringa, Y. Huang, B. Jiang, F. Pan, M. Bermingham, M.X. Zhang, Mater. Sci. Eng. A 779 (2020) 139152, doi:10.1016/j.msea.2020.139152.
[177] H. Zhou, X. Zeng, L. Liu, Y. Zhang, Y. Zhu, W. Ding, J. Mater. Sci. 39 (2004) 7061–7066, doi:10.1023/B:JMSC.0000047551.04037.FE.
[178] I.P. Moreno, T.K. Nandy, J.W. Jones, J.E. Allison, T.M. Pollock, Scr. Mater. 48 (2003) 1029–1034, doi:10.1016/S1359-6462(02)00595-X.
[179] C. Liu, Q. Li, J. Liang, J. Zhou, L. Wang, RSC. Adv. 6 (2016) 30642–30651, doi:10.1039/C5RA27010C.
[180] X. Geng, J. Jiang, X. Zhang, Metals. (Basel) 12 (2022) 1763, doi:10.3390/met12101763.
[181] Z. Li, P. Fu, L. Peng, Y. Wang, H. Jiang, J. Mater. Sci. 48 (2013) 6367–6376, doi:10.1007/s10853-013-7436-0.
[182] C.J. Chen, Q.D. Wang, D.D. Yin, J. Alloys. Compd. 487 (2009) 560–563, doi:10.1016/j.jallcom.2009.07.177.
[183] L. Zhong, Y. Wang, M. Gong, X. Zheng, J. Peng, Mater. Charact. 138 (2018) 284–288, doi:10.1016/j.matchar.2018.02.019.
[184] C. Su, D. Li, A.A. Luo, T. Ying, X. Zeng, J. Alloys. Compd. 747 (2018) 431–437, doi:10.1016/j.jallcom.2018.03.070.
[185] C. Su, D. Li, A.A. Luo, R. Shi, X. Zeng, Metall. Mater. Trans. a Phys. Metall. Mater. Sci. 50 (2019) 1970–1984, doi:10.1007/s11661-019-05136-w.
[186] M. Yamasaki, Y. Kawamura, Scr. Mater. 60 (2009) 264–267, doi:10.1016/j.scriptamat.2008.10.022.
[187] K. Yu, W.X. Li, R.C. Wang, Z.Q. Ma, Zhongguo Youse Jinshu Xuebao/Chinese J. Nonferrous Met. 13 (2003) 277.
[188] S. Arunachalam, B. Kirubasankar, D. Pan, H. Liu, C. Yan, Z. Guo, S. Angaiah, Green Energy Environ. 5 (2020) 259–273, doi:10.1016/j.gee.2020.07.021.
[189] F. Wang, J.J. Bhattacharyya, S.R. Agnew, Mater. Sci. Eng. A 666 (2016) 114–122, doi:10.1016/j.msea.2016.04.056.
[190] D. Liu, Y. Ding, T. Guo, X. Qin, C. Guo, S. Yu, S. Lin, Biomed. Mater. 9 (2014) 015014, doi:10.1088/1748-6041/9/1/015014.
[191] Q. Zhang, Q.A. Li, X.T. Jing, X.Y. Zhang, Cailiao Gongcheng/J. Mater. Eng. (2011).
[192] J. He, W.Z. Chen, Z.J. Zhang, X.M. Chen, J.F. Ma, W.K. Wang, W.C. Zhang, J. Mater. Sci. 57 (2022) 4334–4353, doi:10.1007/s10853-022-06881-x.
[193] W. Fu, R.H. Wang, H. Xue, J. Kuang, J.Y. Zhang, G. Liu, J. Sun, J. Alloys. Compd. 747 (2018) 197–210, doi:10.1016/j.jallcom.2018.02.328.
[194] G. Jia, E. Guo, Y. Feng, L. Wang, C. Wang, Mater. Res. Express. 5 (2018) 036503, doi:10.1088/2053-1591/aab074.
[195] S. Gavras, S. Zhu, M.A. Easton, M.A. Gibson, H. Dieringa, Front. Mater. 6 (2019) 467703, doi:10.3389/fmats.2019.00262.
[196] A. Wu, C. Xia, J. Wang, J. Univ. Sci. Technol. Beijing Miner. Metall. Mater. (Eng. Ed) 13 (2006) 424–428, doi:10.1016/S1005-8850(06)60086-8.
[197] M.A. Easton, S. Zhu, T.B. Abbott, M. Dargusch, M. Murray, G. Savage, N. Hort, M.A. Gibson, Adv. Eng. Mater. 18 (2016) 953–962, doi:10.1002/adem.201500407.
[198] S. Yang, S.K. Tiwari, Z. Zhu, D. Cao, H. He, Y. Chen, K. Thummavichai, N. Wang, M. Jiang, Y. Zhu, Nanomaterials 13 (2023) 827, doi:10.3390/nano13050827.

[199] D. Liu, M. Zeng, Z. Li, Z. Zhu, Y. Chen, K. Thummavichai, O. Ola, N. Wang, Y. Zhu, RSC. Adv. 13 (2023) 8564–8576, doi:10.1039/d3ra00418j.
[200] H. Zhang, Z. Zhu, Y. Sun, M. Zuo, H. Zhou, Y. Chen, L. Han, Adv. Sustain. Syst. 8 (2024) 2400262, doi:10.1002/adsu.202400262.
[201] N. Mo, Q. Tan, M. Bermingham, Y. Huang, H. Dieringa, N. Hort, M.X. Zhang, Mater. Des. 155 (2018) 422–442, doi:10.1016/j.matdes.2018.06.032.
[202] I.P. Moreno, T.K. Nandy, J.W. Jones, J.E. Allison, T.M. Pollock, Scr. Mater. 45 (2001) 1423–1429, doi:10.1016/S1359-6462(01)01179-4.
[203] X. Dong, L. Feng, S. Wang, E.A. Nyberg, S. Ji, J. Magnes. Alloy. 9 (2021) 90–101, doi:10.1016/j.jma.2020.09.012.
[204] Z.H. Huang, W.J. Qi, J. Xu, Trans. Nonferrous Met. Soc. China (English Ed.) 23 (2013) 2568–2576, doi:10.1016/S1003-6326(13)62769-7.
[205] C. Luo, D. Song, Y. Li, W. Qi, N. Zhou, M. Sun, Jinshu Rechuli/Heat Treat. Met. 42 (2017) 127–133, doi:10.13251/j.issn.0254-6051.2017.05.026.
[206] G.L. Jia, L.P. Wang, Y.C. Feng, E.J. Guo, Y.H. Chen, C.L. Wang, Rare Met. 40 (2021) 2197–2205, doi:10.1007/s12598-020-01423-3.
[207] D. Krüger, S. Galli, B. Zeller-Plumhoff, D.C.F. Wieland, N. Peruzzi, B. Wiese, P. Heuser, J. Moosmann, A. Wennerberg, R. Willumeit-Römer, Bioact. Mater. 13 (2022) 37–52, doi:10.1016/j.bioactmat.2021.10.041.
[208] Z. Zhu, S.K. Tiwari, Y. Chen, D. Liu, S. Yang, K. Thummavichai, G. Ma, N. Wang, Y. Zhu, Ceram. Int. 50 (2024) 16813–16825, doi:10.1016/j.ceramint.2024.02.135.
[209] X. Zheng, P. Luo, J. Dong, S. Wang, J. Mater. Eng. Perform. 28 (2019) 1753–1761, doi:10.1007/s11665-019-3878-0.
[210] Z. Liu, L. Wang, L. Wang, Y. Feng, F. Kang, B. Wang, S. Li, C. Hu, J. Mater. Sci. 57 (2022) 15137–15150, doi:10.1007/s10853-022-07569-y.
[211] S.K. Das, Y.B. Kang, T. Ha, I.H. Jung, Acta Mater. 71 (2014) 164–175, doi:10.1016/j.actamat.2014.02.029.
[212] B. Tao, R. Qiu, Y. Zhao, Y. Liu, X. Tan, B. Luan, Q. Liu, J. Alloys. Compd. 748 (2018) 745–757, doi:10.1016/j.jallcom.2018.03.203.
[213] K. Muszka, J. Majta, Ł. Bienias, Metall. Foundry Eng. 32 (2006) 87, doi:10.7494/mafe.2006.32.2.87.
[214] Y. Wang, S. Guan, X. Zeng, W. Ding, Mater. Sci. Eng. A 416 (2006) 109–118, doi:10.1016/j.msea.2005.09.104.
[215] L. Zhong, J. Peng, S. Sun, Y. Wang, Y. Lu, F. Pan, J. Mater. Sci. Technol. 33 (2017) 1240–1248, doi:10.1016/j.jmst.2016.08.026.
[216] S.S. Bashkirov, V.V. Parfenov, L.D. Zaripova, N.V. Boltakova, T.I. Chupakhina, Microeffect of Al addition on the grain refinement and mechanical properties of as-cast Mg–5Y–4Sm alloys, in: Physics of Metals and Metallography, Springer, 2007, pp. 346–350, doi:10.1134/S0031918X07100043.
[217] F. Zhai, L. Wang, X. Gao, Y. Feng, S. Zhao, L. Wang, Trans. Indian Inst. Met 74 (2021) 2639–2649, doi:10.1007/s12666-021-02337-z.
[218] D. Panda, S. Tripathy, R.K. Sabat, S. Suwas, S.K. Sahoo, J. Mater. Eng. Perform. 31 (2022) 9183–9199, doi:10.1007/s11665-022-06934-x.
[219] H.S. Jang, K.H. Kim, N.J. Kim, B.J. Lee, Effect of grain refinment on mechanical properties of microalloyed steels, in: Minerals, Metals & Materials Series, Springer, Cham, 2017, pp. 491–495, doi:10.1007/978-3-319-52392-7_67.
[220] M.S. Nitol, S. Mun, D.E. Dickel, C.D. Barrett, Philos. Mag. 102 (2022) 651–673, doi:10.1080/14786435.2021.2012289.
[221] J. Liu, Z. Cui, L. Ruan, Mater. Sci. Eng. A 529 (2011) 300–310, doi:10.1016/j.msea.2011.09.032.
[222] J.fei Deng, J. Tian, Y. Zhou, Y. Chang, W. Liang, J. Ma, Mater. Des. 218 (2022), doi:10.1016/j.matdes.2022.110678.
[223] K.K. Deng, C.J. Wang, K.B. Nie, X.J. Wang, Acta Metall. Sin. (English Lett.) 32 (2019) 413–425, doi:10.1007/s40195-019-00872-9.
[224] Y.X. Wang, J.W. Fu, Y.S. Yang, Trans. Nonferrous Met. Soc. China (English Ed.) 22 (2012) 1322–1328, doi:10.1016/S1003-6326(11)61321-6.
[225] Z. Zhang, M.P. Wang, S. Zhu, N. Jiang, J. Alloys. Compd. 544 (2012) 159–165, doi:10.1016/j.jallcom.2012.07.116.
[226] Z.J. Li, J.G. Wang, R.F. Yan, Z. Wang, T.Y. Ni, H. Sun, Adv. Eng. Mater. 23 (2021) 2001459, doi:10.1002/adem.202001459.
[227] N. Stanford, Mater. Sci. Eng. A 565 (2013) 469–475, doi:10.1016/j.msea.2012.10.084.
[228] S.M. Zhu, M.A. Gibson, M.A. Easton, J.F. Nie, Scr. Mater. 63 (2010) 698–703, doi:10.1016/j.scriptamat.2010.02.005.
[229] S.A. Alkahtani, E.M. Elgallad, M.M. Tash, A.M. Samuel, F.H. Samuel, Materials. (Basel) 9 (2016) 45, doi:10.3390/ma9010045.
[230] M. Zouari, N. Bozzolo, R.E. Loge, Mater. Sci. Eng. A 655 (2016) 408–424, doi:10.1016/j.msea.2015.12.102.
[231] S. Sandlöbes, Z. Pei, M. Friák, L.F. Zhu, F. Wang, S. Zaefferer, D. Raabe, J. Neugebauer, Acta Mater. 70 (2014) 92–104, doi:10.1016/j.actamat.2014.02.011.
[232] I. Basu, T. Al-Samman, Acta Mater. 96 (2015) 111–132, doi:10.1016/j.actamat.2015.05.044.
[233] E. Cui, H. Sun, Y. Liu, J. Chen, K. He, H. You, L. Wang, L. Jiang, Tezhong Zhuzao Ji Youse Hejin/Special Cast. Nonferrous Alloy. 39 (2019) 1223–1225, doi:10.15980/j.tzzz.2019.11.018.
[234] S. Sandlöbes, M. Friák, S. Zaefferer, A. Dick, S. Yi, D. Letzig, Z. Pei, L.F. Zhu, J. Neugebauer, D. Raabe, Acta Mater. 60 (2012) 3011–3021, doi:10.1016/j.actamat.2012.02.006.
[235] G. Wu, C. Wang, M. Sun, W. Ding, J. Magnes. Alloy. 9 (2021) 1–20, doi:10.1016/J.JMA.2020.06.021.
[236] Z. Li, W. Wang, C. Yang, G. Jiang, Transp. Policy 29 (2013) 170–177, doi:10.1016/J.TRANPOL.2013.06.001.
[237] F. Qi, X. Zhang, G. Wu, W. Liu, X. He, W. Ding, Mater. Sci. Eng. A 813 (2021) 141172, doi:10.1016/j.msea.2021.141172.
[238] J. Wang, Z. Chang, B. Liu, Y. Li, Y. Sun, H. Li, Crystals. (Basel) 12 (2022) 1643, doi:10.3390/cryst12111643.
[239] Z. Zhu, L. Yang, Z. Xiong, D. Liu, B. Hu, N. Wang, O. Ola, Y. Zhu, Nanomaterials 13 (2023) 1664, doi:10.3390/nano13101664.
[240] MD Helicopters MD600N Multi-. https://www.airport-technology.com/projects/md. Accessed Date: 10/07/2025.
[241] J. Bai, Y. Yang, C. Wen, J. Chen, G. Zhou, B. Jiang, X. Peng, F. Pan, J. Magnes. Alloy. 11 (2023) 3609–3619, doi:10.1016/J.JMA.2023.09.015.
[242] L. Yan, Y. Zhang, Y. Zhang, R. Liu, C. Liu, F. Wu, F. Xu, J. Magn. Magn. Mater. 597 (2024) 172003, doi:10.1016/j.jmmm.2024.172003.
[243] Z. Abbasi, E. Shamsaei, X.Y. Fang, B. Ladewig, H. Wang, J. Colloid. Interface Sci. 493 (2017) 150–161, doi:10.1016/j.jcis.2017.01.006.
[244] C. Wang, Y. Chen, S. Xiao, Xiyou Jinshu Cailiao Yu Gongcheng/Rare Met. Mater. Eng. 44 (2015) 2596–2600, doi:10.12442/J.ISSN.1002-185X.2016.44.10.25962600.
[245] X. Zeng, J. Wang, T. Ying, W. Ding, Jinshu Xuebao/Acta Metall. Sin. 58 (2022) 400–411, doi:10.11900/0412.1961.2021.00520.
[246] Z. Savaedi, R. Motallebi, H. Mirzadeh, R. Mehdinavaz Aghdam, R. Mahmudi, Curr. Opin. Solid. State Mater. Sci. 27 (2023) 101058, doi:10.1016/j.cossms.2023.101058.
[247] R. Zeng, W. Dietzel, F. Witte, N. Hort, C. Blawert, Adv. Eng. Mater. 10 (2008) B3–B14, doi:10.1002/adem.200800035.
[248] X. Tong, Y. Han, R. Zhou, W. Jiang, L. Zhu, Y. Li, S. Huang, J. Ma, C. Wen, J. Lin, Acta Biomater. 155 (2023) 684–702, doi:10.1016/j.actbio.2022.10.053.
[249] R. Rettig, S. Virtanen, J. Biomed. Mater. Res. Part A 88A (2009) 359–369, doi:10.1002/JBM.A.31887.
[250] W. Weng, A. Biesiekierski, Y. Li, M. Dargusch, C. Wen, Acta Biomater. 130 (2021) 80–97, doi:10.1016/j.actbio.2021.06.004.
[251] W. Liu, J. Wang, G. Jiang, J. Guo, Q. Li, B. Li, Q. Wang, M. Cheng, G. He, X. Zhang, J. Mater. Chem. B 5 (2017) 7661–7674, doi:10.1039/c7tb00920h.
[252] J. Zan, G. Qian, F. Deng, J. Zhang, Z. Zeng, S. Peng, C. Shuai, J. Mater. Res. Technol. 17 (2022) 2369–2387, doi:10.1016/J.JMRT.2022.01.164.
[253] B.M. Brochu, S.R. Sturm, J.A. Kawase De Queiroz Goncalves, N.A. Mirsky, A.I. Sandino, K.Z. Panthaki, K.Z. Panthaki, V.V. Nayak, S. Daunert, L. Witek, P.G. Coelho, Biomimetics. 9 (2024) 690, doi:10.3390/BIOMIMETICS9110690.
[254] T. Kraus, S.F. Fischerauer, A.C. Hänzi, P.J. Uggowitzer, J.F. Löffler, A.M. Weinberg, Acta Biomater. 8 (2012) 1230–1238, doi:10.1016/j.actbio.2011.11.008.

[255] M. Yang, C. Chen, D. Wang, Y. Shao, W. Zhou, C. Shuai, Y. Yang, X. Ning, J. Magnes. Alloy. 12 (2024) 1260–1282, doi:10.1016/J.JMA.2024.03.014.
[256] X. Zhao, L. ling Shi, J. Xu, J. Mater. Sci. Technol. 29 (2013) 781–787, doi:10.1016/J.JMST.2013.05.017.
[257] Z. Geng, X. Li, Y. Zhang, E. Lin, S.Z. Kure-Chu, X. Li, X. Xiao, Surf. Coatings Technol. 412 (2021) 127042, doi:10.1016/J.SURFCOAT.2021.127042.
[258] C. Zhang, L. Wu, H. Liu, G. Huang, B. Jiang, A. Atrens, F. Pan, Corros. Sci. 174 (2020) 108831, doi:10.1016/J.CORSCI.2020.108831.
[259] A. Soper, A.L. Shaw, P.L.J. Conway, G.S. Pomrehn, M. Ferry, L. Bassman, A. Pribram-Jones, K.J. Laws, Comput. Mater. Sci. 207 (2022) 111240, doi:10.1016/J.COMMATSCI.2022.111240.
[260] Y. Zhang, Y. Huang, F. Feyerabend, C. Blawert, W. Gan, E. Maawad, S. You, S. Gavras, N. Scharnagl, J. Bode, C. Vogt, D. Zander, R. Willumeit-Römer, K.U. Kainer, N. Hort, Acta Biomater. 121 (2021) 695–712, doi:10.1016/J.ACTBIO.2020.11.050.
[261] J. Zhang, Z. Leng, M. Zhang, J. Meng, R. Wu, J. Alloys. Compd. 509 (2011) 1069–1078, doi:10.1016/J.JALLCOM.2010.09.185.
[262] M. Esmaily, Z. Zeng, A.N. Mortazavi, A. Gullino, S. Choudhary, T. Derra, F. Benn, F. D'Elia, M. Müther, S. Thomas, A. Huang, A. Allanore, A. Kopp, N. Birbilis, Addit. Manuf. 35 (2020) 101321, doi:10.1016/J.ADDMA.2020.101321.
[263] L. Liu, F. Yuan, M. Zhao, C. Gao, P. Feng, Y. Yang, S. Yang, C. Shuai, Mater 10 (2017) 477, doi:10.3390/MA10050477.
[264] P. Li, Y. Sun, S. Zhu, L. Wang, S. Guan, J. Wang, Mater. Today Commun. 37 (2023) 107562, doi:10.1016/j.mtcomm.2023.107562.
[265] K. Munir, J. Lin, C. Wen, P.F.A. Wright, Y. Li, Acta Biomater. 102 (2020) 493–507, doi:10.1016/J.ACTBIO.2019.12.001.
[266] S. Jin, D. Zhang, X. Lu, Y. Zhang, L. Tan, Y. Liu, Q. Wang, J. Mater. Sci. Technol. 47 (2020) 190–201, doi:10.1016/J.JMST.2020.02.017.
[267] L.M. Calado, M.J. Carmezim, M.F. Montemor, Front. Mater. 8 (2022) 804906, doi:10.3389/FMATS.2021.804906/XML/NLM.
[268] M. Li, F. Benn, T. Derra, N. Kröger, M. Zinser, R. Smeets, J.M. Molina-Aldareguia, A. Kopp, J. LLorca, Microstructure, mechanical properties, corrosion resistance and cytocompatibility of WE43 Mg alloy scaffolds fabricated by laser powder bed fusion for biomedical applications, Mater. Sci. Eng.: C 119 (2021) 111623.
[269] N. Zhao, N. Watson, Z. Xu, Y. Chen, J. Waterman, J. Sankar, D. Zhu, PLoS. One 9 (2014) e98674, doi:10.1371/JOURNAL.PONE.0098674.
[270] J. Zhang, H. Li, W. Wang, H. Huang, J. Pei, H. Qu, G. Yuan, Y. Li, Acta Biomater. 69 (2018) 372–384, doi:10.1016/j.actbio.2018.01.018.
[271] W. dong Hong, X. wei Chen, W. zhi Wu, Q. huai Zhu, X. rong Chen, Clin. Res. Hepatol. Gastroenterol. 37 (2013) 496–500, doi:10.1016/J.CLINRE.2012.12.002.
[272] I. Antoniac, M. Miculescu, V. Mănescu, A. Stere, P.H. Quan, G. Păltânea, A. Robu, K. Earar, Mater 15 (2022) 1148, doi:10.3390/MA15031148.
[273] H. May, Y. Alper Kati, G. Gumussuyu, T. Yunus Emre, M. Unal, O. Kose, J. Orthop. Traumatol. 21 (2020), doi:10.1186/s10195-020-00547-7.
[274] C. Aktan, M.B. Ertan, A. Turan, O. Kose, Cureus. (2018), doi:10.7759/cureus.3752.
[275] S. Vujović, J. Desnica, D. Stanišić, I. Ognjanović, M. Stevanovic, G. Rosic, Mol 27 (2022) 5529, doi:10.3390/MOLECULES27175529.
[276] S.P. Pilipchuk, A.B. Plonka, A. Monje, A.D. Taut, A. Lanis, B. Kang, W.V. Giannobile, Dent. Mater. 31 (2015) 317–338, doi:10.1016/J.DENTAL.2015.01.006.
[277] J. Ge, C. Yang, Y. Wang, J. Zheng, H. Hua, J. Zhu, Clin. ImPlant Dent. Relat. Res. 20 (2018) 444–454, doi:10.1111/CID.12603;WGROUP:STRING:PUBLICATION.
[278] C.W. Guo, Q. Yu, B.Z. Sun, C.Y. Wang, J.X. Yang, J. Biomater. Tissue Eng. 8 (2018) 1–10, doi:10.1166/JBT.2018.1709.
[279] C.Y. Wang, C.-Y. Kang, S.N. Zhang, J.X. Yang, G. Cheng, J. Biomater. Tissue Eng. 8 (2018) 11–19, doi:10.1166/JBT.2018.1715.
[280] J.H. Lee, H.S. Han, Y.C. Kim, J.Y. Lee, B.K. Lee, J. Cranio-Maxillofacial Surg. 45 (2017) 1639–1646, doi:10.1016/J.JCMS.2017.06.015.
[281] M. Barbeck, L. Kühnel, F. Witte, J. Pissarek, C. Precht, X. Xiong, R. Krastev, N. Wegner, F. Walther, O. Jung, Int. J. Mol. Sci. 21 (2020) 3098, doi:10.3390/IJMS21093098.
[282] K. Xie, L. Wang, Y. Guo, S. Zhao, Y. Yang, D. Dong, W. Ding, K. Dai, W. Gong, G. Yuan, Y. Hao, J. Orthop. Transl. 27 (2021) 96–100, doi:10.1016/J.JOT.2020.11.007.
[283] C. Zhao, P. Hou, J. Ni, P. Han, Y. Chai, X. Zhang, ACS. Appl. Mater. Interfaces. 8 (2016) 5093–5103, doi:10.1021/ACSAMI.5B10825/ASSET/IMAGES/AM-2015-10825D_M002.GIF.